

Rational Design of Organic Electrocatalysts for Hydrogen and Oxygen Electrocatalytic Applications

Ruiqi Cheng, Xiaoqian He, Kaiqi Li, Biao Ran, Xinlong Zhang, Yonghong Qin, Guanjie He, Huanxin Li,* and Chaopeng Fu*

Efficient electrocatalysts are pivotal for advancing green energy conversion technologies. Organic electrocatalysts, as cost-effective alternatives to noble-metal benchmarks, have garnered attention. However, the understanding of the relationships between their properties and electrocatalytic activities remains ambiguous. Plenty of research articles regarding low-cost organic electrocatalysts started to gain momentum in 2010 and have been flourishing recently though, a review article for both entry-level and experienced researchers in this field is still lacking. This review underscores the urgent need to elucidate the structure–activity relationship and design suitable electrode structures, leveraging the unique features of organic electrocatalysts like controllability and compatibility for real-world applications. Organic electrocatalysts are classified into four groups: small molecules, oligomers, polymers, and frameworks, with specific structural and physicochemical properties serving as activity indicators. To unlock the full potential of organic electrocatalysts, five strategies are discussed: integrated structures, surface property modulation, membrane technologies, electrolyte affinity regulation, and addition of anticorrosion species, all aimed at enhancing charge efficiency, mass transfer, and long-term stability during electrocatalytic reactions. The review offers a comprehensive overview of the current state of organic electrocatalysts and their practical applications, bridging the understanding gap and paving the way for future developments of more efficient green energy conversion technologies.

conservation. Over the decades, devices for environmentally-friendly hydrogen and oxygen energy conversion, such as metal–air batteries (MABs), proton/anion exchange membrane fuel cells (PEMFCs/AEMFCs), and water electrolyzers (WEs) have been extensively studied for commercial application.^[1] However, three key electrode reactions of these devices, which are oxygen reduction reaction (ORR), oxygen evolution reaction (OER), and hydrogen evolution reaction (HER), suffer from sluggish reaction kinetics. Therefore, electrocatalysts are urgently required to overcome this deficiency.^[2] Although noble-metals (Pt, Ir, and Ru-based) are known to be effective electrocatalysts, their high-cost and low-availability severely restrict their applications on a broad scale.^[3] As a result, designing low-cost electrocatalysts with low overpotentials to facilitate the electrode reactions and further enhance the energy conversion efficiency is highly preferred. In recent years, various materials have been studied as low-cost electrocatalysts with promising activity, including metal compounds, carbon materials, and organic compounds.^[2d,4] Studies dedicated to metal compounds and carbon materials for

electrocatalytic applications are notably abundant compared to those focusing on organic compounds.^[5] Many cost-effective electrocatalysts are based on metal compounds and carbon materials,^[6] in particular, exhibit comparable, and in some

1. Introduction

Clean and renewable energy has been a topic of extensive research to achieve sustainable development and energy

R. Cheng, X. He, B. Ran, X. Zhang, Y. Qin, C. Fu
 School of Materials Science and Engineering
 Shanghai Jiao Tong University
 Shanghai 200240, P. R. China
 E-mail: chaopengfu@sjtu.edu.cn

K. Li, G. He
 Christopher Ingold Laboratory
 Department of Chemistry
 University College London
 London WC1H 0AJ, UK
 H. Li
 Department of Chemistry
 Physical and Theoretical Chemistry Laboratory
 University of Oxford
 South Parks Road, Oxford OX1 3QZ, UK
 E-mail: huanxin.li@chem.ox.ac.uk
 H. Li
 Electrochemical Innovation Lab
 Department of Chemical Engineering
 University College London
 London WC1E 7JE, UK

 The ORCID identification number(s) for the author(s) of this article can be found under <https://doi.org/10.1002/adma.202402184>

© 2024 The Authors. Advanced Materials published by Wiley-VCH GmbH. This is an open access article under the terms of the [Creative Commons Attribution](#) License, which permits use, distribution and reproduction in any medium, provided the original work is properly cited.

DOI: 10.1002/adma.202402184

instances, even superior catalytic activity when compared to noble-metal benchmarks.^[7] The most commercially promising electrocatalysts currently include well-designed metal-based compounds that can exhibit ultralow overpotentials of HER/OER under large current densities (usually $\geq 1 \text{ A cm}^{-2}$),^[8] scalable produced graphitized carbon materials with extremely high ORR intrinsic activity,^[9] and the composite of metal compound and carbon with superior multifunctional performance in various kinds of devices.^[10] Organic compounds, a new family of low-cost electrocatalysts, have recently garnered certain attention. However, it is not yet clear whether it has prospects, in terms of cost and performance, and what role it will play in electrocatalysis. Therefore, it is necessary to comprehensively summarize its development status.

The advantages of organic electrocatalysts that have been discovered so far are listed as follows: first, many organic compounds are easily obtained through pyrolysis-free synthesis with low-cost organic precursors,^[11] and can be easily recycled or decomposed.^[12] These kinds of materials possess high environmental-friendliness, recyclability, and sustainability.^[13] Second, the modular properties of organic compounds in terms of chemical composition, dimensional structure, and pore distribution allow for the easy integration of specific functional building blocks into their skeletons.^[14] These building blocks play a vital role in determining the overall structural properties.^[15] Through tuning the geometry and dimension of building blocks, the direction of the topological evolution of structural periodicity can be readily modulated, thereby offering great potential for tailoring the mechanical, thermal, electrical, and optical properties of the organic compounds.^[16] Third, due to the high periodicity and degree of order,^[17] the structure of most organic compounds can be easily confirmed, and the relative content of each possible active site can be precisely calculated. With the assistance of the operando measurements and density functional theory (DFT) calculations,^[18] the origin of the electrocatalytic activity in these organic electrocatalysts can be clearly revealed, directly linking the electrocatalytic performance with structural characteristics more directly further filling in the gap in fundamental principles underlying the measured electrochemical performance of noble-metal-free electrocatalysts. Fourth, many organic compounds with robust architectural structures and mechanical properties are favorable for integrating with current collectors to form self-supported electrodes, which can greatly enhance the flexibility and durability of the electrode when assembled in energy-converting devices.^[19] Lastly, organic compounds mainly composed of earth-abundant C, H, O, and N elements do not rely on limited mineral resources, indicating substantial sustainability. These benefits suggest that organic compounds are a promising low-cost alternative to noble-metal-based electrocatalysts. Currently reported electrocatalytic activities of organic electrocatalysts are relatively lower than those of metal-based electrocatalysts (most of the activities of organic electrocatalysts are equivalent to even lower than those of noble-metal benchmarks and many superior well-elaborated non-noble-metal-based electrocatalysts), and the number of published research articles focusing on organic electrocatalysts is much less than those centering around metal-based electrocatalysts. These facts clearly substantiate that the development of organic electrocatalysts is still in its infancy. However, based on the various kinds of merits men-

tioned above, organic electrocatalyst still possess significant potential to be developed as another kind of cost-efficient substitute for commercial noble-metal-based electrocatalysts.

The number of published research articles on low-cost organic electrocatalysts in **Figure 1a** shows that studies on this topic began to emerge in 2000 and thrive since 2012. This statistical data suggest that the development of organic electrocatalysts has gradually become recognized as a more suitable energy development strategy over time, which is favorable for establishing a clean, environmental-friendly, safe, and efficient energy system for low-carbon society. Furthermore, the proportions of research articles focusing on different organic electrocatalysts in **Figure 1b** show that polymers and organic frameworks are currently the most researched organic electrocatalysts compared with small organic molecules and oligomers. This is because in the early development stage of organic electrocatalysts, researchers usually use conventional small organic molecules and oligomers for experimental and exploratory experiments. As the field of organic electrocatalysts gradually matured, more active polymers and organic frameworks with a high degree of polymerization and conjugation were proposed and developed as organic electrocatalysts. The overall development timeline of organic electrocatalyst is displayed in **Figure 1c**. In the beginning, DuVall and McCreery observed that the adsorbed thin layer of catechol small molecules on the glassy carbon electrode could serve as an electrocatalyst for solution-phase redox component in 2000, unearthing the electrocatalytic potential of organic compounds.^[20] Since then, organic electrocatalysts have been found to have many benefits. In 2005, initiated research on evaluating the electrocatalytic hydrogen evolution activities of complexes with BF_2 -bridged diglyoxime ligands in an acidic aqueous solution.^[21] The diglyoxime ligands play a key role in stabilizing the complex, leading to enhanced acid/carbon monoxide resistance during the electrocatalytic hydrogen revolution. Simultaneously, functional groups with less electron-releasing effect on the complex can effectively reduce the energy barrier of HER and the potential for generating H_2 is only -0.28 V versus SCE in CH_3CN , and this reduction protentional is the most positive compared to those of other electrocatalysts under similar conditions. These results manifest that organic compounds with superior structural regulatability and structural stability in actual environments are highly applicable for efficient electrocatalysis. Subsequently, in 2010, with the blooming development of oxygen and hydrogen electrocatalysis, many organic compounds including small organic molecules, oligomers, and polymers were studied as electrocatalysts for catalyzing the electrochemical reactions of green energy-converting devices.^[22] Later, as organic framework materials gradually emerged, their practicality in the field of electrocatalysis was also studied. From 2011 to 2015, electrocatalytic activities of various kinds of metal/covalent organic frameworks had been measured.^[23] From 2016 to the present, not only more and more organic electrocatalysts have been synthesized for more diverse energy storage/harvesting devices, but also advanced in situ characterizations and theoretical simulations have been developed to deeply analyze the electrocatalytic mechanism and the activity origin of organic electrocatalysts.^[24]

Despite ongoing research, there is no conclusive and systematic conclusion regarding the type and reaction mechanism of low-cost organic electrocatalysts, presenting significant

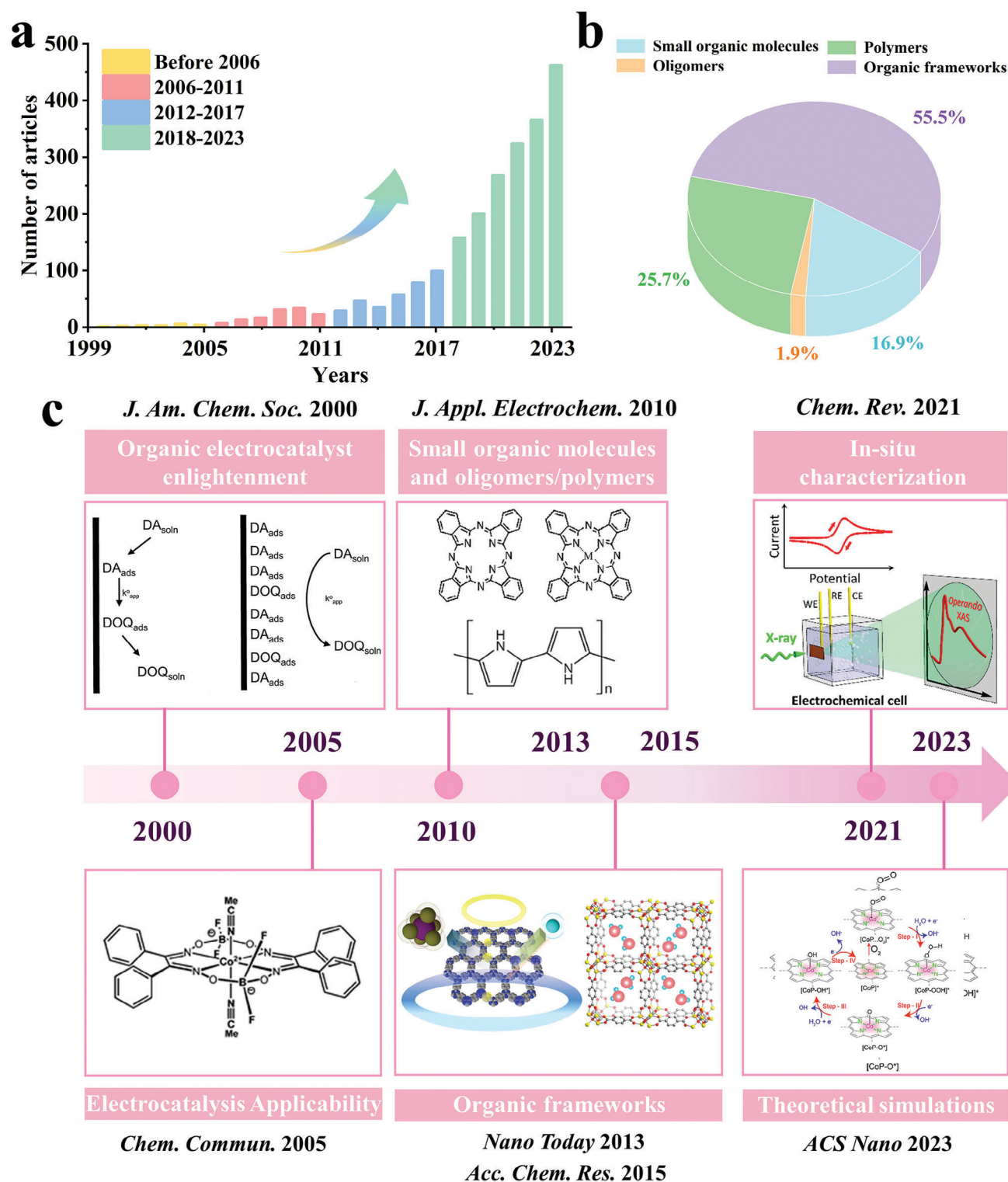


Figure 1. a) Graph of published research articles on organic electrocatalysts before December 31, 2023 (source: Scopus. Limitation: Keywords: Organic electrocatalyst. Excluded keywords: derived). b) Statistical data proportions of published research articles regarding various kinds of organic electrocatalysts since 2000. c) The development timeline of organic electrocatalysts from 2000 to the present. Reproduced with permission.^[20–22,23,24] Copyright 2000, American Chemical Society. Copyright 2005, RSC. Copyright 2010, Springer. Copyright 2013, Elsevier. Copyright 2015, American Chemical Society. Copyright 2021, American Chemical Society. Copyright 2023, American Chemical Society. Copyright 2018, Wiley-VCH. Copyright 2021, American Chemical Society. Copyright 2021, American Chemical Society. Copyright 2015, RSC. Copyright 2022, Wiley-VCH. Copyright 2018, American Chemical Society. Copyright 2022, Wiley-VCH.

challenges in applying these materials to practical electrocatalytic applications. Previous reviews have only summarized some organic electrocatalysts separately.^[25] Nevertheless, a comprehensive analysis of these organic electrocatalysts as well as their reaction mechanisms, is yet to be presented. Additionally, numerous issues appear when putting these low-cost organic electrocatalysts into practical applications. Lots of laboratory-measured electrocatalysts with superior electrocatalytic activity and stability exhibit somehow unsatisfied performance and rapid performance degradation under real conditions when assembled in energy storage/harvesting devices.^[26] It is necessary to use more broadly applicable methods to fully reveal the activity of electrocatalysts.

While various kinds of organic compounds have been investigated as electrocatalysts, designing low-cost, high-performance electrocatalysts remains a challenge due to the lack of a comprehensive understanding of organic electrocatalysts. Moreover, the nascent stage of applying these organic compounds in practical applications under an actual environment also significantly hampers the advancement of green energy storage/harvesting technologies.

Herein, a systematic and comprehensive overview of organic materials for electrocatalytic ORR, OER, and HER will be given in this review, offering guidance to both novice and experienced researchers in this field. The reported organic electrocatalysts to date can be classified into four types: small organic molecules, oligomers, polymers, and organic frameworks. Each type of organic compound possesses unique properties that contribute to various electrocatalytic mechanisms. The molecular structure, heteroatom dopant, and combined catalytic active substrate of small organic molecules are key factors determining the electrocatalytic performance. While for oligomers with a certain degree of polymerization, the molecular weight and number/kind of linked functional groups are more important. The electrocatalytic mechanisms of these electrocatalysts with a low molecular weight involve interactions between surface electroactive species and reactants. By modulating these interactions, the reaction intermediate binding energy on the small organic molecule electrocatalyst can be optimized, thereby achieving a lower reaction energy barrier. For organic compounds with a higher degree of polymerization, structures with low crystallinity are categorized as polymers, while those with a high degree of crystallinity are classified as organic frameworks. The electrocatalytic activities of these structures are mainly controlled by four factors: degree of conjugation, type of combined conductive enhancer, concertation of active species, and morphological/electronic structure of the global support. All these structural/physicochemical properties of organic compounds can directly affect many substantial indicators/descriptors of electrocatalytic activity. Therefore, by tuning various structural/physicochemical properties of organic electrocatalysts, these electrolytic active indicators/descriptors are significantly modulated, and the overall electrocatalytic activity of organic electrocatalysts can be rationally optimized. It should be noted that electrocatalytic mechanisms of electrocatalysts with a high molecular weight are diverse. For example, the electrocatalytic mechanisms of metal organic framework (MOF) based electrocatalysts can be generalized as follows: through screening out appropriate ligand structures and metal sources, the charge density on the active site (usually the metal site or its

adjacent atoms) and the reaction energy barrier of the assembled MOF can be successfully optimized.^[27] The electrocatalytic mechanisms of covalent organic framework (COF)-based electrocatalysts are correlated with the electron distribution of the COF global support. By selecting different building blocks, the interunit charge density difference of the polymerized COF and the charge density and reaction energy barrier of the active site can be regulated.^[28] In the following section, four fundamental electrochemical characteristics of organic electrocatalysts during electrocatalytic reactions are widely acknowledged to quantify the electrocatalytic activity, which are the number of active sites, mass transfer, charge transfer, and intrinsic activity. Deciphering the activity through finding appropriate activity indicators/descriptors originating from the structural/physicochemical properties can construct novel structure–activity relationships, and these relationships can provide better instruction for the rational design of high-performance organic electrocatalysts. Additionally, in the future, these well-designed organic electrocatalysts will ultimately be applied in various kinds of actual devices for practical applications. Given that the performances of most reported hydrogen and oxygen energy converting devices including MABs, PEMFCs/AEMFCs, and WEs are determined by the electrode structure and interaction between components of electrode and solute in the electrolyte, strategies for designing excellent electrode architecture are crucial to achieving superior performance and stability. In short, three strategies for better demonstrating the original electrocatalytic activity of these organic compounds into practical applications include constructing integrated electrode structure, tuning the surface property of the electrode, and fabricating membrane electrode assembly. Meanwhile, two other strategies namely electrolyte affinity regulating and corrosion-resistant species applying for maintaining the electrode integrity and inhibiting the decomposition/transformation of organic electrocatalysts are also prompted. All these five strategies leverage the modifiable characteristics of organic electrocatalysts with tunable activities and compatibility. This work not only systematically outlines concepts and setup factors related to electrocatalytic reactions of organic compound-based materials, but also elaborates on methods for better converting the original activity of electrocatalysts into practical applications and achieving long-term stability in an actual environment, thereby providing a clear understanding as guidance for the development of low-cost organic electrocatalysts for green energy use. The systematic overview of this review is thoroughly illustrated in **Figure 2**.

2. Categories of Organic Electrocatalysts

Numerous studies have reported organic electrocatalysts with activities comparable to noble metals and have analyzed the origins of their catalytic activities. However, the relationships between various physicochemical properties and electrocatalytic activity in organic electrocatalysts remain unclear. This can be largely attributed to the wide variety of organic electrocatalysts, each with different electrocatalytic mechanisms. Fortunately, due to the clear chemical compositions and molecular structures of organic electrocatalysts, compared with other electrocatalysts, bridging the gap between the measured electrocatalytic activity and their structural/physicochemical properties is more

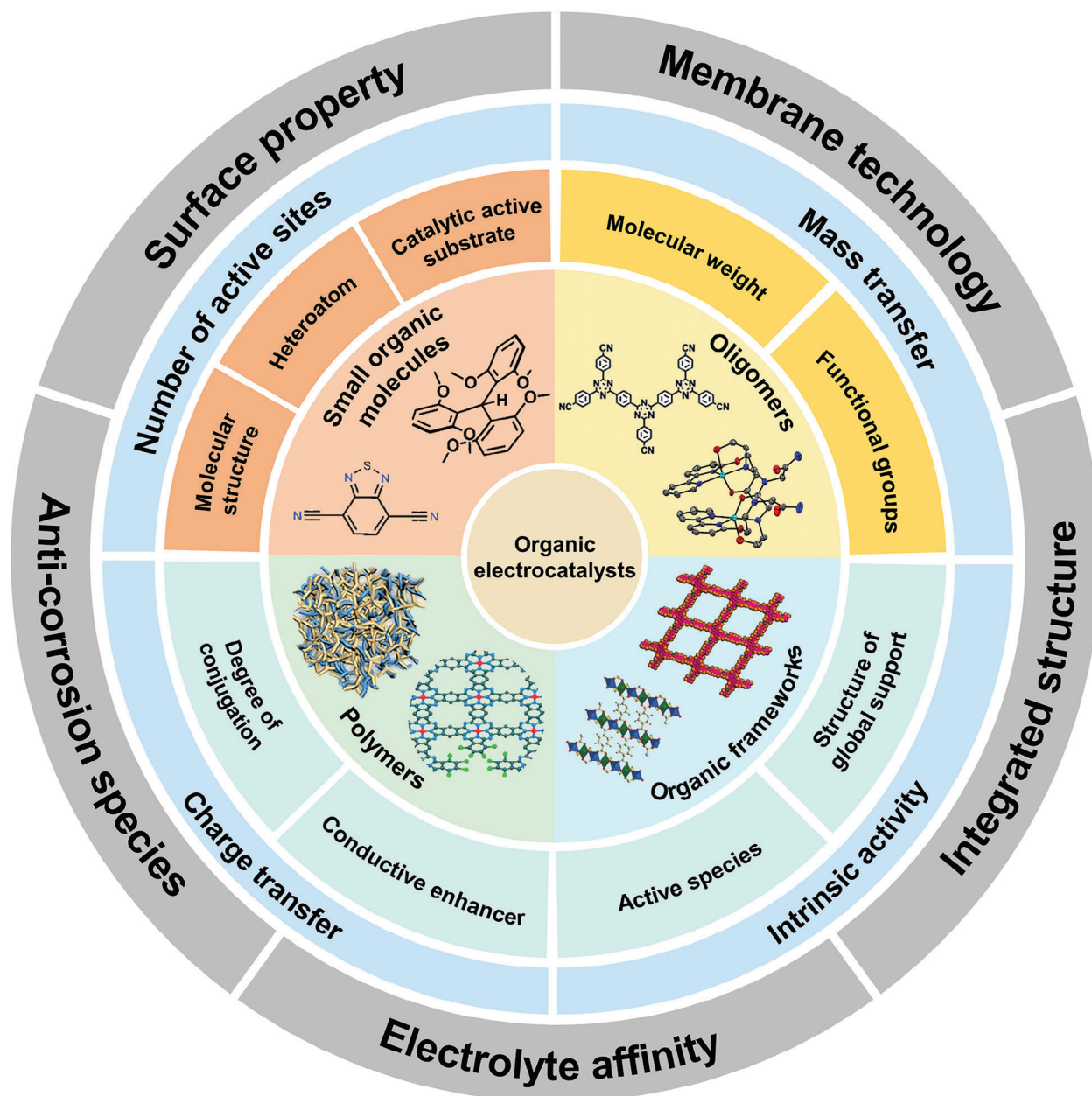


Figure 2. Comprehensive graphic illustration of organic electrocatalysts. Reproduced with permission.^[14,28,29] Copyright 2021, American Chemical Society (small organic molecules, left image) and Copyright 2018, American Chemical Society (small organic molecules, right image). Copyright 2015, RSC (oligomers, left image) and Copyright 2021, American Chemical Society (oligomers, right image). Copyright 2019, American Chemical Society (polymers, left image) and Copyright 2022, Wiley-VCH (polymers, right image). Copyright 2018, Wiley-VCH (organic frameworks, left image) and Copyright 2022, Wiley-VCH (organic frameworks, right image).

feasible and desirable. This is beneficial for providing a universal guide for the rational design of low-cost, organic compound-based electrocatalysts.^[30]

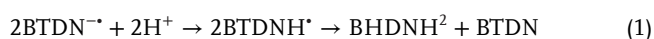
In this section, organic compound-based electrocatalysts for electrochemical applications are categorized into four main types: small organic molecules, oligomers, polymers, and organic frameworks. Among small organic molecules, those decorated with oxygen/nitrogen/sulfur-containing functional groups (also known as oxygen/nitrogen/sulfur-based small molecules) are the most representative. Importantly, through modulat-

ing their molecular structures, contained heteroatoms, and combined catalytic active substrates, they can be designed as electron donors/acceptors for releasing/extracting electrons to the adsorbed reaction intermediates during electrocatalytic reactions.^[29c] Oligomers, usually obtained through incomplete polymerization and typically having a molecular weight of $\approx 10\,000$,^[31] can have their electrocatalytic activity greatly affected by tuning the molecular weight, which modulates the number of exposed terminal residual functional groups and surface properties. Polymers and organic frameworks, both possess high de-

grees of polymerization. The difference between organic frameworks and polymers is that organic frameworks exhibit high crystallinity while polymers possess amorphous crystal structures.^[28] The electron mobility in the skeleton of these polymerized components is determined by the degree of conjugation, type of conductive enhancer, and structure of the global support.^[32] Furthermore, the overall electrocatalytic performance of organic frameworks and polymers is primarily controlled by the concentration of active species (such as electrocatalytic active functional groups and atomic metal centers) in their skeletons. The exhibited electrocatalytic activities of organic frameworks and polymers are mainly controlled by these four factors. In this review, we have compiled these four types of organic materials used as oxygen and hydrogen electrocatalysts, each with their unique physicochemical properties that can affect the electrocatalytic performance, and discussed in detail in the following sections.

2.1. Small Organic Molecules

Small organic molecules are typically employed as ligands for synthesizing metal complexes or as building blocks for organic polymers.^[26] However, their direct use as catalysts for electrocatalytic reactions has not been extensively explored. H heteroatom-doped small organic molecules, possessing cyclic conjugated aromatic structures, can serve as efficient electrocatalysts. This is because specific functional groups with heteroatoms on the structure's edge can be functionalized as active sites, adsorbing electroactive species and further catalyzing electrocatalytic reactions.^[33] Axelsson et al. utilized 2,1,3- benzothiadiazole-4,7-dicarbonitrile (BTDN) with S heteroatoms for catalyzing HER.^[29c] The reaction mechanism of BTDN is elucidated by spectroelectrochemical strategies. As shown in **Figure 3a**, the CV curve of BTDN exhibits two characteristic peaks at -1.06 V and -1.88 V (V vs Fc/Fc⁺). Upon the addition of salicylic acid (SAL, identifier of the electrocatalytic behavior of BTDN), the first characteristic peak negatively shifts and can be ascribed to the transformation of BTDN to BTDN^{•-} (electrochemical step) and then to BTDNH[•] (chemical step). The second characteristic peak gradually vanishes as the concentration of SAL increases, a phenomenon interpreted by in-situ UV-vis spectra (**Figure 3b,c**). When the external potential is set at -1.9 V, the addition of SAL results in the appearance of two absorption peaks at 520 and 555 nm (characteristic peak of BTDN²⁻), indicating the protonation of BTDN^{•-}. Beyond that, with the addition of SAL, the peak at 340 nm decreases with the negative shift of extremal potential, suggesting the reformation of BTDN post-electrocatalysis. The reformation of BTDN follows the transformation equation given below



Based on the above analysis, the overall reaction mechanism can be illustrated (**Figure 3d**). The heteroatom-containing cyclic structure at the molecule's edge can function as an active site for the adsorption/desorption of hydrogen intermediates, thereby catalyzing HER.

Compared with graphitic carbon-based electrocatalysts, small organic molecule electrocatalysts typically display distinct and well-defined active sites, which is more advantageous for elu-

cidating the structure-activity relationships. By adjusting the quantity and type of oxygen-containing functional groups on the skeleton of small organic molecules, Yan et al. have effectively demonstrated the impact of functional groups on the electronic structure and, subsequently, the two-electron ORR electrocatalytic activity of small organic molecule electrocatalysts.^[1] Simulation results reveal that samples with one-side oxidized structures (Pyr-2CO, Pyr-2OH, and Pyr-2OMe) exhibit enhanced dipole moments and asymmetric charge distribution on the oxygen-containing functional groups (**Figure 3e**). Among them, Pyr-2OMe displays the highest charge density on the oxygen-containing functional groups, which is more conducive to adsorbing oxygen intermediates and catalyzing two-electron ORR.

The electron interaction between reaction intermediates on organic molecule electrocatalysts and reactant substrate also plays a pivotal role in determining the overall electrocatalytic efficiency. Hoque et al. employed manganese-tetraphenylporphyrin (Mn(TPP)) as bifunctional oxygen electrocatalysts at both electrodes in a electrochemical cell to produce manganese-oxo further producing two equivalents of sulfoxide with a single equivalent of dioxygen without electron consumption (**Figure 3f**).^[35] The cathodic ORR accompanied by monooxygenase reaction and anodic OER accompanied by dehydrogenase reaction are both highly active (**Figure 3g**), which can be attributed to the electron interaction between the adsorbed oxygen species on Mn(TPP) and applied substrates. This results in $\approx 200\%$ Faradic efficiencies of the system for oxidation of various types of organic molecules. Another approach involves applying small organic molecules to an electrocatalytic active substrate to optimize its electronic structure and achieve higher activity. Wang et al. have employed a submonolayer p-aminothiophenol (PATP) molecule on the surface of Pt nanoparticles (PtNPs) to enhance their HER catalytic activity (**Figure 3h**).^[36] The amino group can act as an electron acceptor to extract electrons from the PtNP substrate, thereby reducing the charge density on the surface of PtNPs and facilitating the adsorption/desorption of the reaction intermediate (**Figure 3i**). Moreover, DFT simulations have confirmed that due to the formation of electron donor/acceptor pairs with charge redistribution effect, the absorption of PATP can effectively change the electron distribution of PtNPs substrate, thus thereby lowering the reaction energy barrier for HER (**Figure 3j**).

In short, small organic molecule electrocatalysts, with their tunable molecular structure and surface properties possess many advantages including monodispersity, batch-to-batch reproducibility, clear molecular construction, etc. Apart from that, small organic molecules can be doped with heteroatoms or decorated on other electroactive substrates to further boost the overall electrocatalytic activity. Consequently, studies focusing on the electrocatalytic activity of small organic molecules are highly significant for the rational design of cost-effective organic electrocatalysts.

2.2. Oligomers

Compared with polymers and frameworks, oligomers usually possess a significantly lower molecular weight ($\approx 10\,000$) and more terminal residual functional groups.^[37] With fewer repeating well-defined units, they can be considered as segments

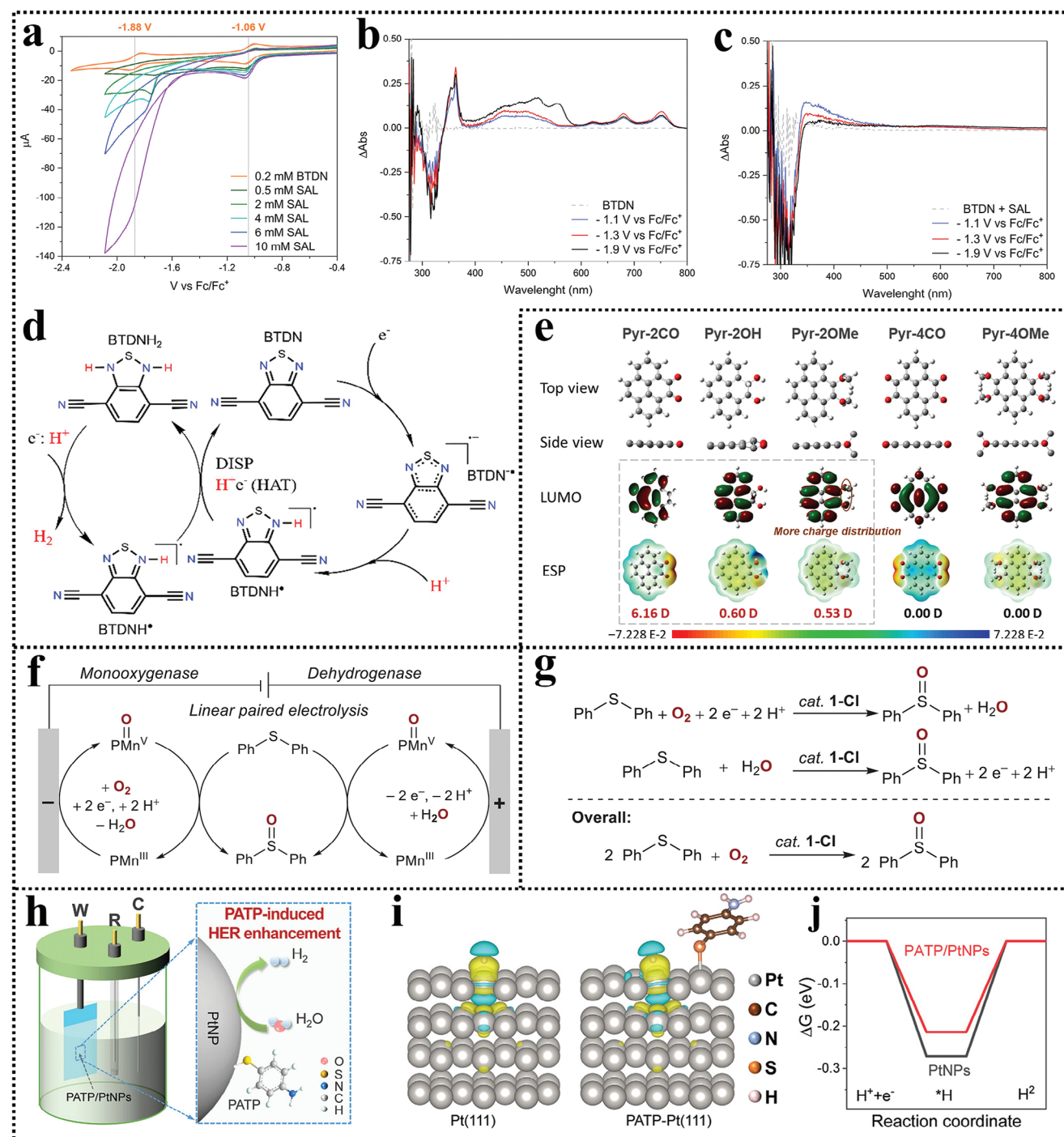


Figure 3. a) CV curves of BTDN with/without SAL. b,c) In situ UV-vis spectra of BTDN with/without SAL. d) Inferred reaction mechanism for hydrogen evolution of BTDN. Reproduced with permission.^[29c] Copyright 2021, American Chemical Society. e) Simulated molecular configuration, charge distribution, and electrostatic potential of pyrene-based small organic molecules. Reproduced with permission.^[34] Copyright 2022, Elsevier. f) Figure illustration and g) corresponding chemical equation of electrochemical oxygen reductive activation and H₂O oxidative activation of H₂O for Ph₂S oxygenation. Reproduced with permission.^[35] Copyright 2024, Science. h) Illustration of combining PATP with PtNP for boosting HER. i) Charge distributions and j) free energy diagram of PtNPs and PATP combined PtNPs. Reproduced with permission.^[36] Copyright 2023, Wiley-VCH.

of polymers/frameworks, which can expose more active sites to achieve much higher catalytic activity. Furthermore, with a lower molecular weight, tuning molecular energy level structures and specific functional groups on oligomers becomes much simpler.^[38] By introducing a surfactant in the synthesis, a series kind of covalent reticular oligomers (CROs) have been obtained. These oligomers exhibit much better HER and OER catalytic activity compared with their organic framework counterparts when assembled with Ru and biomimetic poly(3,4-ethylenedioxythiophene) (PEDOT).^[39] The X-ray diffraction (XRD) patterns indicate that these oligomers possess high crystallinity, and the FTIR spectra indicate the existence of C=N bonds in their skeletons (Figure 4a,b), both of which are constant with their organic framework counterparts. The estimated size of the CRO structure, based on Chem-draw software, is 8–12 nm (Figure 4c). Due to the presence of numerous terminal residual functional groups, all CROs possess a much higher hydrophilic feature with nearly zero contact angle compared with their organic framework counterparts, suggesting much-facilitated mass transfer of these CROs during electrocatalytic reaction. The UV-vis spectra of various kinds of CROs and organic frameworks show that CROs exhibit much narrower bandgaps compared with their organic framework counterparts (Figure 4d–f), suggesting better conductivity. Hence, it can be concluded that CROs possess both accelerated mass transfer and better conductivity, explaining their better electrocatalytic activity.

In addition, surface functional groups can significantly enhance the electrocatalytic activity of an oligomer by directly serving as active sites. Wang et al. have used a novel kind of p-phenylenediamine oligomer (pPO) with superior ORR/OER catalytic activity to mediate the change potential of Li–O₂ battery.^[40] Due to the presence of a special benzoquinone group on the link of pPO, during discharging (ORR), pPO was reduced and transferred into pPO with extra oxygen-containing functional groups (pPO_O). On the contrary, during charging (OER), pPO was oxidized to pPO with extra nitrogen-containing functional groups (pPO_N) (Figure 4g). The Li–O₂ battery with pPO cathodic electrocatalyst exhibits three pairs of redox peaks in the CV curve, indicating that the benzoquinone groups on the link of pPO provide massive active sites for both ORR and OER (inset of Figure 4g). The in situ UV-vis spectra manifest peaks at 318 (π–π stacking) and 541 nm (benzene ring) that intensify/weaken with the discharging/charging process, indicating the combination/separation of lithium and pPO (Figure 4h). Furthermore, the in situ XRD pattern shows that both peaks at ≈32° and 35° intensify during discharging and weaken during charging (Figure 4i), again confirming the reversible formation and decomposition of the discharge product on pPO electrocatalysts in Li–O₂ battery.

In a word, although oligomers possess lower molecular weight, they can still retain high crystallinity and specific functional groups on their skeletons. This inherent advantage of oligomers provides great convenience for in-depth study of electrocatalytic mechanisms at the molecular or atomic level. Additionally, tuning the molecular weight of oligomers can modulate the exposure of active sites. Furthermore, numerous terminal residual functional groups in oligomers can not only boost the hydrophilicity to facilitate the mass transfer but also optimize the electronic structure through forming electron donor–acceptor pairs with backbones to accelerate the electron transfer. This suggests

that oligomers have great potential to be developed as highly efficient low-cost organic electrocatalysts.

2.3. Polymers

Polymers, characterized by high thermal stability, low solubility in aqueous solution, and tunable structures, are also considered as a type of desired organic electrocatalysts.^[41] However, most polymers possess limited electrocatalytic activity due to the low degree of conjugation. Strategies for the rational design of efficient organic polymer electrocatalysts usually focus on altering the conjugated molecular structure on their skeleton, such as introducing heteroatom and tuning the degree of conjugation. These modifications further optimize the electronic structure, band structure, and energy barrier for electrocatalytic reaction.^[42] Li et al. have discovered that the number of phenyl rings with conjugated π-bonds on the skeleton of covalent organic polymer (COP) plays a crucial role in determining its ORR catalytic activity.^[43] The addition of phenyl rings to the skeleton of COP decreases the charge density on the COP global support (Figure 5a,b), which is beneficial for adsorbing negatively charged ORR reaction intermediates onto COP. Apart from that, the electron fluidity increases with the addition of phenyl rings, suggesting improved charge transfer ability, which is also confirmed by the density of state (DOS) simulation (Figure 5c–f). The simulated bandgap narrows with the addition of phenyl rings, confirming better charge transfer of COP with more phenyl rings. Additionally, functional groups linked to the skeleton of COP can also be utilized as active species and play a key role in enhancing the electrocatalytic activity of COP. Through the polymerization with triformyl phloroglucinol (Tp), the specific porphyrin structure in 5, 10, 15, 20-tetra(4-aminophenyl)–21H,23H-porphyrin (PAM) can be inherited into the obtained COP (denoted as TpPAM, Figure 5g).^[44] The HER progress of TpPAM is illustrated in Figure 5h, and the volcano plot manifests that the position of TpPAM is much closer to the volcano peak compared with other metal electrocatalyst counterparts (Figure 5i), suggesting the porphyrin structure in COP TpPAM can serve as a highly efficient active site for HER.

Moreover, similar to oligomers, the relatively low conductivity of COP also limits their catalytic performance. Integrating with graphitic carbon conductive enhancers (such as CNT, carbon black, etc.) is a promising approach to address this issue. The unique synergy effect between graphitic carbon conductive enhancer and COP is responsible for the high electrocatalytic activity. Guo et al. have synthesized a COP/reduced graphene oxide (rGO) hybrid through a one-step self-assembly strategy (Figure 5j).^[41a] Simulating the charge transfer between COP and single-layer/ multilayer graphene reveals that for both models, the charge transfer between COP and graphene is neglectable, substantiating that integrating with rGO can hardly modulate the electronic structure (Figure 5k,l). The only way for rGO to benefit the catalytic activity of COP is to enhance the conductivity as well as facilitate the electron transfer from the current collector to active sites on COP. As a consequence, the synergy effect of the COP/rGO can be illustrated as follows: the rGO serves as a highly efficient electron pathway and the COP provides efficient active sites, thereby endowing the hybrid with boosted ORR efficiency.

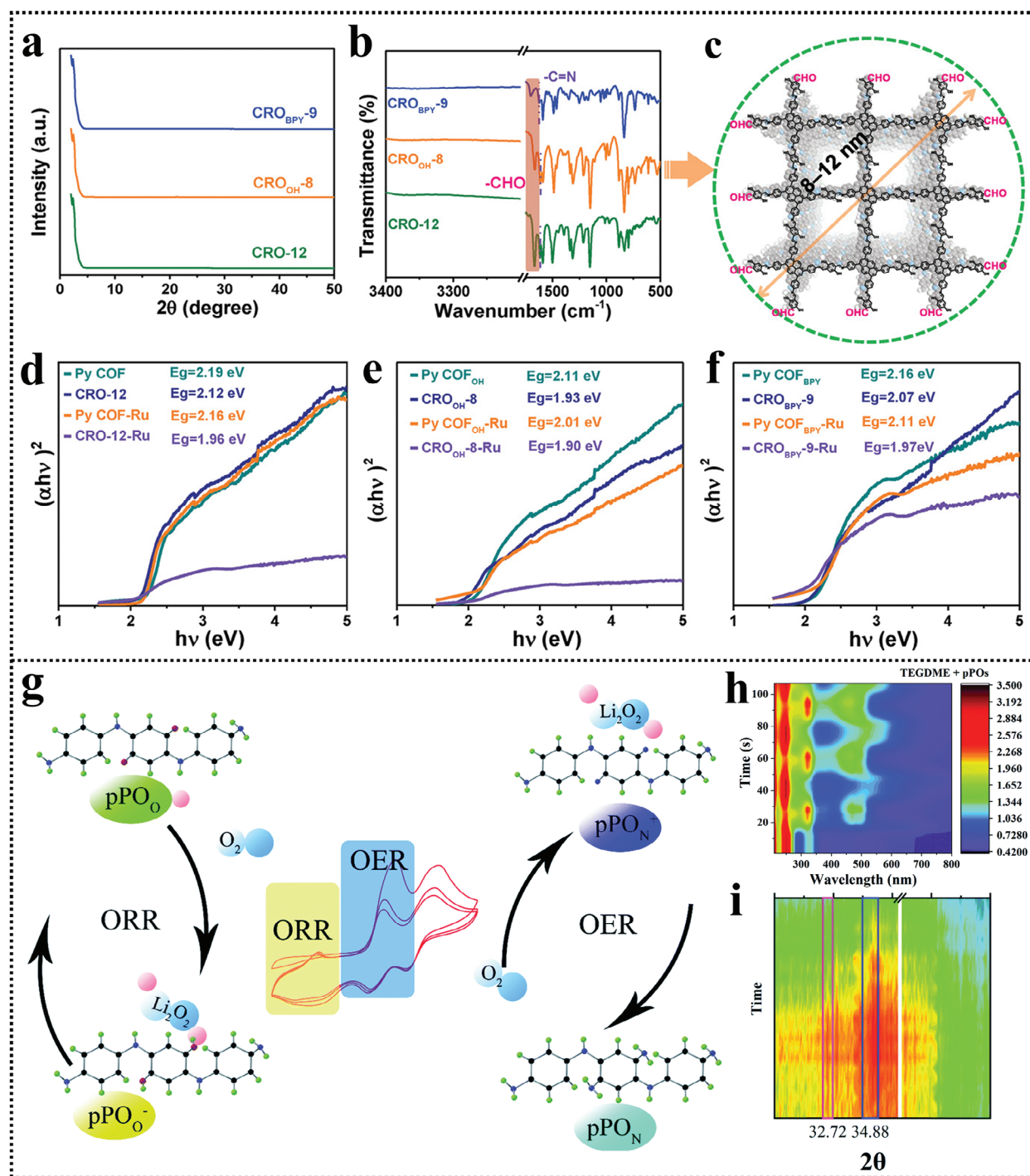


Figure 4. a) XRD patterns and b) FTIR spectra of CROs. c) Estimated size of CRO. d–f) Bandgap calculation of various CROs and their organic framework counterparts.^[39] Reproduced with permission. Copyright 2023, Wiley-VCH. g) Schematic illustration of ORR and OER processes on pPO during charging–discharging in a Li–air battery. h) In situ UV–vis spectra and i) in situ XRD pattern of battery with pPO. Reproduced with permission.^[40] Copyright 2020, RSC.

Generally speaking, compared with oligomers, polymers possess a higher degree of polymerization and low crystallinity. The exhibited electrocatalytic activity of polymer is mainly determined by the properties of its skeleton, such as charge distribution on the global support, degree of conjugation, and ac-

tive species such as linked functional groups and metal centers. Apart from that, combining polymers with conductive enhancers can better reveal the electrocatalytic activity of polymer electrocatalysts by accelerating the transportation of electrons to active sites.

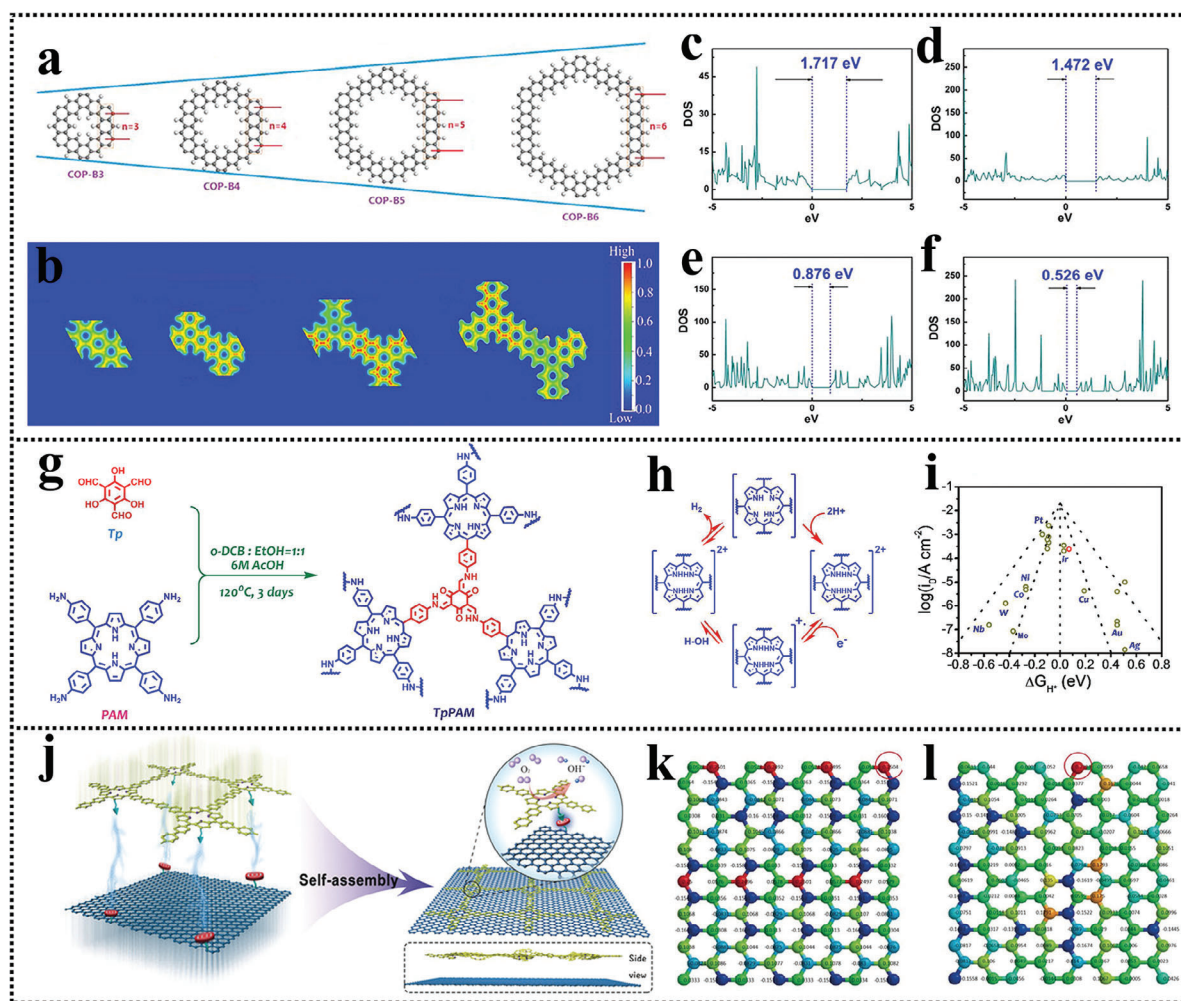


Figure 5. a,b) Molecular structures with charge distributions of different sizes of COPs. c–f) Calculated DOS plots of different sizes of COPs. Reproduced with permission.^[43] Copyright 2019, Frontiers. g) Synthesis of TpPAM. h) Inferred HER mechanism on TpPAM. i) Volcano plot for TpPAM and other transition-metal electrocatalysts. Reproduced with permission.^[44] Copyright 2017, American Chemical Society. j) Illustration of the self-assembly strategy to obtain COP/rGO hybrid. Charge distributions on k) pure graphene layer and l) COP–graphene hybrid. Reproduced with permission.^[41a] Copyright 2018, Wiley-VCH.

2.4. Organic Frameworks

Organic frameworks can be categorized into two types: metal organic frameworks (MOFs) and covalent organic frameworks (COFs). MOFs are usually obtained through forming chemical bonds between inorganic and organic building blocks,^[45] while COFs, which bear similarities to polymers, are usually obtained through condensation reactions, and various units on COFs are also connected through covalent bonds.^[46] Both MOFs and COFs exhibit high crystallinity with distinct lattice fringes, markedly different from other organic polymers.^[47] Additionally, organic frameworks are more long-range ordered, and the chemical bonds connecting these high-crystallized organic frameworks are more robust and less reversible, contributing to their chemical stability.^[48] Another distinction between organic frameworks and polymers is that organic frameworks can be synthesized by different combinations of building blocks, whereas polymers are formed by relatively sin-

gular chemical bonding starting from one or more monomers. This leads to the fact that organic frameworks tend to exhibit much higher porosity and specific surface area than polymers. These unique properties of organic frameworks suggest that they are favorable for electrocatalytic applications. The ordered and controllable structure can provide a clear configuration of active sites which is convenient for illustrating the origin of the activity from DFT simulations, the high porosity can expose more active sites in the electrolyte, thus facilitating the reaction kinetics, and the superior chemical stability can ensure them remain stable under different electrolytes/potentials.^[49] All these advantages of organic frameworks suggest that organic frameworks can be used as desirable low-cost organic electrocatalysts for substituting commercial noble-metal benchmarks.

Atoms around the metal centers of MOF can normally be utilized as highly efficient active sites for electrocatalytic reactions. Therefore, the coordination environment of the ligands plays

a key role in determining the electrocatalytic activity of MOF, and this can be efficaciously regulated by tuning the structure of the coordinated organic ligands. Cheng et al. partially replaced the carboxyl ligand with thiol ligand into the skeleton of Ni-benzenedicarboxylic acid (BDC)-based MOF to regulate the coordination environment of the Ni metal site thereby boosting the HER activity.^[50] The S K-edge spectra of S-NiBDC manifest the existence of S–Ni bond in S-NiBDC (Figure 6a), and Fourier transform-extended X-ray absorption fine structure (EXAFS) fitting of the Ni K-edge EXAFS spectra further confirms the configuration of the metal site in S-NiBDC is Ni–O₅S₁ (Figure 6b), which is similar to that of the Fe–S core in [FeFe]-hydrogenase (Figure 6c). Moreover, through DFT simulation, it can be observed that the introduction of S in NiBDC MOF can shift the *p*-d-band center (ϵ_p) closer to the Fermi level, leading to improved HER activity (Figure 6d). Besides, after introducing thiol ligand in the skeleton of NiBDC, the valence of Ni is enhanced because the electron-withdrawing –SH group can extract more electrons from the metal center compared with the –COOH group. This results in the presence of electron-rich S group on the organic part of S-NiBDC with an optimized coordination environment that can generate S–H* intermediate for facilitating the Heyrovsky step during HER, but also the strengthening of Ni–O bonds for anchoring the Ni metal center and retaining the MOF structure beneficial for the enhancement of electrocatalytic stability when used as electrocatalysts. The in situ Raman spectra of NiBDC and S-NiBDC at –0.3 V versus RHE show that the signal intensity of MOF structure decreases finitely for S-NiBDC while rapidly for NiBDC over time, proving the enhanced stability of S-NiBDC attributed to the optimization of coordination environment (Figure 6e,f).

Moreover, the structure of the ligand itself is also a crucial factor affecting the electronic structure of metal centers and the overall electrocatalytic activity of MOFs. The chosen ligand typically possesses advanced physicochemical properties such as appropriate degree of π -conjugation, redox-activity, connectivity, and hydrophilicity/hydrophobicity. These properties are advantageous for constructing highly efficient active sites with boosted charge/mass transfer.^[51] However, due to the limited conductivity of these organic ligands, the exploration of electrocatalytic applications of MOFs primarily focuses on OER and HER.^[52]

Carboxylic acid ligands including terephthalic acid,^[14b,53] hexacarboxylic acid,^[54] triphenylenedicarboxylate acid,^[55] iophenedicarboxylate acid,^[56] etc., are commonly adopted for synthesizing MOF-based electrocatalysts for efficient oxygen evolution. These ligands, with their electron-rich functional groups, are beneficial for increasing the charge density and modifying the coordination environment of the adjacent metal site.^[57] As reported by Liu's group,^[58] the introduction of various types of electron-donating/electron-withdrawing monocarboxylate ligands into the skeleton of Ni-BDC MOF significantly influences its exhibited OER electrocatalytic activity (Figure 6g). The Ni 2p XPS spectra in Figure 6h reveal that the peak position shifts negatively after introducing electronic-rich ligands (4-aminobenzoic acid and ferrocenedicarboxylic acid) and shifts positively after introducing electron-deficient ligands (4-nitrobenzoic acid). This shift occurs because electron-rich ligands can donate electrons to the metal Ni site in Ni-BDC while electron-

deficient ligands extract electrons from it. Since the DFT simulation result proves that active sites are not on ferrocene derivatives, the OER performances of various kinds of MOFs are mainly determined by the charge density and intrinsic activity of Ni sites. The linear sweep voltammetry (LSV) curves suggest that electronic-rich ligands are more favorable for improving the OER activity due to their electron-donating property (Figure 6i).

Conversely, ligands with electron-deficient conjugated structures such as pyridine,^[59] tetramine,^[60] dithiolene,^[61] aminothiol,^[62] etc., are highly favored for coordinating metal atoms, thereby exposing their unoccupied positions to benefit the hydrogen evolution process. After coordinating with metal atoms, these ligands can extract electrons from them and elevate their degree of unsaturation, which is extremely beneficial for electrocatalytic reactions that consume electrons, such as HER. In the work conducted by Huang et al., the advantages of electron-deficient ligands toward HER have been studied.^[60] In the hexaiminohexaazatrinaphthalene (HAHATN), the electron-deficient bidentate tertamine can coordinate with Ni ion to form a two-coordinated Ni–N₂ moiety with a high degree of unsaturation. Simultaneously, the electron-rich ortho-amine at the edge can coordinate with Ni to construct Ni–N₄ moiety with a low degree of unsaturation, thus forming the polymerized Ni₃(Ni₃•HAHATN)₂ MOF (Figure 6j). The Ni₃(Ni₃•HAHATN)₂ MOF displayed a much higher HER activity than the Ni₃(HITP)₂ MOF with only Ni–N₄ moieties (Figure 6k). The simulated bond length of the N–H bond after adsorbing a H* on the Ni–N₂ site is also shorter than that after adsorbing a H* on the Ni–N₄ site, suggesting that Ni–N₂ moieties possess better H* adsorbing ability. Moreover, the partial density of states (PDOSs) manifest that the d-orbit of the Ni atom in the Ni–N₂ site is also closer to the Fermi level compared with that in the Ni–N₄ site, further proving the superior H* bonding capacity of Ni–N₂ site.

As discussed earlier, the ligand structure can significantly influence the electronic properties and the intrinsic electrocatalytic activity of the MOF metal sites. Electron-donating ligands can transfer electrons to the adjacent metal site, thereby increasing its charge density. This increase is advantageous for activating electrocatalytic oxidation reactions such as OER on the metal site. On the contrary, electron-withdrawing ligands can extract electrons from the adjacent metal site, leading to charge depletion. The resulting metal atom, characterized by low charge density and a high degree of unsaturation, emerges as a promising active site for electrocatalytic reactions that consume electrons, including the ORR and HER.^[2d] By choosing suitable ligands, it is possible to optimize the charge distribution on the MOF metal site successfully, thereby achieving high activity for various electrocatalytic reactions.

Similar to MOF electrocatalysts, identifying the active site and deciphering its electronic structure are also important for illustrating the origin of electrocatalytic activities of COF electrocatalysts.^[63] The overall catalytic activity of COF electrocatalyst is usually determined not only by the configuration and local coordination environment of active sites but also by the charge transfer ability of the organic global support.^[24a,64] Yan et al. have utilized the special property of unsaturated bonds (UBs) in COF to design them as highly efficient electrocatalytic

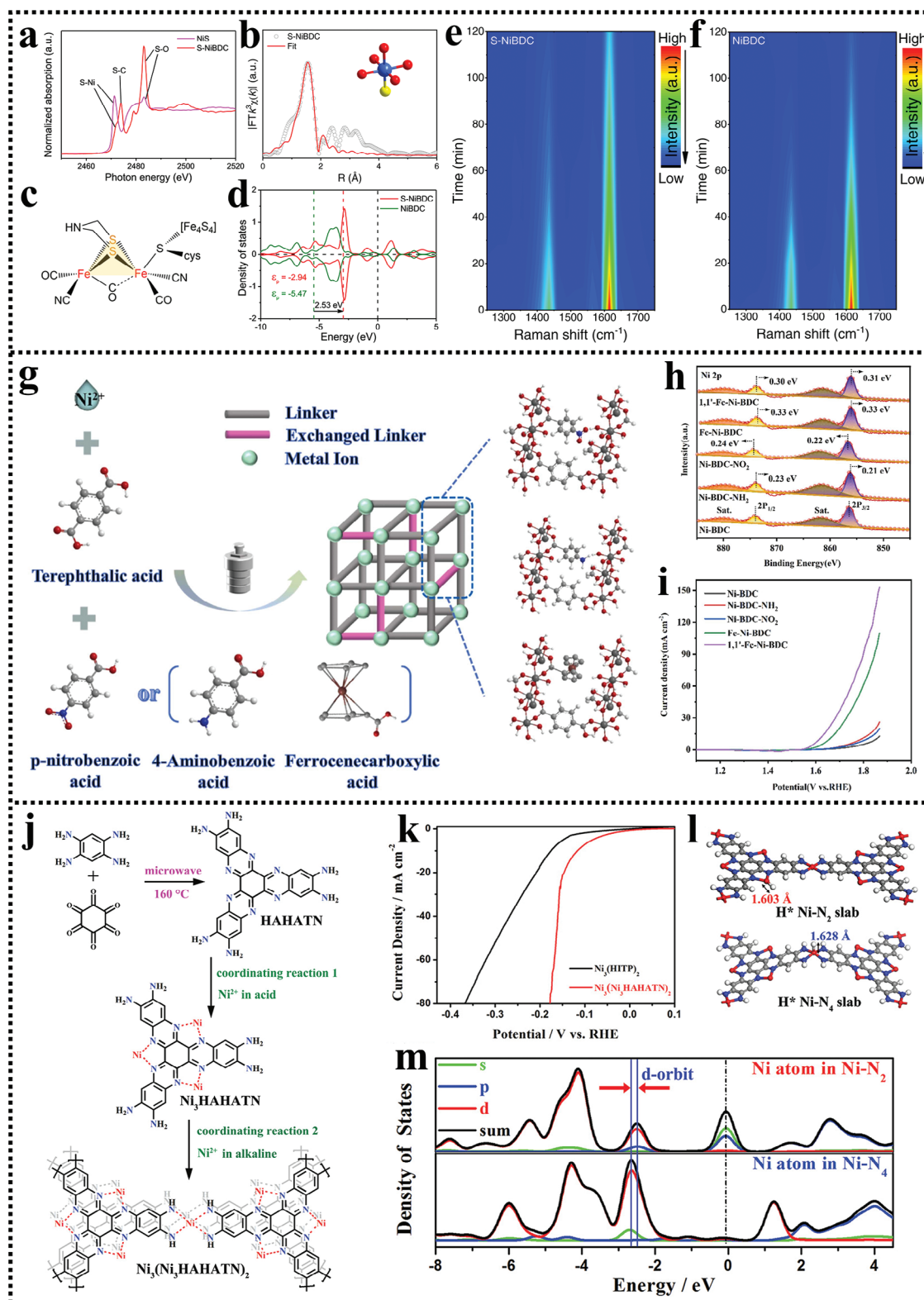


Figure 6. a) S K-edge spectra and b) EXAFS fitting of S-NiBDC. c) Structure of [FeFe]-hydrogenase with Fe-S core. d) Simulated PDOS of NiBDC and S-NiBDC. e, f) In situ Raman contour plots of NiBDC and S-NiBDC. Reproduced with permission.^[50] Copyright 2022, Nature. g) Syntheses of Ni-BDC MOFs with different kinds of doped ligands. h) XPS spectra and i) LSV curves of Ni-BDC MOFs. Reproduced with permission.^[58] Copyright 2023, Elsevier. j) Synthesis of $\text{Ni}_3(\text{Ni}_3\bullet\text{HAHATN})_2$ MOF. k) LSV curves of $\text{Ni}_3(\text{Ni}_3\bullet\text{HAHATN})_2$ and $\text{Ni}_3(\text{HITP})_2$ MOFs. l) Configurations of $\text{Ni}_3(\text{Ni}_3\bullet\text{HAHATN})_2$ with H^* adsorption on $\text{Ni}-\text{N}_2$ and $\text{Ni}-\text{N}_4$ sites. m) PDOSs of Ni atom in $\text{Ni}-\text{N}_2$ and $\text{Ni}-\text{N}_4$ of $\text{Ni}_3(\text{Ni}_3\bullet\text{HAHATN})_2$ slab. Reproduced with permission.^[60] Copyright 2020, Wiley-VCH.

active sites for ORR.^[29f] These UBs, with parallel directions can not only expand the inner space but also increase the electron cloud overlap of COF, resulting in facilitated mass transfer and optimized electronic structure. It is worth noteworthy that the UBs are electron-withdrawing groups, which can serve as highly efficient active sites for adsorbing oxygen intermediates.^[65] To obtain better electrocatalytic activity, the electronic structure of UBs should be precisely fixed. By inserting C=C and N=N bonds into the skeleton of COF (**Figure 7a**), the charge density of the adjacent carbon atoms can be modulated (**Figure 7b**). The electron localization and Fukui functions of these COFs indicate that charge is only distributed to the adjacent C=N bond (**Figure 7c**), suggesting the C=N bonds in these COFs are the active sites for ORR. The introduction of C=C and N=N can also affect the charge distribution on the C=N bond at the linkage, implying that the introduction of UBs can effectively tune the oxygen intermediate adsorption ability of the C=N bond. This inference is also confirmed with in situ Raman spectra. For COF with N=N bonds (Azo-COF), the characteristic peak of C=N...OOH (1603 cm⁻¹) appears with the negative shift of external potential, while the other two COFs remain nearly unchanged regardless of the external potential in the Raman spectra (**Figure 7d,e**). This phenomenon suggests that the insertion of N=N in the COF skeleton can optimize the electronic structure of the adjacent C=N bonds further activating them to modulate the adsorption of oxygen intermediates to obtain a lower ORR energy barrier. In addition, an insightful and quantitative description of charge distribution on the global support of COF is conducive to analyzing its charge distribution and donor-acceptor property. The dipole moment can be used to quantify the symmetry and intermolecular charge polarity of the COF monomer, and the electrostatic potential (ESP) can confirm the charge distribution on that,^[14a] both of which are instrumental to deciding whether the choice of specific monomer is appropriate for constructing highly efficient active sites in COF with suitable charge density. Huang et al. have used these two parameters to select favorable building blocks for efficient two-electron ORR.^[66] The results demonstrate that the usage of electron-rich N-containing monomers (revealed by ESP) with a high dipole moment can enhance the interunit charge density difference in the skeleton of COF further increasing the charge density on the adjacent thiophene-S active sites with electron acceptor properties for achieving lower ORR energy barrier. This work greatly highlights the benefit of the quantitative description of charge distribution for selecting appropriate monomers to synthesize efficient COF electrocatalysts.

Heterocyclic COFs can also serve as highly efficient electrocatalysts because active species linked to the building block of COF can serve as active sites for catalyzing electrocatalytic reactions.^[67] These active species include functional groups and atomic metal centers, both of which are favorable for adsorbing reaction intermediates. You et al. prepared a series of meal-free carbon-based COFs for ORR.^[14a] Through introducing methyl group (MG) in COF, the ortho carbon (site 5) can be activated, therefore creating more active sites for ORR (**Figure 7f**). This activation of the ortho carbon stems from the optimized electronic structure. As shown in **Figure 7g**, the simulated bandgap of the COF can be effectively narrowed through bounded MG decoration, indicating enhanced charge transfer for ORR. Besides that,

the Gibbs energy diagram in **Figure 7h** confirms the reduced ORR energy barrier of the bounded MG decorated COF. Beyond that, the facilitated ORR with a reduced energy barrier of rate-determining step (O₂ to OOH*) is further confirmed through theoretical/in situ Raman analysis (**Figure 7i,j**). The theoretical Raman spectra manifest the position of OOH...C=C and O₂...C=C characteristic peaks, and the in situ Raman spectra display the presence and strength of similar peaks, suggesting the boosted ORR kinetic of bounded MG decorated COF. Similarly, atomic metal centers with a high degree of unsaturation are also considered as efficient active sites for boosting the electrocatalytic activity of COF. In the research conducted by Li et al.,^[68] two kinds of nitrogen-coordinated atomic cobalt active sites (Co-N₄ and Co-N₂) have been created in a novel fully conjugated COF (denoted as Co-PorBpy-Co) for boosting the ORR activity. When the oxygen intermediate is absorbed on these two kinds of Co sites, the Co-O bond length of Co-N₄ is longer than that of Co-N₂, indicating Co-N₂ is more favorable for adsorbing and dissociation of oxygen (**Figure 7k**). Beyond that, the Co-N₂ active site exhibits not only lower free energies of all ORR steps but also lower calculated limiting ORR energy barrier compared to those of Co-N₄ (**Figure 7l,m**), suggesting its higher ORR activity.

In general, modular structures of organic frameworks enable them to incorporate definite building blocks with active species, which is advantageous for the rational design of effective organic electrocatalysts. The origin of the electrocatalytic activity of organic framework should also be clarified. The degree of conjugation, charge distribution of global support, and integrated conductive enhancer all play important roles in controlling charge transfer and reaction rate in electrocatalytic processes. More importantly, the type and configuration of active species should also be discerned. For MOF electrocatalysts, their catalytic activities are mainly controlled by the coordination environment and electronic structure of the confirmed metal centers. While for COF electrocatalysts, their catalytic activities are determined by the content of active species such as functional groups, nonmetallic heteroatoms, and atomic metal centers linked/coordinated on their skeletons. Both of these organic frameworks can be directionally and precisely designed by selecting appropriate building blocks with favorable active species for efficiently catalyzing electrocatalytic reactions.

In conclusion, the physicochemical properties that determine the electrocatalytic performance vary among different types of organic electrocatalysts. The electrocatalytic activity of small organic molecule-based electrocatalysts is mainly influenced by the molecular structure, heteroatom/dopant, and the catalytic activity of the integrated substrate. For oligomers, the electrocatalytic performance is determined by two factors: the molecular weight and the decorated functional groups. In the case of polymers and organic frameworks, their activity-controlled properties are consistent due to their similar high degree of polymerization. The major four factors are the degree of conjugation, the added conductive enhancer, the active species, and the global support structure. By categorizing and organizing these factors of different organic electrocatalysts, the optimization of their performance becomes more systematic and guided.

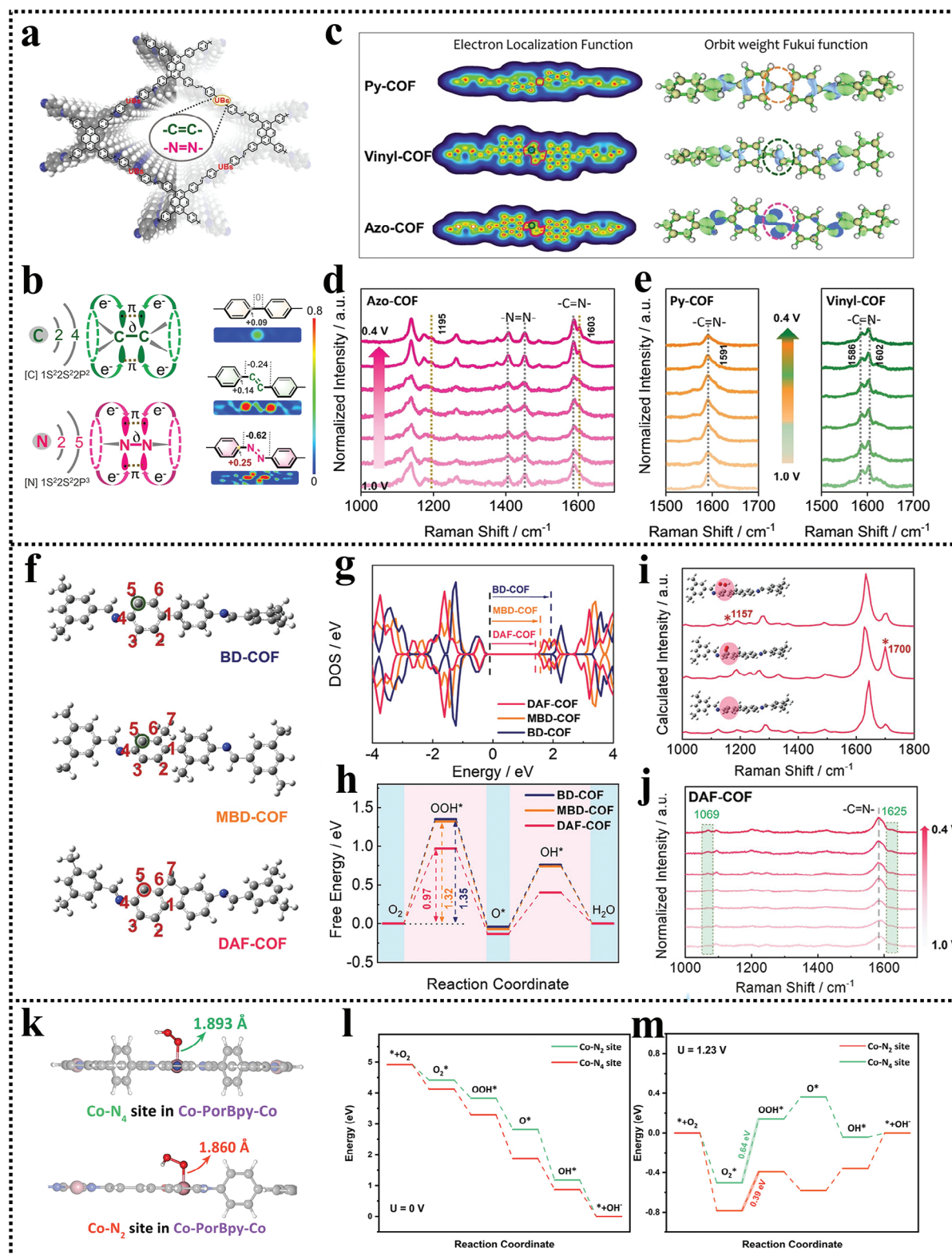


Figure 7. a) Structure of COF with UBS. b) Electronic structure of C=C and N=N bonds and charge distributions of building blocks with/without C=C/N=N bonds. c) Electron localization and Fukui functions of COFs with/without C=C/N=N bonds. d,e) In situ Raman spectra of these COFs. Reproduced with permission.^[29f] Copyright 2022, Wiley-VCH. f) Structures of COFs with/without bounded MG decoration. g) Calculated DOS and h) ORR energy barriers of these COFs. i) Simulated and j) in situ measured Raman spectra of COF with bounded MG decoration. Reproduced with permission.^[14a] Copyright 2023, Wiley-VCH. k) Structure configurations of Co-N₄ and Co-N₂ active sites adsorbed with oxygen intermediate in Co-PorBpy-Co. l,m) Free energy diagrams of Co-N₄ and Co-N₂ active sites at the external potential of 0 and 1.23 V. Reproduced with permission.^[68] Copyright 2023, Wiley-VCH.

3. Structure–Activity Relationships of Organic Electrocatalysts

More importantly, linking the structural/physicochemical properties with the electrocatalytic activity of these organic electrocatalysts is critical for explaining the electrocatalytic mechanism and further searching for relevant regular patterns for designing organic electrocatalysts with promising catalytic performances.^[69] Therefore, raising illustrative indicators/descriptors of electrocatalytic activities based on structural/physicochemical properties of organic electrocatalysts summarized in the previous section is crucial for constructing accurate structure–activity relationships. Moreover, optimized simulation methods are highly preferred for discerning these indicators/descriptors. For example, directly combining the explicit solvation with the system can more precisely determine the rate-limiting step to judge whether the reaction on the electrocatalyst is limited by mass transfer or charge transfer, and calculating the energy barrier at the catalyst–electrolyte interface is more in line with the actual situation of electrocatalysts during use.^[70]

For electrocatalytic reactions, the overall electrocatalytic activity is directly determined by four key electrocatalytic characteristics including the number of active sites, mass transfer, charge transfer, and intrinsic activity.^[1a,71] The first two characteristics are more related to the morphological structure, and the latter two characteristics are more related to the electronic structure of electrocatalysts. The effect of these characteristics on the electrocatalytic performance is illustrated in **Figure 8**. Through morphological structure modulation (such as specific surface area, crystallinity, channel structure, etc.), not only the concentration of active species and the electrochemical specific surface area (ECSA) can be tuned resulting in the change of the number of exposed active sites, but also the gas/reactant diffusion rate further the mass transfer can also be effectively affected.^[60,72] As for electronic structure modulation, not only the conductivity and charge transfer during electrocatalytic reactions but also the electronic structure on the potential active sites can significantly affect their adsorption/desorption energies of reaction intermediates further intrinsic activity (examined by turnover frequency, current density based on ECSA, etc.) can also be successfully modulated.^[73] Hence, it is important to correlate the structural/physicochemical properties of organic electrocatalysts with those four characteristics determining the electrocatalytic performance discussed above for providing instructions for designing cost-effective organic electrocatalysts with promising electrocatalytic performance.

For organic electrocatalysts, their most representative structural and physicochemical properties can be considered as “indicators” or “descriptors” for constructing appropriate structural–activity relationships with their measured electrocatalytic activities. By optimizing different electrochemical characteristics, each indicator or descriptor can be categorized, which is beneficial for clarifying details for the activity improvement of organic electrocatalysts further bridging the activity and structural/physicochemical properties. Strategies focusing on tuning these structural/physicochemical properties of organic electrocatalysts for achieving better electrocatalytic performance through optimizing different kinds of specific electrocatalytic characteristics will be detailed in the following sections.

3.1. Number of Active Sites

In organic electrocatalysts, the most widely used strategy to improve the number of active sites during electrocatalytic reactions is to increase the area of the three-phase interface to expose more active sites.^[74] Notably, in organic compounds, the π – π electron interaction that is closely related to the number of exposed active sites should be particularly concerned since a strong π – π stacking effect may contribute to the agglomeration and therefore decrease the number of active sites. **Figure 9a** shows an example of increasing the number of available active sites of organic electrocatalysts through morphology engineering.^[75] Two kinds of metal-free COF with quasi-3D (Q-3D) structures, namely, JUC-610 and JUC-611, have been synthesized through the solvothermal method. Due to the weak interlayered π – π electron interaction of the Q-3D COF, it can be easily exfoliated into nanosheets. The exfoliated JUC-610 is denoted as JUC-610-CON, which enlarges the area of the reaction zone (usually the three-phase interface and quantified by ECSA). The LSV curves show that the onset potentials of JUC-610 and JUC-610-CON are very close (**Figure 9b**). This is because the types of active sites and their ORR thermodynamic electrocatalytic efficiency in these two samples are equivalent. Whereas, the Tafel slope of JUC-610-CON is lower than that of JUC-610 (**Figure 9c**), suggesting the facilitated reaction kinetic, which is attributed to the exposure of more active sites (identified by the highest ECSA of JUC-610-CON in **Figure 9d**). Moreover, controlling the conjugation degree of the organic electrocatalysts is also beneficial to the full exposure of active sites. Wang et al. discovered that after introducing unconjugated quaternary ammonium groups on the skeleton of COF,^[76] the agglomeration caused by strong π – π electron interaction is inhibited and more active sites can be exposed in the electrolyte for catalyzing OER, leading to a more than fourfold increase in ECSA.

Apart from that, intentionally tuning the morphological structure of organic electrocatalysts by introducing conductive substrates for better dispersing active sites to prevent agglomeration between them is also favored. Liu et al. utilized carbon nanotubes (CNTs) as substrate and in situ decorated thienothiophenepyrrene COF on them (**Figure 9e**).^[77] By varying the mass ratios of added CNTs to the COF precursor, they obtained a 1D van der Waals heterostructural composite, CC-X, exhibiting a core–shell structure. As shown in the TEM image of CC-3, CNT, and COF serve as core and shell, respectively (**Figure 9f**). The thickness of the COF shell determines the overall specific surface area of the composite, further affecting the ECSA. The composite with a lower mass ratio of added CNTs to the COF precursor possesses the larger ECSA (**Figure 9g**) and ORR electrocatalytic activity. A similar phenomenon is also observed in polymer-based electrocatalysts.^[78] Due to the intrinsic properties of polymers with more functional groups, they can provide numerous easily accessible active sites, facilitating the kinetics of the electrocatalytic reaction.

In most cases, strategies for increasing the number of active sites often function in multiple ways simultaneously. In organic electrocatalysts, many strategies for introducing more active species in the original material may also optimize the morphological structure for achieving a larger ECSA and more exposed active sites. In the work conducted by Li et al.,^[67] different alde-

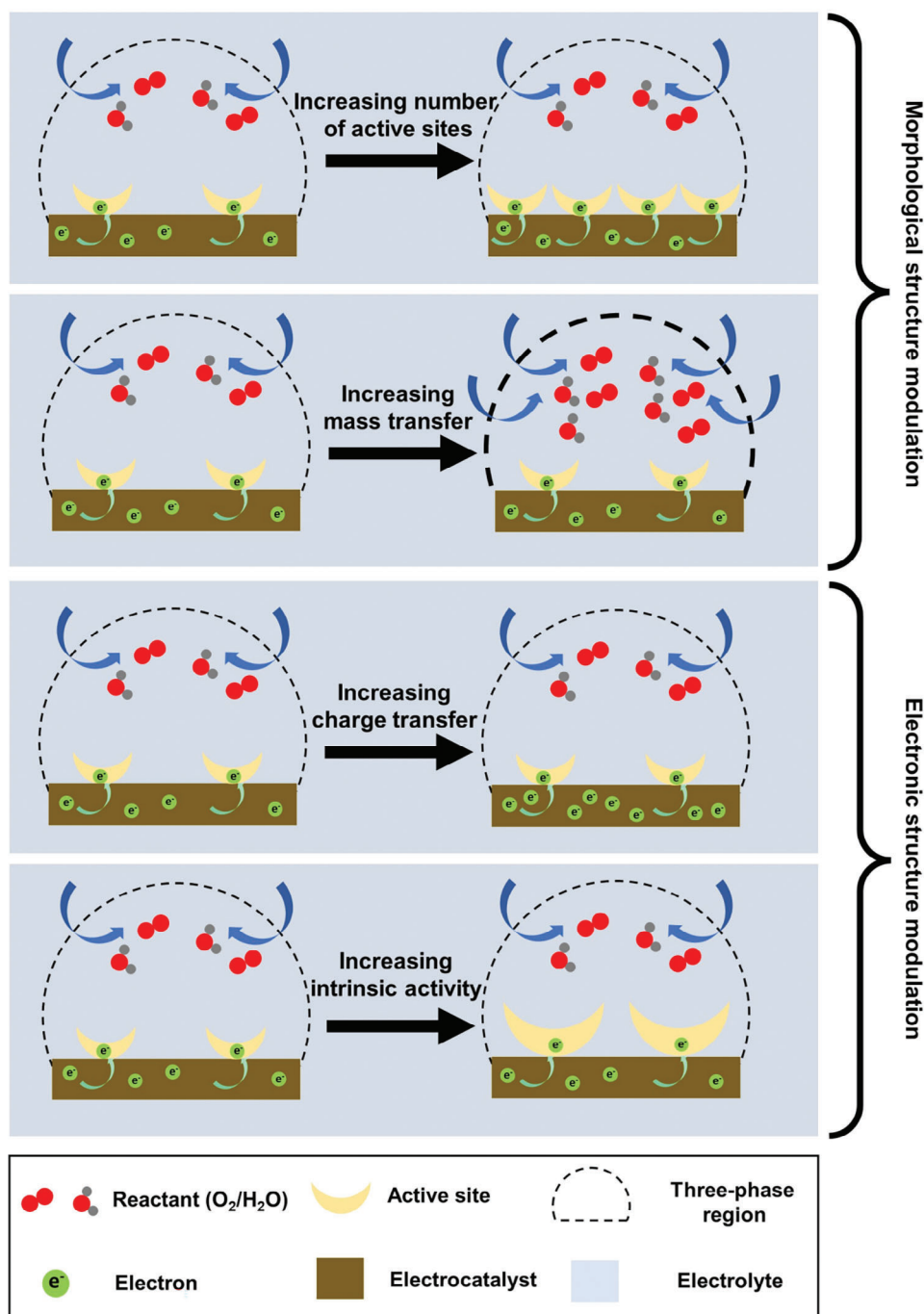


Figure 8. Schematic illustration of four electrocatalytic characteristics that directly affect the electrocatalytic activity.

hyde monomers with varying numbers of thiophene groups were polymerized with an amine monomer. Resultant products, JUC-527 and JUC-528, with different concentrations of unsaturated sulfur species serving as efficient ORR active sites also exhibit different ring sizes and specific surface areas. The JUC-528 with higher content of active unsaturated sulfur species and a larger ECSA (Figure 9h,i) exhibits better ORR performance in Figure 9j with much positive onset potential (E_{onset}) of 0.82 V and half-wave potential ($E_{1/2}$) of 0.70 V compared with JUC-527 (E_{onset} =

0.77 V and $E_{1/2}$ = 0.63 V). Besides, the crystallinity usually affects the catalytic activity of organic electrocatalysts by influencing the number of exposed active sites. Reducing the crystallinity of organic composites can often promote electrocatalytic activity by enlarging the three-phase boundary and increasing the effective collision probability between reactants and active sites.^[79] With the aid of synchrotron radiation atomic characterization, the impact of tuning the crystallinity can be assessed. By examining a type of bimetallic NiFe-based MOF through X-ray absorption

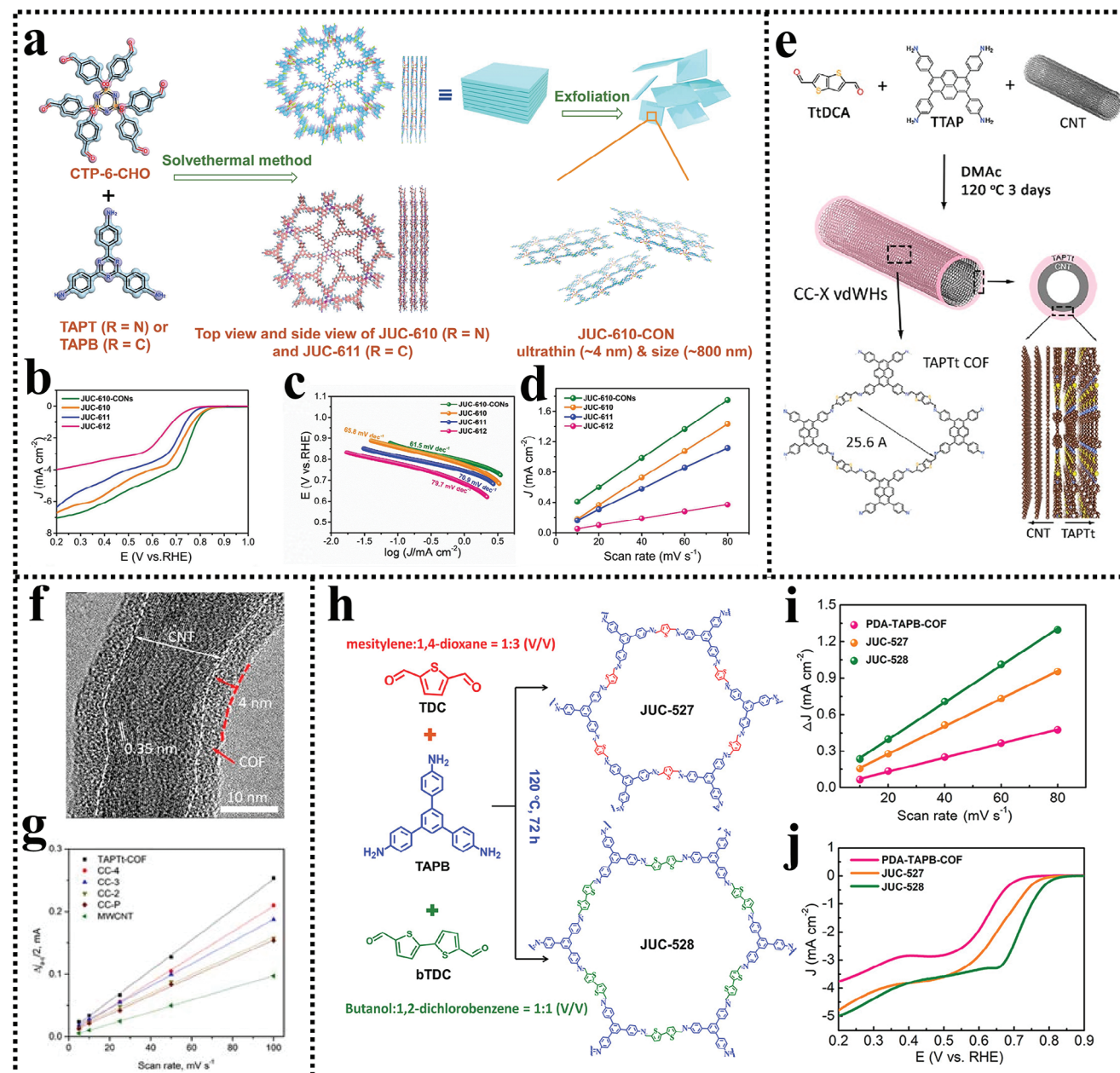


Figure 9. a) Synthesis of JUC-610 and JUC-610-CON with Q-3D structure. b) LSV curves, c) Tafel slopes, and d) electrochemical bilayer capacitances of JUC-610 and JUC-610-CON. Reproduced with permission.^[75] Copyright 2023, Springer. e) Synthesis CC-X. f) TEM image of CC-3. g) Calculated ECSAs of CC-X. Reproduced with permission.^[77] Copyright 2021, American Chemical Society. h) Synthesis and molecular structures, i) calculated ECSAs, and j) LSV curves of JUC-527 and JUC-528. Reproduced with permission.^[67] Copyright 2020, American Chemical Society.

spectroscopy (XAS), Li et al. discovered that introducing Ni into the Fe-based MOF can greatly increase the distortion index and elongate the Fe–O bond length. This results in the formation of a low-crystalline structure with more exposed active sites and boosted OER activity.^[80]

Based on the preceding discussion, it can be acknowledged that for organic materials with much clearer atomic and morphological structures used as electrocatalysts, DFT calculation, in situ electrochemical spectroscopic studies, and atomic characterizations can better assist in discerning their potential active

species compared with other materials. Meanwhile, the structural/physicochemical properties of organic materials, including ECSA, concentration of active species, and crystallinity, can be controlled and modulated with greater ease and precision compared to other materials. Therefore, they can be regarded as activity indicators/descriptors for conveniently analyzing the molecular structures of organic electrocatalysts, thereby establishing clear relationships between these structural/physicochemical properties and electrocatalytic performances. Furthermore, with these explicit relationships, the proposed strategies for tuning the

structural and physicochemical properties of organic electrocatalysts, as mentioned above, to increase the number of active sites, prove to be more effective and reliable.

3.2. Mass Transfer

The mass transfer of reactant through an electrocatalyst significantly influences the kinetics of the electrocatalytic reactions.^[81] To compete with other heterogeneous electrocatalysts, organic electrocatalysts ought to deliver high current densities. However, many organic electrocatalysts still exhibit low current densities when the external potential can activate nearly all active sites. This inferiority is mainly caused by mass transport limitations.^[82] Mariano et al. discovered that controlling mass transport during ORR by optimizing the structure of gas diffusion electrolyzes can greatly increase the oxygen reduction rate of 2D conductive MOF by several orders of magnitude.^[83] Compared with $\text{Ni}_3(\text{HITP})_2$ deposited on regular radiating ring-disk electrode (RRDE), when the $\text{Ni}_3(\text{HITP})_2$ was integrated with a gas diffusion electrode (GDE) or deposited on the indium-tin oxide (ITO) window of scanning electrochemical cell microscopy (SECCM), the ORR current (an indicator of electrocatalytic activity) improves by several orders of magnitude (Figure 10a,b). This improvement is attributed to the immediate replenishment of fresh oxygen into the oxygen depletion zone adjacent to the organic electrocatalyst, maintaining the reaction kinetics, after optimizing the structure of gas diffusion electrolyzes. Mass transfer is a key determinant of the catalytic activity exhibited by an organic electrocatalyst. To better describe the effect of mass transfer toward the electrocatalytic process, Yin et al. introduced a new parameter k_{O_2} , calculated by dividing the thickness of the diffusion layer by diffusion coefficient along with some constants.^[84] The obtained k_{O_2} serve as a characteristic parameter to evaluate mass transfer, specifically the mass transfer limited coefficient, on the electrode with the electrocatalyst. As a consequence, the rational design of the electrode structure of organic electrocatalysts is crucial in revealing their activities in practical applications.^[60]

Moreover, structural/physicochemical properties such as polymerization, size, and pore distribution have a strong influence on mass transfer. Zhang et al. adopted an aqueous micellar strategy to obtain a novel kind of conjugated reticular oligomer (CRO).^[39] By assembling CRO on PEDOT conductive polymer, a novel “muscle”-biomimetic organic structure consisting of CRO “blood cells” and PEDOT “neurons” is successfully constructed. This structure can significantly accelerate mass transfer and further benefit the electrocatalytic OER and HER processes. The size of various types of CROs, with more terminal residual groups, is much smaller compared with their COF counterparts. This gifts them better hydrophily, which considerably boosts the probability of effective collision between reactants and active sites, accordingly accelerating the mass transfer (Figure 10c). The OER and HER overpotential diagrams of these organic materials with different sizes demonstrate that with the reduction of size (Figure 10d,e), overpotentials also decrease. This indicates the great contribution to the optimized size of CROs and promoted mass transfer.

Constructing superstructures is another effective strategy for obtaining mass transfer of organic materials for electrocatalytic

applications. These well-designed superstructures usually possess consecutive tunnel structures, which can serve as efficient pathways for transferring various kinds of reactants and reaction intermediates.^[85] In the study conducted by Li et al., focusing on nonaqueous Li–air batteries,^[86] a novel porous COF was synthesized on carbon nanotubes to facilitate mass transfer and address the issues of high instability and low lifespan of Li–air batteries in ambient air. The resulting composites can function as snorkels, transporting oxygen exclusively to active sites for reduction (Figure 10f). The ring size of the various COFs is largely determined by the length of the monomer (Figure 10g,h). By modulating the ring size of COF, the Knudsen diffusion of the solvent molecules can be confined while perfectly retaining the gas diffusion channels. Molecular dynamic simulations confirmed the solvent-free tunnel (Figure 10i). It was observed that the concentration of the penetrated solvent molecules in COF-1 with a smaller ring size (1.41 nm) is much lower than that in COF-4 with a larger ring size (2.42 nm). This indicates the improved mass transport rate of COF-1 during the ORR, with less hindrance caused by the blocking effect of solvent molecules.

In this section, mass transfer, including transferring reactants and reaction intermediates also makes a great contribution to determining the reaction kinetics and further electrocatalytic activity of the electrocatalyst. For organic compounds, by selecting various monomers and polymerizing using specific methods, the size and pore/channel structure of the organic materials with better wettability can be easily controlled. Therefore, by optimizing these two activity indicators/descriptors, it becomes more convenient for organic materials to obtain desirable structures with facilitated mass transfer when used as electrocatalysts.

3.3. Charge Transfer

In addition to the mass transfer process, the charge transfer process is also a crucial characteristic that should be considered when optimizing the design of organic electrocatalysts. The charge transfer is closely related to the electronic structure of the material. Organic materials with π -conjugated structures consisting of benzene- or triphenylene-based segments (framework, polymers, oligomer, etc.) are known to be effective electrical insulators due to their superior conductivity of electrical charge.^[87] Because of this, fabricating a π -conjugated structure can greatly enhance the charge transfer ability, further facilitating the rate of charge transport toward the active site and reaction kinetics in organic electrocatalysts. Through facile solvothermal reaction, Wang et al. synthesized a topological organic salphen organic framework (SOF) with a fully π -conjugated structure for anchoring atomic cobalt metal ions, which functions as metal active sites for ORR (Figure 11a).^[88] Through using monomers with phenolic aldehyde and o-diamine structure to coordinate Co atom, a novel CoN_2O_2 configuration with N_2O_2 ligands can be constructed. Through the ligand-mediation effect, electrons can be redistributed on the CoN_2O_2 for better adsorbing oxygen intermediate, and the fully π -conjugated SOF structure with more electrons serves as a highly conductive substrate to transport more electrons to the metal–ligand region for reducing oxygen. With the assistance of Ketjen black (KB), the LSV curve of CoN_2O_2 -SOF combination with a remarkable $E_{1/2}$ of 0.959 V

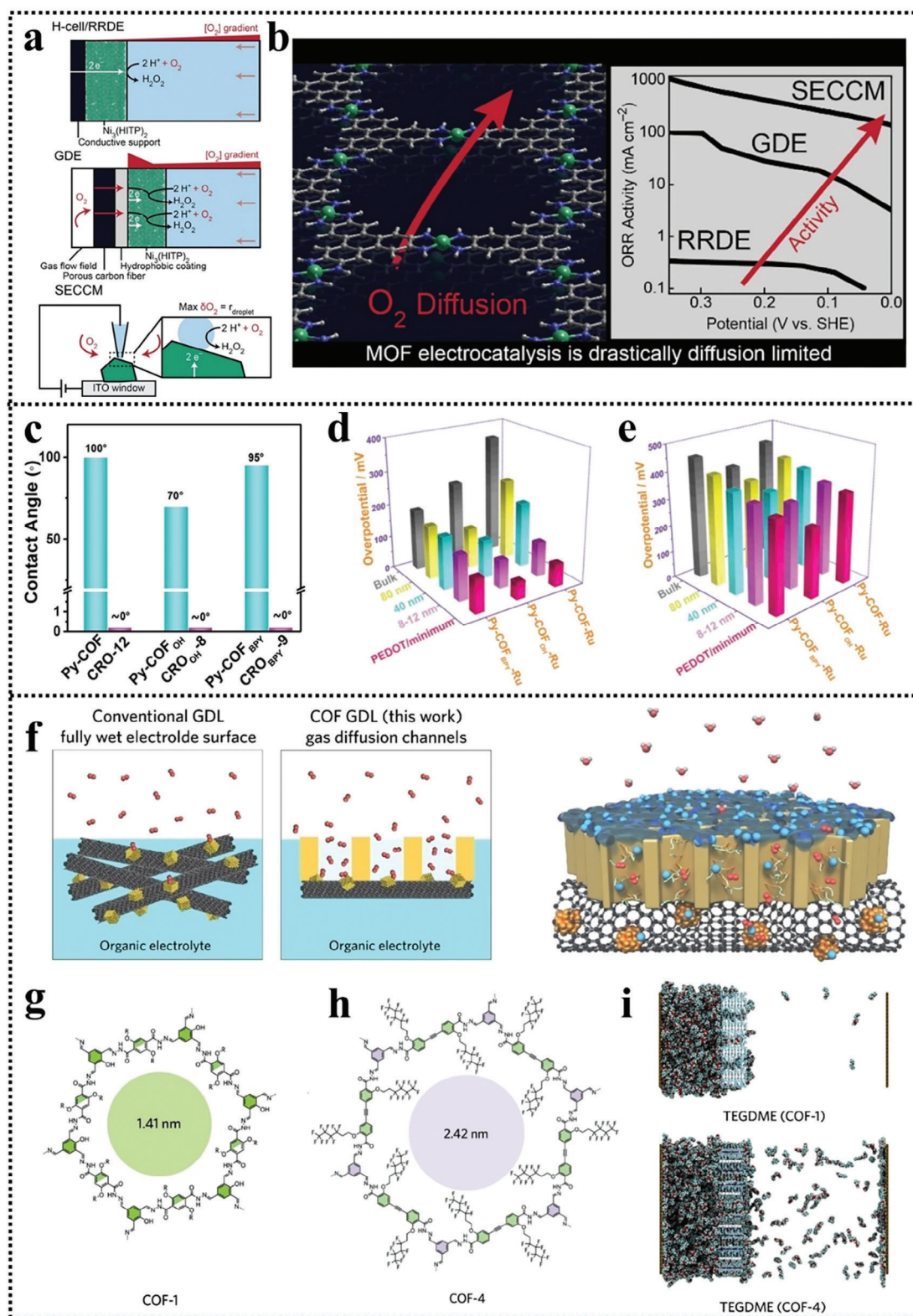


Figure 10. a) Schematic illustration of the ORR progress and b) measured ORR current of $\text{Ni}_3(\text{HITP})_2$ in systems with H-cell RRDE, GDE, and SECCM. Reproduced with permission.^[83] Copyright 2022, American Chemical Society. c) Comparison of contact angles of CROs with their COF counterparts. d) OER and e) HER overpotentials of various CROs and COFs. Reproduced with permission.^[39] Copyright 2022, Wiley-VCH. f) Schematic illustration of the function of the superstructured COF gas diffusion layer. g,h) Molecular structures and ring sizes of COF-1 and COF-4. i) Molecular dynamic simulations of organic solvent molecules penetrating through COF-1 and COF-4. Reproduced with permission.^[86] Copyright 2023, Wiley-VCH.

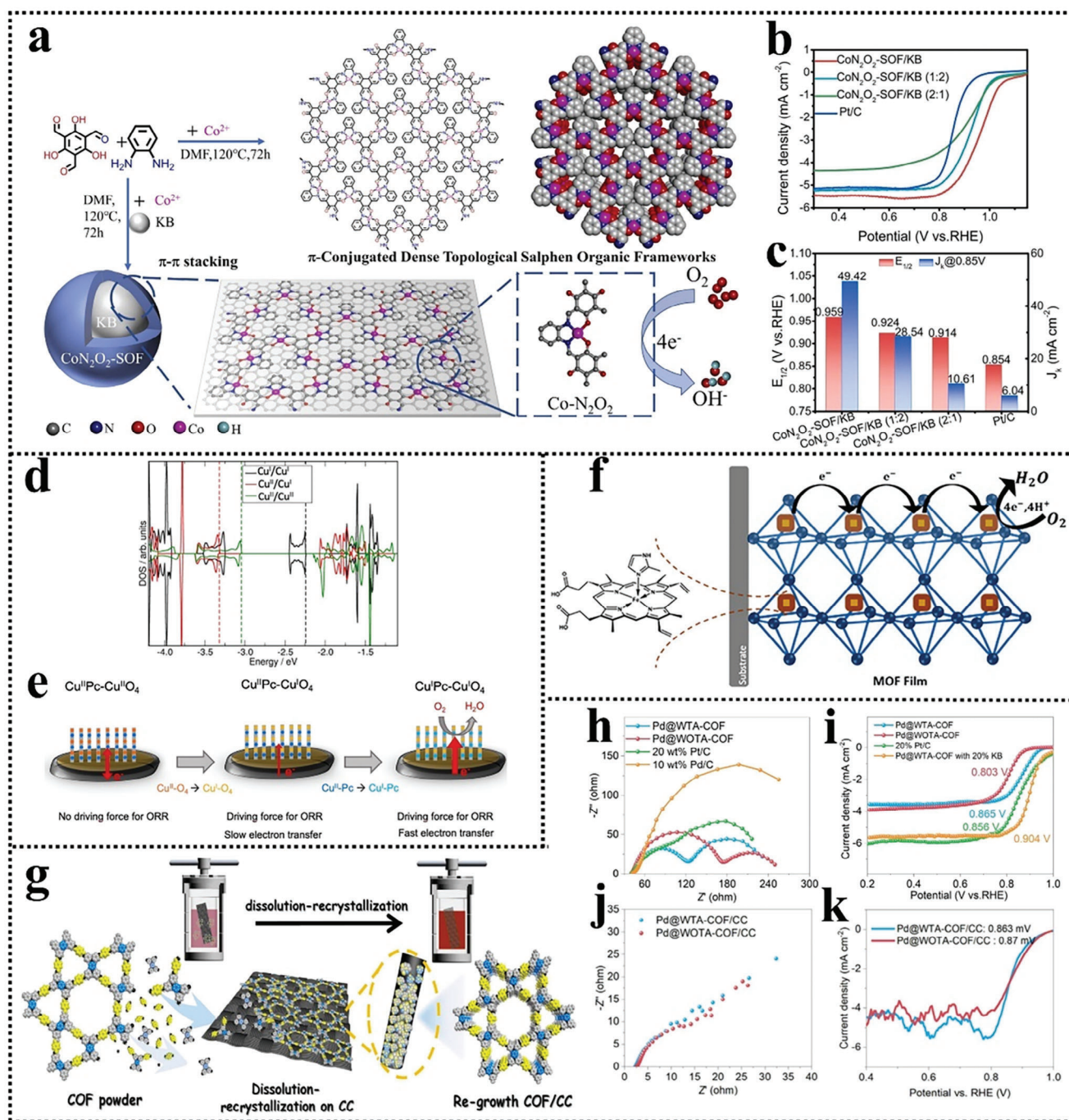


Figure 11. a) Synthesis of conjugated topological organic SOF/KB composite. b) LSV curves and c) corresponding $E_{1/2}$ and J_k of various topological organic SOF/KB composites with Pt/C benchmark. Reproduced with permission.^[88] Copyright 2022, Elsevier. d) Density of states of Cu^I/Cu^I, Cu^{II}/Cu^I, and Cu^I/Cu^{II} samples. e) Schematic illustration of the oxidation states of different copper metal sites toward the electron transfer. Reproduced with permission.^[90] Copyright 2023, American Chemical Society. f) Structure of the UIO-66@Hemin MOF film with axial coordinating MeIM. Reproduced with permission.^[91] Copyright 2020, American Chemical Society. g) Illustration of the dissolution-recrystallization strategy for decorating COFs on CC. Nyquist plots and LSV curves of h,i) Pd@WTA-COF and j,k) Pd@WOTA-COF. Reproduced with permission.^[94] Copyright 2023, Elsevier.

in 0.1 M KOH is much more positive than the Pt/C benchmark (Figure 11b,c). Besides that, kinetic current densities (J_k) at 0.85 V of these samples were also calculated in Figure 11c, the CoN₂O₂-SOF/KB, the CoN₂O₂-SOF also exhibits the highest J_k of 49.42 mA cm⁻², proving the highest overall intrinsic activity of

CoN₂O₂-SOF resulting from both the high activated atomic active sites and facilitated charge transfer of SOF π -conjugated structure. Notably, the electronic interaction between metal and ligands in organic electrocatalysts also has a huge impact on charge transfer during electrocatalytic reactions. Li et al. prepared a

series of thiazolo[5,4-d]thiazole-bridged covalent organic polymers, team, and pointed out that the thiazolo[5,4-d]thiazol unit can extract electrons from the surrounding unit with different types of halogen atoms (including F, Cl, Br, and I), and the intensity of this electron extraction effect is determined by the electronegativity of the halogen atom.^[89] The polymer containing F exhibited the highest ORR activity with the lowest energy barrier of the electron transfer potential-determining step, which is associated with the fastest charge transfer between the thiazolo[5,4-d]thiazol unit and F atoms with the highest electronegativity.

Besides, charge transfer inside the organic materials during electrocatalytic reactions can also be successfully tuned by modulating energy band structures. The energy band structure consists of a conductive band (E_c), valence band (E_v), and bandgap ($\Delta E = E_c - E_v$), and ΔE can be considered as a descriptor of conductivity and E_v can reflect the energy barrier for electrons to participate in the catalytic reaction.^[77] By modulating the oxidation state of the different copper metal centers of a well-designed 2D MOF with π -conjugation, Dominic et al. have constructed a clear relationship between the band structure and ORR electrocatalytic performance.^[90] The density of states of simulated MOFs with different copper species (Cu^I and Cu^{II}) in two kinds of metal centers (denoted as Cu^X/Cu^Y , where X and Y are the oxidation states of the copper species) in Figure 11d exhibit the calculated bandgaps of Cu^I/Cu^I , $\text{Cu}^{II}/\text{Cu}^{II}$, and $\text{Cu}^I/\text{Cu}^{II}$ are 0.51, 0.92, and 1.25 eV, respectively. Considering electrons are more likely to transfer from the E_v to the E_c and participate in electrocatalytic reactions, the Cu^I/Cu^I with the lowest bandgap possess the best ORR performance, which can be attributed to the fast electron transport brought by the narrow bandgap. This facilitated charge transfer on $\text{Cu}^I\text{Pc}-\text{Cu}^I\text{O}_4$ originates from the formation of the metal–ligand–metal efficient electron transfer pathway. Due to the electron state optimization (transforming Cu^{II} to Cu^I) of metal centers, the conjugation degree of the organic part at the linkage is enhanced, leading to a higher electron flow rate in MOF (Figure 11e). Yet, the accelerated charge transfer, narrowed bandgap, and increased conductivity of organic electrocatalysts should be in-depth analyzed. Taking MOF-based electrocatalysts as examples, the combination of ligand and the metal site can greatly affect the charge transfer during electrocatalytic reactions. Liberman et al. have discovered that the axial coordinating electron-donating ligand can dramatically facilitate charge propagation through hopping between neighboring redox-active metal sites of MOF. In Figure 11f, the introduction of axially coordinated 2-methylimidazole (MeIM) on the metal site of UIO-66@Hemin MOF enormously increases the charge hopping rate (k_{hopping}), thus greatly accelerating the charge transfer for ORR.^[91] This is because the electron-rich MeIM ligand can inject electrons to the adjacent coordinated metal site through metal-to-ligand charge transfer, thus increasing the mobility of electrons in the UIO-66@Hemin MOF further enabling more electrons involved in the ORR.^[92] Nevertheless, it should be noted separately that although increasing the degree of conjugation can effectively boost the charge transfer, the strengthened π – π interaction accordingly can cause structure agglomeration and even destruction,^[75] which leads to a significant reduction of active sites and limited mass transfer. As a consequence, an appropriate degree of conjugation should be adopted to achieve a trade-off between charge transfer and mass transfer.

Furthermore, metal sites in MOFs with a hybrid coordination environment usually possess better charge transfer ability due to its broken neutrality of the original structure with a higher carrier concentration, and ligands with functional groups possessing great affinity to reaction intermediate are also helpful for improving the charge transfer.^[93] Tian et al. synthesized a type of P-doped MOF using 2-amino-1,4- benzene dicarboxylic acid ligand ($\text{BDC}(\text{NH}_2)$) to simultaneously catalyze OER and HER in an alkaline electrolyte.^[27] The P atoms were doped into the octahedron of metal sites to break its neutrality, and the NH_2 groups in $\text{BDC}(\text{NH}_2)$ ligand reacted with the adsorbed OH^- ions and released electrons during electrocatalytic reactions, which both are conducive to the charge transfer process of bifunctional electrocatalysis on MOF.

In addition to combining with reaction intermediates, functional groups on the surface of organic electrocatalysts have another vital effect on charge transfer especially when the organic materials are decorated on current conductors (such as carbon cloth, Ni foam, Cu foam, etc.) or composited with conductivity enhancers (such as carbon nanotube, carbon black, etc.) for electrocatalytic reactions. In the study conducted by Wang et al.,^[94] two kinds of Pd-inserted COFs with different content of functional groups (labeled as Pd@WTA-COF or Pd@WOTA-COF , and Pd@WOTA-COF possesses more oxygen-containing functional groups) are synthesized. These synthesized COFs were decorated on the surface of a carbon cloth (CC) current collector through a dissolution–recrystallization strategy. The obtained Pd@WTA-COF/CC and Pd@WOTA-COF/CC integrated compositions were used as air cathodes in the zinc–air batteries (Figure 11g). The fitted EIS curves and LSV curves of Pd@WTA-COF and Pd@WOTA-COF in Figure 11h,i show that Pd@WTA-COF exhibits lower charge transfer resistance and more positive $E_{1/2}$ compared to Pd@WOTA-COF . This is because the oxygen-containing functional groups affect the conjugated structure of the COF skeleton, leading to decreased charge transfer during ORR. Interestingly, after decorating these two types of COFs on the surface of CC, for Pd@WTA-COF/CC , the charge transfer resistance becomes higher and $E_{1/2}$ becomes more negative compared with Pd@WOTA-COF/CC (Figure 11j,k). This is because the oxygen-containing functional groups on Pd@WOTA-COF can increase the dispersity of the COF layer further preventing uncontrolled stacking of thicker COF layers during the dissolution–recrystallization decoration process, contributing to increased charge transfer of the Pd@WOTA-COF/CC air cathode during discharging. As a result, it is clear that when discussing the charge transfer process of organic electrocatalysts in practical applications, the structural/physicochemical interaction between the organic materials with other substrates/collectors should also be considered.

In a word, charge transfer is another important characteristic that affects the ultimate electrocatalytic activity. For organic electrocatalysts, structural/physicochemical properties including the degree of conjugation, energy band structure, and structural/physicochemical interaction with other materials are the main deciders of the charge transfer ability. To rationally design organic electrocatalysts with high charge transport rates, it would be more vivid and controllable to start by regulating the aforementioned structural/physicochemical properties as activity indicators/descriptors to achieve better electrocatalytic activity.

3.4. Intrinsic Activity

For organic electrocatalysts with clear and confirmed structures or active sites, modulating the electronic structure can significantly increase the intrinsic activity while maintaining their original structure and active site configuration.^[95] Structural/physicochemical properties, including charge density on active sites and the valence electron number of the atom serving as active sites, directly influence the thermodynamic energy barrier of electrocatalyst reactions. Sun et al. have discovered that after introducing a Fe atom into the penta-coordinated metal site of Mil53 Ni-based MOF, the number of electrons in d-orbital per metal atom increases due to the enhanced metal–ligand effect.^[14b] In this respect, the enhanced electronegativity of Ni atoms is accompanied by a decrease in the adsorption energy of oxygen intermediate on them, which enhances the intrinsic activity per Ni metal active site toward OER. The effect of charge density at the active site on the adsorption energy of its reaction intermediates is more pronounced on small molecule electrocatalysts with only one active site. As reported by Xue et al.,^[96] changing the bonding position of a H atom on the Ni metal center of planar Ni(II) porphyrinoid complex small organic molecule electrocatalyst, from fused benzo units side to meso-aryl side, can considerably reduce its HER energy barrier. This is because the position change of the bonded H atom modulates the charge density of the whole organic molecule, resulting in charge redistribution further boosting the intrinsic activity.

Furthermore, the design of COF or COP electrocatalysts with defined active sites can be effectively optimized by tuning inherent parameters related to the electronic structure. Li et al. precisely modulated the intrinsic activity of iron active sites in the COPs with confirmed covalent porphyrin structures and Fe–N₄ active sites.^[28] Observations show that the substitution of fluorine atoms on the surrounded benzene ring increases the charge density of the iron site for the adsorption of oxygen intermediates from 1.03 to 1.20, leading to high electron-transition intensity (Figure 12a,b). Given that the ORR is an electron-consuming process, a higher charge density and electron-transition intensity on the iron active site is beneficial for enabling the adsorbed oxygen to obtain electrons and undergo reduction. This inference is confirmed by the theoretical calculation of the thermodynamic energy barriers of pure COP and F-decorated COP (Figure 12c). The F-decorated COP (oxygen intermediates adsorbed on the metal site) exhibits the lowest energy barrier, which can be attributed to the high charge density of the iron atom. Beyond that, the fluorine group with electron-withdrawing property can reduce the adsorption energy of reaction intermediates and push the kinetic activity closer to the volcano peak. This makes it much easier for the oxygen intermediates to be desorbed from the active site, thereby achieving a high activity level for the iron active site (Figure 12d).

Besides, to further illustrate the inherent relationship between the electronic structure and the electrocatalytic activity of confirmed active sites configuration for better directing the rational design of highly efficient organic electrocatalysts, another series of Ni-MOFs with different second metal sources are synthesized and in-situ decorated in the nickel foam through an interface-mediated strategy for OER applications (Figure 12e).^[97] Considering the binding between oxygen intermediates and metal sites is on account of the coupling between the d-orbitals of the tran-

sition metal atom and p-orbitals of the oxygen atom, and this coupling brings about the development of partially occupied antibonding states and filled bonding states (Figure 12f). The introduction of second metal sources in the metal site of Ni-MOF can greatly tune the charge density on the metal site with modulated d-band center and e_g filling (Figure 12g), while these two electronic properties can be used as activity descriptors to simulate the adsorption free energy of various reaction intermediates and further thermodynamic reaction barrier/overpotential of OER (Figure 12h). Although these descriptors have been thoroughly studied in many metal-based inorganic electrocatalysts, the correlation between them and the electrocatalytic activity in organic electrocatalysts should be established additionally because unlike inorganic electrocatalysts, the electron properties of the metal site in organic electrocatalysts are strongly determined by its coordinated ligand. As a result, simulation of these d-orbital characteristics in organic electrocatalysts should focus on the whole metal–ligand unit rather than the only metal site. Subsequently, as a function of the d-band center and e_g filling, a computed OER overpotential contour diagram of Ni-M-MOFs is shown in Figure 12i. From the red region (Fe-substitution) to the green area (Co-substitution), and finally, to the blue area (Cu, Mn, and Zn-substitution), the OER overpotential improves steadily, and the bimetallic NiFe-MOF in the middle of the red region with a d-band center of ≈ -1 eV and e_g filling of ≈ 2.5 has the highest electrocatalytic activity of all Ni-M-MOFs thanks to its optimum electronic structure with the lowest overpotential for the oxygen evolution on the metal active site, indicating the highest intrinsic electrocatalytic activity of the metal active site.

Nevertheless, illuminating the intrinsic activities of organic electrocatalysts only through theoretical analysis is not sufficient. Characterizations focusing on structural elements of the organic part and bonds between metal and ligand are highly in demand to fill the gap between electrocatalytic activity and intrinsic properties.^[98] The examination of the structural and bond information through synchrotron radiation measurement is instrumental in figuring out the electrocatalytic mechanism of organic electrocatalysts. Zhou et al. tailored the Ni-MOF structure through constructing defects in the organic part to obtain defective Ni-MOF (D-Ni-MOF) with a higher intrinsic activity.^[99] XAS examination reveals that the oxidation state of the Ni site increases while the coordination number decreases after defect engineering in the organic part. This is because the partial absence of ligands contributes to fewer electrons being extracted from the metal center, resulting in rapid adsorption of OH[−]/H₂O and reduced energy barrier to form OH* and H* on the Ni metal site further boosting intrinsic activity. Additionally, due to the unique structure of MOF with metal–ligand units, changes during electrocatalytic reactions of the overall structural and bond length between metal and ligands can also be identified for deducing the electrocatalytic mechanism through operando XAS test. As reported by Zhao's group,^[100] after shaping the NiCo-MOF into ultrathin nanosheets (NiCo-UMOFNs), the Ni-K edge X-ray absorption near-edge structure (XANES) peak positions of NiCo-UMOFNs with potential range from 1.43 to 1.53 V are positive than those of bulk NiCo-MOF (Figure 12j), revealing the metal site in NiCo-UMOFNs tend to transfer more electrons to its coordinated ligands as the external potential positively shifts. The EXAFS spectra also show that the Ni–O/Ni–C/Ni–Ni bond length

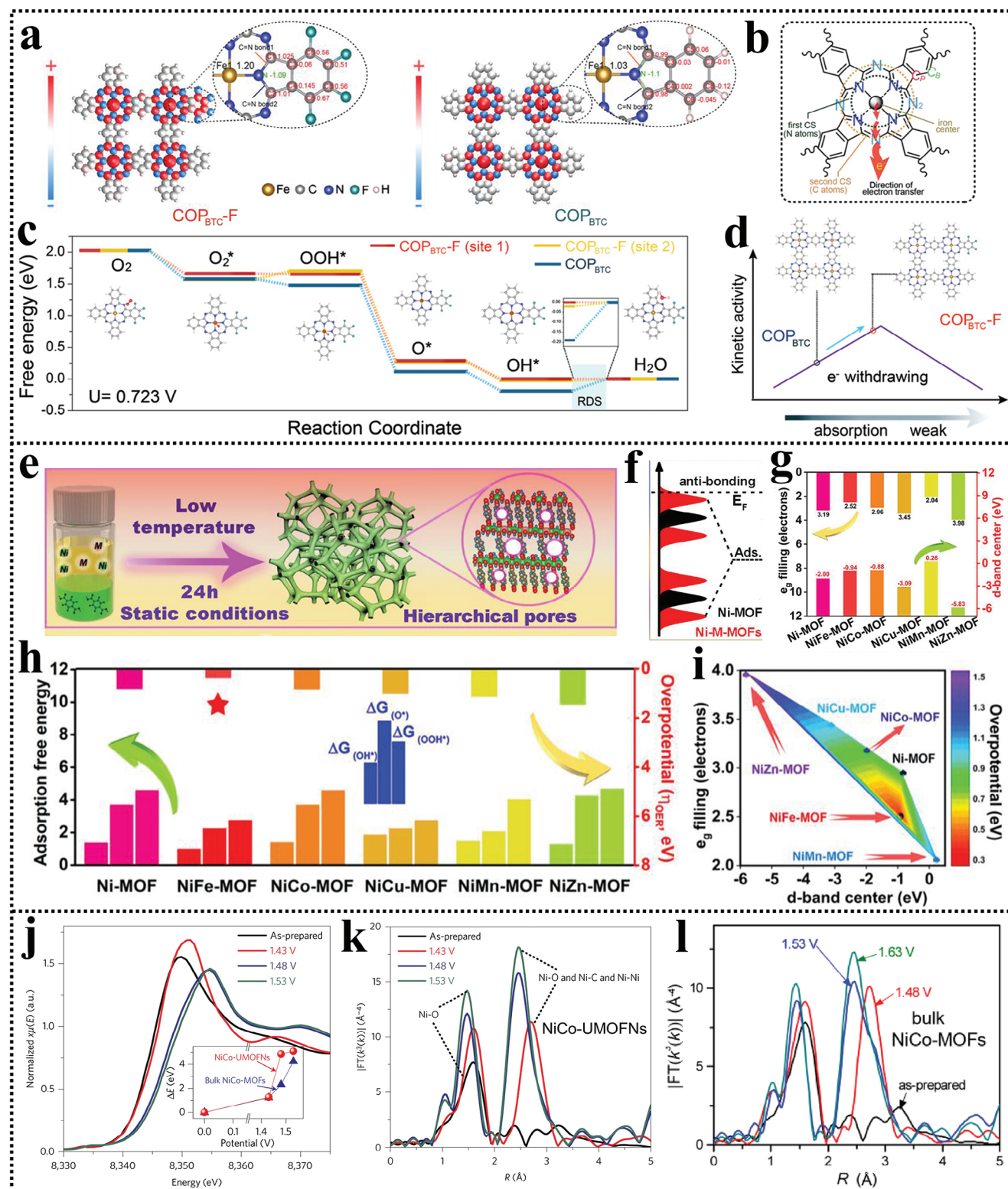


Figure 12. a) Charge distribution of pure COP and COP with fluorine substitution. b) Schematic illustration of the electron-transition effect on the metal sites of COP-F. c) Free energy diagrams and d) volcano plots of pure COP and COP with fluorine substitution. Reproduced with permission.^[28] Copyright 2022, Wiley-VCH. e) Synthesis of Ni-MOF on nickel foam. f) Schematic illustration of bond formation of coupling effect. g) d-band center and e_g filling, h) adsorption free energy and overpotential Ni-M-OFs, and i) the fitted contour diagram of the computed OER overpotential of various Ni-M-OFs. Reproduced with permission.^[97] Copyright 2021, Wiley-VCH. j) Operando Ni K-edge XANES spectra of NiCo-UMOFNs (inset: relative energy shift of NiCo-UMOFNs and bulk NiCo-MOF). k), l) Ni K-edge EXAFS spectra of NiCo-UMOFNs and bulk NiCo-MOF. Reproduced with permission.^[100] Copyright 2016, Nature.

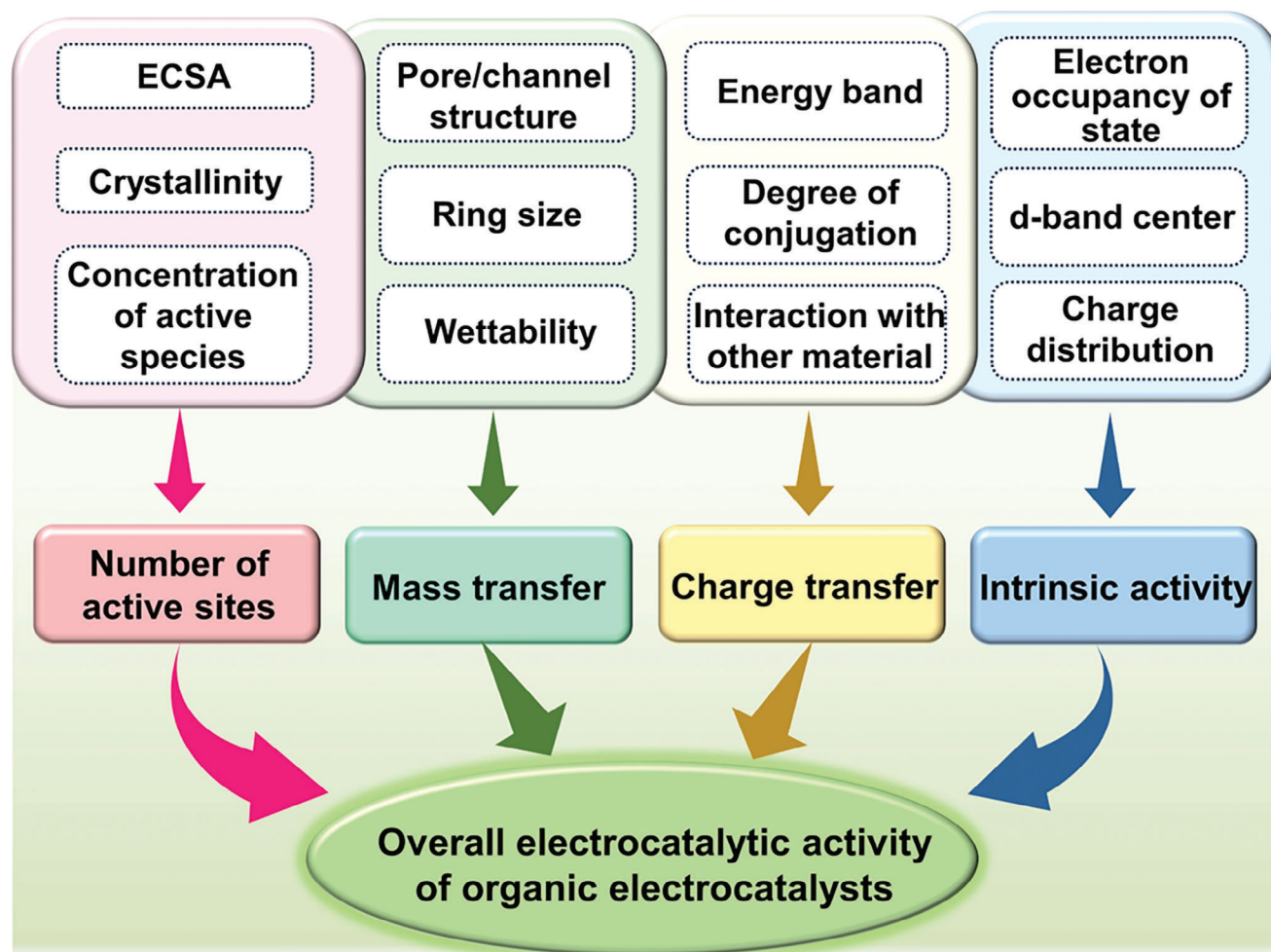


Figure 13. Schematic illustration of various activity indicators/descriptors affecting the overall electrocatalytic activity of organic electrocatalysts.

of NiCo-UMOFNs shrunk at a lower potential compared with those of bulk NiCo-MOF (Figure 12k,l). These are highly responsible for the improved intrinsic activity of NiCo-UMOFNs.

The intrinsic activity of confirmed active species directly determines the overall electrocatalytic performance of the organic electrocatalyst. For metal-free organic materials, structural/physicochemical properties, including overall electronegativity and charge distribution, can significantly affect intrinsic activity. For transitional metal-contained organic materials, structural/physicochemical properties such as electron occupancy of state, d-band center, and charge density on the metal sites are closely related to the intrinsic activity. Optimizing the electrocatalytic activity of organic electrocatalysts by modulating these activity indicators/descriptors provides a more concise and clear approach for directionally enhancing the electrocatalytic performance and revealing the interrelationship between the electronic structure and the intrinsic activity of organic electrocatalysts.

In conclusion, the unique and diverse structural/physicochemical properties of organic electrocatalysts can serve as specific indicators or descriptors of electrocatalytic activities. These properties can be used to correspond to various electrochemical characteristics that directly influence the

overall performance of electrocatalysis. These activity indicators/descriptors can be classified into four categories based on different electrochemical characteristics (Figure 13). From the perspective of morphological structure modulation, first, the ECSA, content of active sites, and crystallinity can directly affect the number of exposed active sites for electrocatalyst reactions. Second, the pore/channel structure, wettability, and ring size in polymerized structure determine the mass transfer process. Along with that, it can be noticed that these structural/physicochemical properties are also interrelated, making their modulation extremely effective for tuning the electrocatalytic activity of organic materials. Likewise, from the perspective of electronic structure modulation, structural/physicochemical properties such as energy band structure, degree of conjugation, and interaction with other materials (such as conductive carbon substrate) can effectively tune the overall electronic structure of organic materials. This further affects the charge transfer process during electrocatalytic reactions. Similarly, for organic electrocatalysts with defined molecular structures and atomic active sites, the actual configuration is consistent with the theoretical model. Therefore, the simulation results from DFT calculation toward electrocatalytic reactions on organic

electrocatalysts are more reliable. As a result, the d-band center and the electron occupancy of the state of metal active sites in metal-contained organic materials are pivotal and useful for analyzing the electrocatalytic activity. Additionally, for both metal-contained and metal-free organic materials, their charge distribution can reveal the charge density on the confirmed active sites. Accordingly, the electrocatalytic activity of the active site can be easily evaluated. This section concludes various special structural/physicochemical properties of organic materials, which can be considered as activity indicators/descriptors. This further constructs a much clearer structure–activity relationship between structural/physicochemical properties and electrocatalytic activities of organic electrocatalysts. We believe this relationship can provide meaningful instructions for how one can prepare a low-cost organic catalyst that exhibits excellent electrocatalytic performance.

3.5. Roadmap for Obtaining Highly Active Organic Electrocatalysts

With the successful construction of the reliable structure–activity relationship of low-cost efficient organic electrocatalysts discussed in the previous section, designing excellent organic electrocatalysts has become more oriented. A systematic roadmap for future designing organic electrocatalysts with excellent performance can be depicted based on accumulated past to present experience. **Table 1** summarizes the activity enhancement strategies and electrocatalytic performances of many organic electrocatalysts as well as some inorganic electrocatalysts in recent years (including noble-metal benchmarks and some other well-performed carbon/metal-based electrocatalysts). Although many organic electrocatalysts exhibit promising electrocatalytic activity, further improvements are still needed to commercialize them.

Basically, from the past to the present, activity optimization of organic electrocatalysts is usually conducted from five aspects, namely, pore/channel structure, surface group, charge distribution, electron state, and conjugation degree. The pore/channel structure and surface group are more related to the number of active sites and mass transfer, while the charge distribution and electron state are usually associated with the charge transfer and intrinsic activity. Additionally, the conjugation degree affects nearly all four electrochemical characteristics.^[124]

Moreover, these five aspects are also strongly correlated to the morphology and molecular structure of the organic electrocatalyst. The morphology of the organic electrocatalyst usually determines its pore/channel structure and conjugation degree, while the molecular structure often defines its surface groups, charge distribution, and electron state. Based on these clear relationships, methods for implementing these optimizations of organic electrocatalysts are raised. To optimize their electrocatalytic performance, appropriate building blocks can be selected to precisely control the morphology and molecular structure of the prepared organic electrocatalysts.

Combined with the flourishing trend of organic electrocatalysts over the decade and the valuable achievements that have been made so far, a development timeline for preparing well-performed organic electrocatalysts through controlling

these morphology and molecular structure can be depicted (**Figure 14a**). As organic materials have gradually been widely studied in the field of electrocatalysis since 2013, Jahan et al. discovered morphology of MOF significantly changed and led to a great increment of the specific surface area when it was composed with GO.^[125] In another study conducted next year, Liu et al. used a nitrogen- and sulfur-rich conductive polymer to decorate a glassy carbon electrode.^[126] The charge transfer resistance was greatly reduced, implying the conductive molecular structure of organic materials can effectively benefit the charge transfer process during HER. Then in 2015, the conjugate property of organic electrocatalysts was proposed to link with the electrocatalytic activity. Although organic materials with high conjugation degrees usually possess electron transfer ability, the π – π electron interaction between stacked layers will lead to agglomeration, thereby burying the active site and limiting mass diffusion. As a result, making the best use of the advantages and bypassing the disadvantages of a high conjugation degree is highly desired. For example, strategies such as using the Langmuir–Blodgett route to obtain a nonstacked single-layer film can significantly prevent agglomeration and preserve the active sites,^[127] and integrating with conjugated carbon material generates a conjugation effect between carbon and organic materials that can enhance the charge transfer.^[128] With the further development of organic electrocatalysts, in 2018, the focus of researchers was gradually deepening to the atomic level. Che et al. found that after adsorbing organic structures with different surface groups on the PEDOT polymers,^[129] the morphology of the obtained composites is significantly different, further resulting in discrepant electrocatalytic activity. Simultaneously, In the study conducted by Sun et al., the number of 3d electrons in a Ni-based MOF cell increased after incorporating Fe into the atomic metal center, explaining its enhanced intrinsic activity originated from the ligand electronic effect.^[14b] Notably, the ligand morphological effect should not be neglected. In the work of Zhou et al. conducted in 2020,^[130] the morphology of MOFs can be controlled by manipulating the proportion of Mn, Fe, and Ni. This is because tuning the ligand–metal bond strength can control the growth direction of MOFs, resulting in optimized morphology for promoting the mass transfer and exposure of active sites. A year later, the ligand effect toward electrocatalytic performance in MOFs was quantified through defining accurate activity descriptors,^[97] namely, d-band center and d-orbital occupancy. The descriptors can greatly help in selecting appropriate ligands and metals to obtain an organic structure with the lowest overpotential based on the theoretical volcano-type relationship curve. At present, adopting appropriate building blocks to obtain efficient organic electrocatalysts becomes much more reliable due to the improved accuracy and speed of theoretical calculations. This is because not only the molecular dimension and overall morphology can be successfully controlled by manipulating the configuration of building blocks,^[102] but also can directly quantify the charge density on the potential active sites can be quantified using electron static potential (ESP) analysis and further proving great convenience and accuracy for simulating the electrocatalytic activity.^[66] This development timeline outlined the progress of organic electrocatalyst construction over the past decade from the initial macroscopic regulation of conductivity and morphology, delved into controlling the molecular

Table 1. Activity enhancement strategies and electrocatalytic performances of various kinds of organic electrocatalysts, noble-metal benchmarks, and some other well-performed carbon/metal-based electrocatalysts.

Electrocatalyst (type)	Catalyzed reaction	Active species	Activity enhancement strategy	Electrocatalytic performance	Refs.
Dpa (small organic molecule)	Acidic 2e [−] ORR	pyridyl-N and amino-N	Charge distribution optimization	$N \approx 2.4$	[101]
PYTA-TPEDH-COF (COF)	Alkaline 2e [−] ORR	—C=N—	Pore/channel structure optimization	$N = 2.28$	[102]
PBT (polymer)	Alkaline 2e [−] ORR	C at the linkage	Charge distribution optimization	$N = 2.2$	[103]
PCC ₉₀₀ (carbon)	Alkaline 2e [−] ORR	—C=O	Surface group optimization	$N \approx 2.08$	[104]
FePc-BBL COF (COF)	Alkaline 4e [−] ORR	Fe	Conjugation degree optimization	$E_{1/2} = 0.933$ V versus RHE	[105]
Co-TP-COF (COF)	Alkaline 4e [−] ORR	Co	Electron state optimization	$E_{1/2} = 0.73$ V versus RHE	[106]
Co-CNT@COF-Pyr (COF)	Alkaline 4e [−] ORR	Co	Surface group optimization	$E_{1/2} = 0.52$ V versus RHE	[107]
Pt ₁ -Fe/Fe ₂ O ₃ (012) (metal compounds)	Alkaline 4e [−] ORR	Pt	Charge distribution optimization	$E_{1/2} = 1.05$ V versus RHE	[108]
Pt/C (benchmark)	Alkaline 4e [−] ORR	Pt	—	$E_{1/2} = 0.86$ V versus RHE	[109]
Co _{0.8} Ni _{0.2} Fc-MOF (MOF)	Alkaline OER	CoNi	Charge distribution optimization	$\eta = 209/252$ mV@10/200 mA cm ^{−2}	[110]
FeNi-MOF (MOF)	Alkaline OER	FeNi	Electron state optimization	$\eta = 249/303$ mV@10/100 mA cm ^{−2}	[111]
CoBDC-Fc (MOF)	Alkaline OER	Co	Electron state optimization	$\eta = 178/241$ mV@10/100 mA cm ^{−2}	[112]
Co-TpBpy (COF)	Alkaline OER	Co	Charge distribution optimization	$\eta = 400$ mV@1 mA cm ^{−2}	[113]
Ni-MOF-FA (MOF)	Alkaline OER	Ni	Pore/channel structure optimization	$\eta = 386$ mV@10 mA cm ^{−2}	[114]
NiFeO ₄ (metal compounds)	Alkaline OER	Fe, Ni, Al, Mo, Co, and Cr	Electron state optimization	$\eta = 195/288$ mV@100/300 mA cm ^{−2}	[115]
RuO ₂ (benchmark)	Alkaline OER	Ru	—	$\eta = 265$ mV@10 mA cm ^{−2}	[116]
IrO ₂ (benchmark)	Alkaline OER	Ir	—	$\eta = 340$ mV@10 mA cm ^{−2}	[117]
CoTAPP-CoTNPP (polymer)	Acidic HER	Co	Charge distribution optimization	$\eta = 170$ mV@10 mA cm ^{−2}	[118]
Ru@COF-1 (COF)	Acidic HER	Ru	Conjugation degree optimization	$\eta = 200$ mV@10 mA cm ^{−2}	[119]
C ₆ -TRZ-TFP COF (COF)	Acidic HER	C	Conjugation degree optimization	$\eta = 200/235$ mV@10/50 mA cm ^{−2}	[120]
V—CoP ₂ /CC (metal compounds)	Acidic HER	V and Co	Electron state optimization	$\eta = 50/134$ mV @10/50 mA cm ^{−2}	[121]
Pt (benchmark)	Acidic HER	Pt	—	$\eta = 32$ mV@10 mA cm ^{−2}	[122]
PEDOT/CRO _{OH} -8-Ru (oligomer)	Alkaline HER	Ru	Electron state optimization	$\eta = 64$ mV@10 mA cm ^{−2}	[39]
FeCoNiCuPd (metal alloy)	Alkaline HER	Fe, Co, Ni, Cu, and Pd	Electron state optimization	$\eta = 30$ mV@10 mA cm ^{−2}	[123]
Pt/C (benchmark)	Alkaline HER	Pt	—	$\eta = 35$ mV@10 mA cm ^{−2}	[123]

functional groups and ligands, and finally delved into selecting atom configuration and electron state based on simulation results to achieve the design of an efficient organic electrocatalyst. Accordingly, selecting appropriate building blocks is fundamental to design a type of highly active organic electrocatalysts. This is because the geometry and size of building blocks directly affect the pore/channel structure and conjugation degree. More-

over, as mentioned in previous sections, building blocks with electron-deficient functional groups are favorable for constructing efficient organic electrocatalysts for ORR and HER because these unsaturated species with low charge density can serve as active sites to catalyze reaction consumption electrons. On the contrary, building blocks with electron-rich functional groups can construct region with negative charge, which is considerable

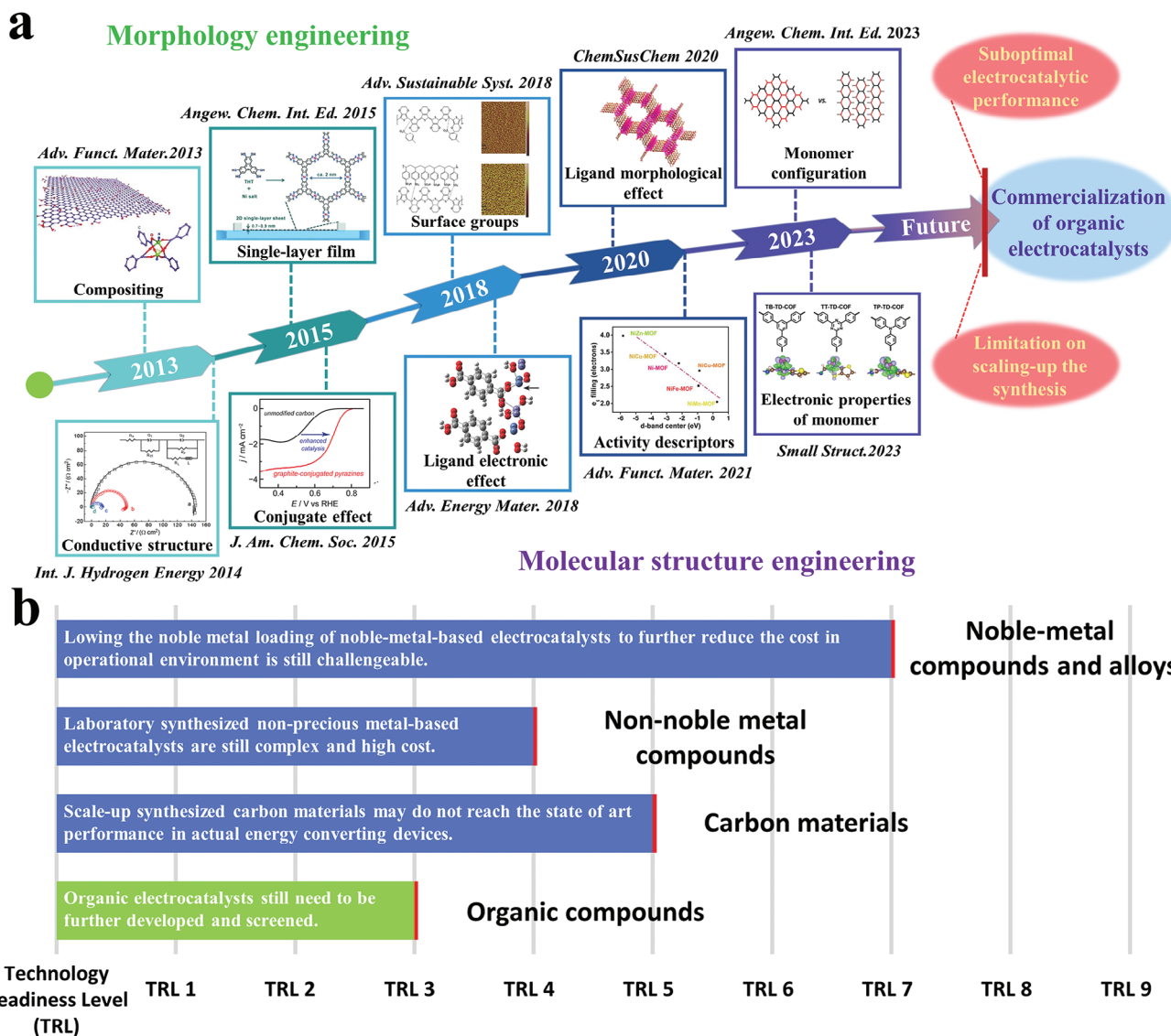


Figure 14. a) Development timeline of well-performed organic electrocatalysts preparation through morphology engineering and molecular structure engineering. b) TRLs of noble-metal compounds and alloys, non-noble-metal compounds, carbon materials, and organic compounds when used as electrocatalysts. Reproduced with permission. [14b,66,97,102,125–130] Copyright 2023, Wiley-VCH. Copyright 2021, Wiley-VCH. Copyright 2020, Wiley-VCH. Copyright 2018, Wiley-VCH. Copyright 2015, ACS. Copyright 2015, Wiley-VCH. Copyright 2014, Elsevier. Copyright 2013, Wiley-VCH.

reaction zone for oxidation reaction such as OER. Furthermore, the strategic selection of low-cost ligands and the use of facile green syntheses are also beneficial for the scale-up production of cost-efficient organic electrocatalysts. This is primarily because choosing low-cost ligands can directly reduce the cost of raw materials and facile green syntheses involving fewer steps and less complicated procedures often lead to increased efficiency and reduced the total production cost. Additionally, it is crucial to note that the selected ligand and its associated functional groups should possess stable chemical properties in aqueous, acidic, and alkaline environments with superior resistance to degradation. This factor is crucial for maintaining the durability of organic electrocatalysts during long-term use in real-world applications. Through adopting carefully considered building blocks for facile green synthesizing, a highly

efficient organic electrocatalyst with low cost is expected to be obtained.

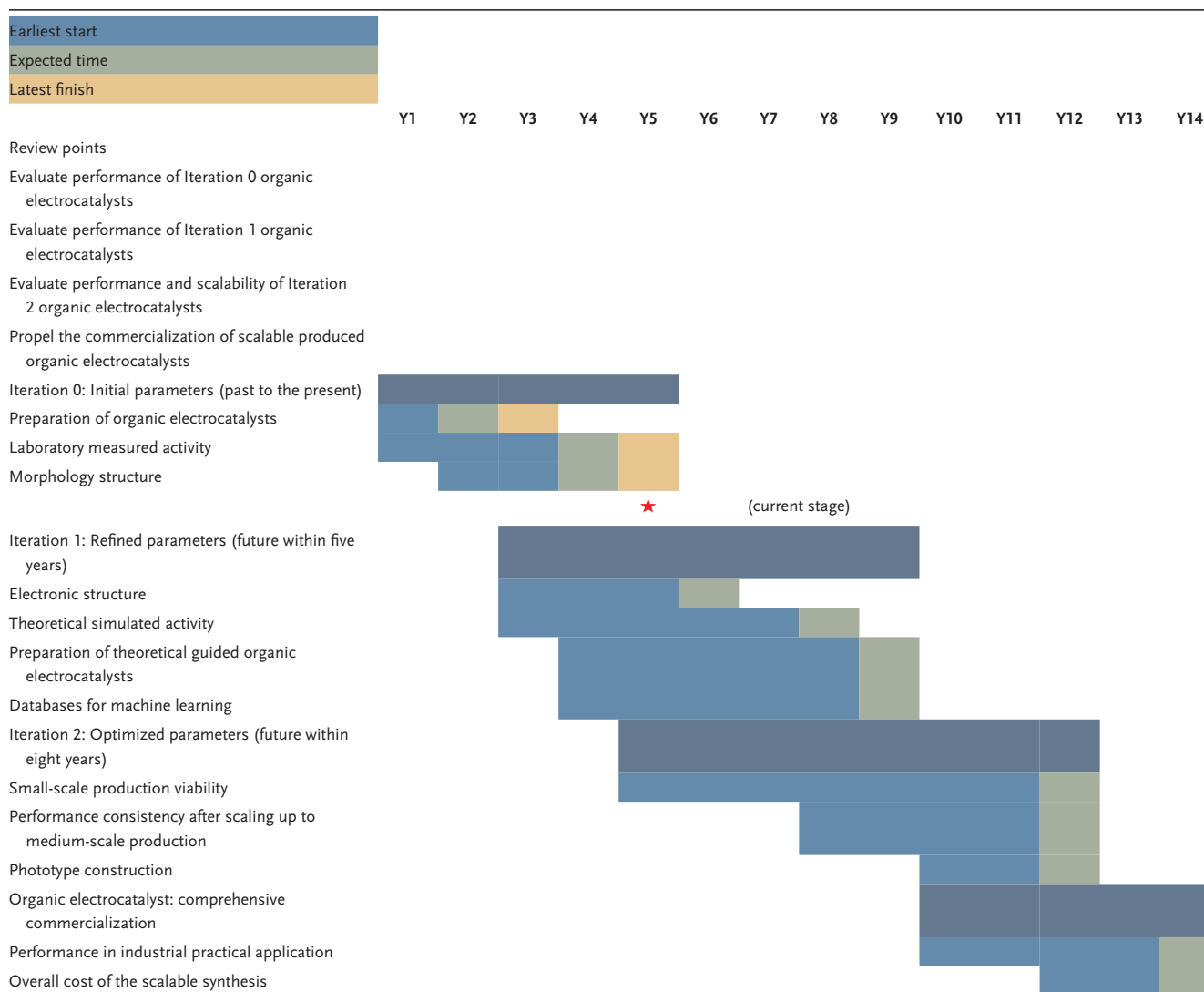
Although selecting fitted building blocks (including ligands and small organic molecule monomers) to regulate the morphology and molecular structure of the ultimate organic electrocatalyst becomes much more viable with the advancement of theoretical simulation and progressive refinement of electrocatalytic theory, the development of organic electrocatalysts is still in its early stages. A more detailed graph in Figure 14b reflects the technology readiness levels (TRLs) of organic electrocatalysts with other types of electrocatalysts currently being studied. Among them, noble-metal compounds and alloys are currently the most mature in development for hydrogen and oxygen electrocatalysts, available at a TRL of 7 (technology fully demonstrated in relevant environments with certain system prototype design in

operational environments) in fuel cells.^[131] After successfully lowering the noble-metal loading and scaling up the production, they are closest to comprehensive commercialization in an operational environment (TRL 9). For non-noble-metal compounds, the biggest challenge is that many laboratory-synthesized electrocatalysts are still complex and expensive,^[132] suggesting they are still limited at TRL 4. As a result, after extending them to relevant environments, further technology validations are still required. Carbon materials with concise synthesis usually possess considerable activity after scaling up the production in a relevant environment (TRL 5).^[133] However, inherent shortcomings of carbon materials such as oxidability and instability still limit demonstrating their performance in actual devices.^[134] Compared to the aforementioned electrocatalysts, organic electrocatalysts were the latest to be studied. The current TRL of organic electrocatalysts is only 3, which is because not only the moderate electrocatalytic performance of organic electrocatalysts com-

pared with metal-based electrocatalysts and noble-metal benchmarks but also the limitation on scaling up the synthesis. Many current studies have raised some scalable synthesis of organic electrocatalysts, however, their exhibited electrocatalytic activity is usually not competitive,^[135] indicating further research is still required for producing cost-effective organic electrocatalysts on a large scale. Therefore, future studies of organic electrocatalysts should focus on further screening cost-efficient organic electrocatalysts through both experimental proofing and theoretical simulating and simultaneously scaling-up the synthesis to pave the way for their future large-scale commercialization in various kinds of energy-converting devices.

To guide future research directions and prospect the development goals of organic electrocatalysts in the next decade, a Gantt chart of key research parameters of organic electrocatalysts for each iteration has been provided. As shown in **Table 2**, prior to now (Y1–Y5), only electrochemical measurements and

Table 2. Gantt chart for overviewing key research parameters of organic electrocatalysts in each iteration from the past to the future (The current stage of development is marked with a red star).



morphology characterizations of organic electrocatalysts were relatively thorough based on the general experience accumulated from previous research on other electrocatalysts.^[136] Moreover, in the past two years (Y3–Y5), the electronic structure and DFT simulation were also used to characterize organic electrocatalysts further revealing their electron and band properties and origin of activity.^[137] Moreover, with the assistance of machine learning, a database can be set up for effectively screening more well-performed organic electrocatalysts.^[138] Optimizing all these refined parameters can make the synthesis of efficient organic electrocatalysts more directed.^[139] However, analysis based on these parameters has not yet reached a completely thorough level and more in-depth studies need to be supplemented in the next few years (Y6–Y9). After all these difficulties are resolved, preparing high-efficient organic electrocatalysts in the laboratory becomes effortless and the TRL of organic electrocatalysts can progress from 3 to 4. Then, the production of well-designed organic electrocatalysts should be scaled up to meet the requirement of electrocatalyst application and demonstrated in a relevant environment.^[140] Meanwhile, the activity consistency of organic electrocatalysts before and after scaling up the production should also be validated. After settling all these concerns in a few more years (Y10–Y12), prototypes of efficient organic electrocatalysts can be constructed for competitive large-scale manufacturing and the corresponding TRL can reach 7. Subsequently, systems including large-scale manufacturing and applying cost-efficient organic electrocatalysts in various actual devices under operational conditions ought to be established for overviewing and qualifying the commercial value. Finally, after considering the practical and commercial optimizations of the system such as simplifying the synthesis, reducing the cost of building blocks, and increasing recyclability, the ultimate goal of organic electrocatalysts—comprehensive commercialization in operational environment (TRL 9)—will be achieved. Based on the past rapid development trend of organic electrocatalysts, we believe that achieving comprehensive commercialization of organic electrocatalysts is highly possible in the next decade (Y5–Y14).

4. Optimization of Organic Electrocatalysts for Practical Applications

As mentioned in the previous section, the ultimate goal in designing highly efficient organic electrocatalysts is to apply them to various kinds of actual devices. As indicated in Table 3, organic electrocatalysts can be utilized in numerous practical applications for energy storage and harvesting. However, applying various kinds of well-designed electrocatalysts in practical applications still confronts many challenges. This is primarily because many electrocatalysts with high laboratory-measured activity perform suboptimally under actual circumstances when assembled in devices. Additionally, the uncertain surface properties of many active substances result in poor compatibility with other ingredients while assembling electrodes.^[26] The former leads to unsatisfactory performance of the assembled device, which is inconsistent with the used electrocatalyst with originally excellent activity and the latter contributes to the low electrochemical durability and structural instability of the electrode, both of which significantly hinder the practical application of these green energy devices. The degradation in actual environments is due to laboratory measurements are only used to screen optimal electrocatalysts. When applying them in practical applications, many actual problems that can significantly affect the actual performance appear including low electrode wettability, low electrolyte affinity, structural instability of electrode under large currents, electrode powdering, inappropriate electrocatalyst loading, poor gas permeability of the electrode, etc. The noble-metal-based electrocatalysts are typical examples,^[141] in these electrocatalysts, noble-metal nanoparticles are usually mixed with carbon black to obtain better conductivity and dispersity.^[142] Nonetheless, these nanoparticles possess low compatibility with the carbon black substrate, which can be ascribed to the corrosion of the metal nanoparticles and the subsequent dissolution of the active substances especially in acid media under large currents. This results in poor stability and attenuated activity of these electrocatalysts and low performance of devices assembled with them.^[2f,143] Accordingly, materials that

Table 3. Organic electrocatalysts for oxygen and hydrogen electrocatalytic applications.

Electrocatalyst	Catalyst type	Catalyzed reaction	Application	Refs.
Ni(II) complexes	Small organic molecules	HER	Alkaline hydrogen production	[96]
Et-FI ⁺	Small organic molecules	OER	Acid water oxidation	[148]
PhAcrl	Small organic molecules	HER	Acid hydrogen production	[149]
PEDOT/CRO _{OH} -8-Ru	Oligomers	OER/HER	Alkaline water splitting	[39]
15-H ₂ O@CNT@GC	Oligomers	OER	Alkaline water oxidation	[150]
Cu ₂ (BEE) ₂	Oligomers	OER	Neutral water oxidation	[29b]
TAT-TFBE	Polymer	OER/HER	Alkaline water splitting	[151]
Au@PD-COP-II	Polymer	OER/HER	Alkaline water splitting	[152]
Co-COP	Polymer	ORR/OER	Zn–air battery	[153]
NiCoFe–NDA	MOF	OER	AEMWE	[154]
NCF-MOF	MOF	OER/HER	Alkaline water splitting	[155]
CdFe-BDC	MOF	OER/HER	Sea water splitting	[156]
Ni-TAPP-Co	COF	ORR/OER	Li–O ₂ battery	[157]
FePc-BBL COF	COF	ORR	Zn–air battery	[105]
TAPPCo-QA	COF	ORR	AEMFC	[158]

possess high activity compatibility in assembled electrodes (including substrate, current collector, binder, conductive enhancer, ionomer, etc.) of actual devices should be proposed to realize the practical application of low-cost electrocatalysts.

Building on the previous discussion, the electrocatalytic activities of organic compounds can be optimized by adjusting their intrinsic properties, thereby maximizing four major electrochemical characteristics, namely, the number of active sites, mass transfer, charge transfer, and intrinsic activity. Concurrently, organic electrocatalysts with massive functional groups exhibit high surface energy, endowing them with great compatibility in the electrode and electrolyte compared to inorganic electrocatalysts.^[144] This compatibility of organic electrocatalysts is determined by the oxidation/reduction potential of their surface functional groups and their interactions with other components. The functional groups' oxidation/reduction potential determines whether the organic electrocatalyst can maintain its original structure during electrocatalytic oxidation/reduction reactions,^[145] and the interactions between functional groups and other components are crucial for preserving the composition and architecture of the electrode.^[146] Consequently, the compatibility of an organic electrocatalyst can be effectively regulated by tuning the surface functional groups based on their oxidation/reduction potential and interaction strength with other components.

Overall, electrocatalysts based on organic compounds with optimizable electrocatalytic activity and compatibility hold significant potential for development as reliable electrocatalysts. These catalysts can offer excellent performance and durability in actual energy storage devices. Nevertheless, the aggregation and decomposition/transformation of organic structures, along with the corrosion of active species during use, are inherent shortcomings. These issues contribute to suboptimized performances and poor stabilities in energy storage/harvesting devices during operation, thereby limiting their practical applications.^[147] Here, three strategies have been proposed by utilizing the good compatibility and tunability of organic compounds in the electrode for fully demonstrating the activity of the original electrocatalysts further benefiting the performance of the assembled devices: 1) electrode structure designing, 2) electrode surface property modulating, and 3) membrane electrode fabricating. These strategies are critical for optimizing not only the mass/charge transfer process of the electrode with organic electrocatalysts during electrocatalytic reactions, but also the structural/compositional maintenance of the electrode. Simultaneously, two additional strategies focusing on the stability improvement of organic electrocatalysts in practical applications are also raised: 1) regulating electrolyte affinity and 2) introducing corrosion-resistant species. All these strategies are discussed in detail in the following section.

4.1. Integrated Electrode Structure Design

An electrode with a well-designed structure can usually exhibit superior performance in energy-converting devices. For organic compounds, their high compatibility characteristic allows the fabricated electrode with an organic electrocatalyst to demonstrate excellent performance and durability. This is primarily due

to reduced charge transfer resistance and dense contact between active substances and other components such as conductive enhancers and current collectors.^[56,159] Xue et al. designed a robust integrated electrode through in situ electrodeposition of polyaniline (PANI) and NiFe-OH on nickel foam (**Figure 15a**).^[146a] The introduction of PANI can not only enhance the integral structural compatibility but also optimize the oxidation state of NiFe-OH to further OER electrocatalytic activity. The Nyquist plots exhibit that the NF/PANI/NiFe-OH possesses not only the lowest charge transfer resistance of 1.27 Ω but also the highest intrinsic activity revealed by TOF calculation among all samples (**Figure 15b,c**). The improved electrocatalytic performance of NF/PANI/NiFe-OH with a freestanding structure can be ascribed to the tight interactions between the PANI layer, NiFe-OH, and NF. The chronoamperometric curves at different current densities in **Figure 15d** show that the NF/PANI/NiFe-OH can maintain stable plateaus under 100/350 mA cm⁻², and the surface structure of NF/PANI/NiFe-OH after 26 h can also be retained without destruction (inset of **Figure 15d**). The PANI serves as a medium with a stabilizing effect (caused by the surface NH— functional groups with high oxidation potential) for forming densely contacted freestanding structures with high compatibility, explaining the superior electrochemical durability and structural durability of NF/PANI/NiFe-OH.

For MOF-based electrocatalysts, the existence of functional groups on organic ligands that can react with the metal collector allows the in situ coordinated MOF to directly grow on the surface of the metal collector to form a freestanding electrode without a binder and conductive enhancer.^[14b] Xu et al. used a hydrothermal method to in situ decorate Ni-ZIF on the surface of nickel foam, and then the integrated Ni-ZIF@NF was boronized to form Ni-ZIF/Ni-B@NF with a freestanding structure.^[160] Due to the extended structure caused by the in situ growth of Ni-ZIF, abundant crystalline-amorphous phase boundaries can be exposed to provide more active sites, accelerating the mass diffusion for both OER and HER. The performance of the water electrolyzer with Ni-ZIF/Ni-B@NF anode and cathode greatly outperforms that with Pt/C cathode and IrO₂ anode, which can be associated with the facilitated mass transfer of Ni-ZIF/Ni-B@NF with freestanding structure.

Elucidating the role of each component and revealing the interaction between different components in the electrode can provide insightful instruction for the rational design of electrode structure, which can fully demonstrate the activity of organic electrocatalyst. Electrospinning is an efficient strategy for weaving self-supporting electrodes. In a study conducted by Yang et al.,^[19a] the role of various compounds in the composited electrode is clearly illustrated. The fabrication progress of the composited electrode involves directly polymerizing the cobalt-based covalent organic polymer (Co-COP) on the surface of acid-functionalized graphite carbon (AFGC) to form Co-COP/AFGC. The Co site in the Co-COP is highly efficient for ORR, and the AFGC can not only enhance the conductivity but also increase the diffusion rate of oxygen of Co-COP/AFGC (**Figure 15e**). Then, the Co-COP/AFGC was uniformly mixed with polyacrylic acid (PAA), polyvinyl alcohol (PVA), and binder for electrospinning. After esterification, the cross-linked nanofibers consisting of PAA and PVA serve as substrates for uniformly dispersing Co-COP/AFGC.

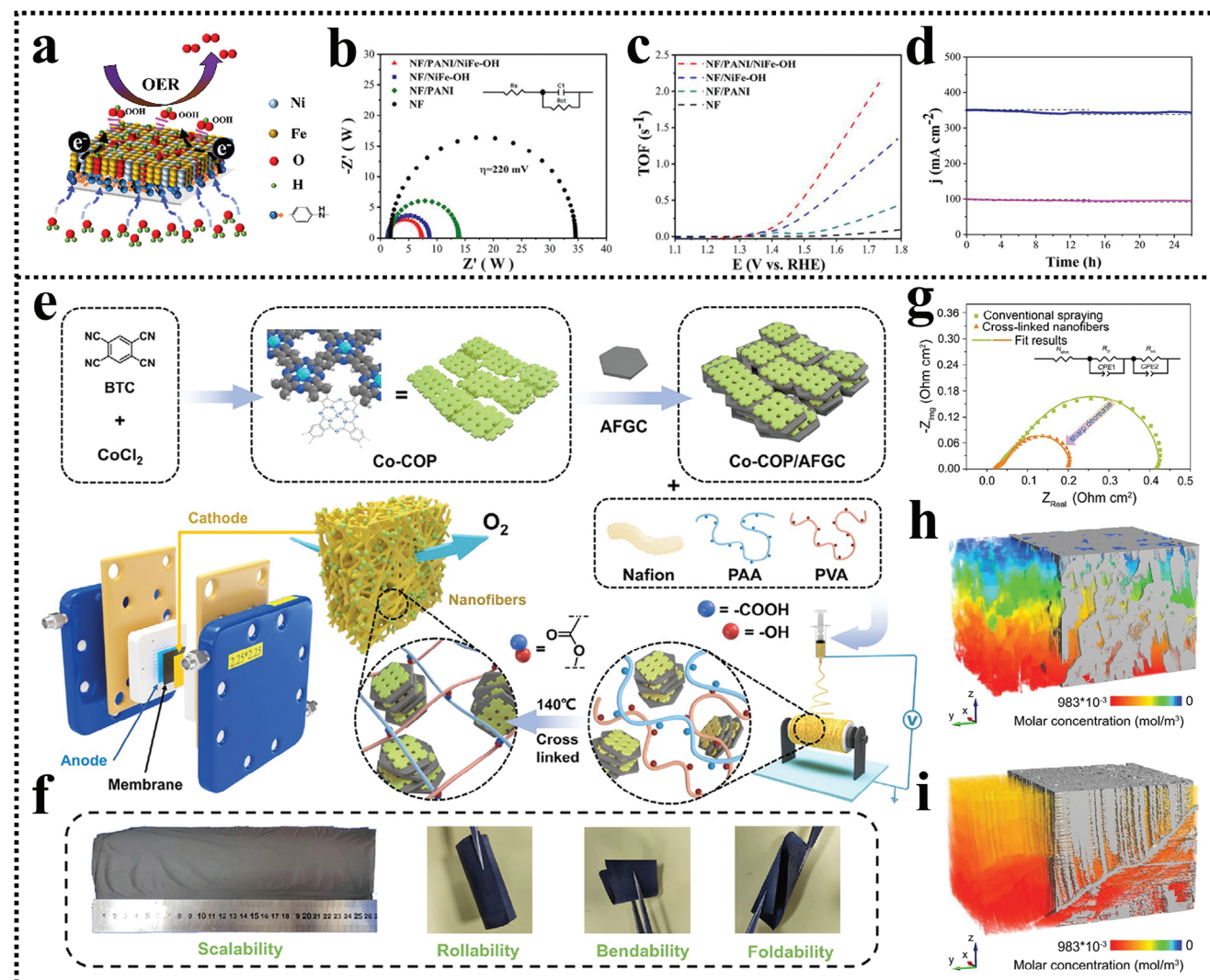


Figure 15. a) OER mechanism of NF/PANI/NiFe-OH. b) EIS plots and c) LSV curves of NF/PANI/NiFe-OH and its counterparts. d) Stability chronoamperometric test of NF/PANI/NiFe-OH under different current densities. Reproduced with permission.^[146a] Copyright 2022, Elsevier. e) Electrospinning assisted fabrication progress and f) optic photos of the uniform composited nanofiber electrode with Co-COP/AFGC. g) EIS plots of composited nanofiber electrode and conventional spraying electrode. Oxygen diffusion at h) composited nanofiber electrode and i) conventional spraying electrode. Reproduced with permission.^[19a] Copyright 2023, Wiley-VCH.

Due to the interaction between functional groups, the Co-COP forms dense contacts with AFGC and cross-linked nanofibers through both chemical and hydrogen bonds, resulting in a uniform nanofiber membrane (Figure 15f). This phenomenon manifests the high compatibility of organic electrocatalysts. The obtained composited freestanding air cathode possesses high flexibility, even more, the EIS measurement suggests that the fabricated electrode possesses much lower charge transfer resistance (Figure 15g). Furthermore, through computational fluid dynamics simulation, the oxygen diffusion in the freestanding nanofiber electrode and conventional slurry-casted electrode are shown in Figure 15h,i. The nanofiber air cathode exhibits a much larger area for oxygen and Co-COP contact, which is extremely beneficial for fast transferring oxygen to the Co active site for thorough ORR. The improved charge transfer and mass transfer of the freestanding nanofiber electrode can be attributed to

the high compatibility of Co-COP with conductive enhancers and organic substrates. This result also highlights the advantages and uniqueness of organic materials in the preparation of electrodes.

4.2. Electrode Surface Property Modulation

The control of surface wettability at active sites has been employed to alter the activity and selectivity by manipulating the interactions between heterogeneous electrocatalysts and reactants.^[161] Furthermore, in practical applications, the surface properties of the electrode can greatly affect the exhibited electrocatalytic performance by controlling the effective collision between reactants and active centers on the surface of the electrode.^[81] For organic compounds, their surface properties

(such as hydrophilic/hydrophobic properties) are mainly determined by the functional groups attached to their skeletons. These surface properties can be precisely and flexibly regulated.^[162] For instance, fluorine-containing groups can effectively enhance the hydrophobicity,^[163] while oxygen-containing functional groups can improve the hydrophilicity.^[164] This is because the polarity of the linked functional groups has a strong correlation with wettability; functional groups with high polarity are much more favorable for solvating in nonpolar solvents (such as water).^[165] For that reason, assembling well-designed organic compounds in the electrode can effectively optimize the electrode surface properties to achieve better performance.

For energy-converting devices using ion exchange membranes including AEMFC/PEMFCs, the surface properties of the membrane electrode assembly (MEA) are critical for fully unlocking the full potential of the electrocatalyst to achieve better performance in a real-world environment. Due to the tunable surface property and high compatibility of organic compounds, assembling them into the MEA can effectively boost the performance of the energy-converting device with ion exchange membranes. During the electrocatalytic reaction, the organic compound in MEA can be considered as a type of cocatalyst by strengthening the catalyst-ionomer reaction.^[166] Zhai et al. synthesized a novel kind of COF functionalized with phosphotungstic acid (P-COF) and incorporated it into the MEA of PEMFC (Figure 16a).^[167] The bonded phosphotungstic acid on COF greatly increases its hydrophilicity further enhancing the water uptake. Apart from that, the strong acidity of phosphotungstic acid in P-COF can accelerate the proton transfer in MEA during discharging, which greatly facilitates the electrocatalytic reaction on the electrode. These benefits of P-COF result in the ultrahigh maximum power density of PEMFC with P-COF.

In addition, the interaction between reactants and active sites on the electrode is also a critical factor controlling the catalytic efficiency and the ultimate performance of energy-converting devices.^[168] Assembling organic electrocatalysts with tunable surface properties into the electrode is beneficial for obtaining electrodes with desirable hydrophilicity/hydrophobicity for electrocatalytic reactions. Li et al. have coated a porphyrin covalent organic framework (POF) on the surface of CNTs to construct an interwoven film as the air cathode for a Zn-air battery.^[169] Due to the rich functional groups on POF, its surface exhibits high hydrophilicity. After integrating with CNTs, the contact angle of the CNT@POF composite is greatly reduced (Figure 16b). By the way, the CNT@POF exhibits excellent flexibility under bending (Figure 16c), which can be attributed to the high compatibility of POF with CNTs. This is because the conjugated POF tends to grow on the analogously conjugated graphited surface of the CNT through intermolecular π - π interactions, as a result, this growth mechanism can finely retain the original 1D structure of the CNT scaffold (Figure 16d). The fabricated CNT@POF freestanding air cathode exhibits superior charging/discharging performance in a Zn-air battery with great stability after 200 cycles (Figure 16e), which can be attributed to the optimized surface properties and structural robustness of the electrode. In situations with gas reactants, the adhered gas reactants on the electrode isolate the electrolyte and active sites, which greatly reduce the three-phase boundary and further hinder the electrocatalytic reaction. Accord-

ingly, increasing the hydrophobicity of electrodes can boost the desorption rate of gas reactants, further alleviate the block effect of gas reactants to the active sites, and enhance reaction kinetics. Cao et al. used fluorinated COF named TpF6 to decorate the FeNi LDH.^[71e] With massive fluorine groups, TpF6 can greatly enhance the hydrophobicity of the electrode. Digital images of the electrodes with FeNi LDH and TpF6 decorated FeNi LDH (denoted as FeNi LDH-TpF6-2) show that the released oxygen bubble can remain nearly unchanged after 10 s on the surface of FeNi LDH-TpF6-2, suggesting its superior hydrophobicity, which is beneficial for not only the oxygen transportation on the surface of the electrode during ORR but also the oxygen desorption during OER (Figure 16f,g). This superior hydrophobicity of FeNi LDH-TpF6-2 cathode is further confirmed by its largest measured contact angles and oxygen adhesion force (Figure 16h,i). Moreover, theoretical calculation is also conducted to evaluate the oxygen adsorption on FeNi LDH-TpF6-2. Oxygen molecules transport much faster on the surface of TpF6 compared with its COF counterparts without fluorine decoration, further suggesting that fluorine chains in TpF6 play a key role in facilitating the oxygen delivery on the electrode (Figure 16j). Furthermore, the Zn-air battery with FeNi LDH-TpF6-2 cathode exhibits great charge/discharge performance with excellent durability after 800 cycles, which is also ascribed to the construction of the efficient oxygen transport pathway in TpF6 with high hydrophobicity (Figure 16k).

4.3. Membrane Electrode Fabrication

Another approach for fully unleashing the electrocatalytic potential of organic electrocatalysts in practical applications (such as fuel cells and water electrolyzers) involves designing an MEA system to promote the mass and charge transfer on the electrode to obtain better performance.^[28,154] Organic electrocatalysts with their unique regulatability and compatibility can be used to optimize the structure of the electrode. For example, Chang et al. incorporated COF in the catalyst layer during the assembling process of MEA. Through mixing in the catalyst layer (CL) and integrating with the microporous layer, a novel kind of gradient catalyst layer (G-CL) is constructed (Figure 17a).^[170] The introduction of COF can boost not only the proton transferability but also the electron transfer. The EIS curves show that incorporating COF into MEA has a negligible effect on the ultralow ohmic resistance (R_1) of the MEA ($\approx 0.4 \Omega$, mainly contact resistance of different layers). Moreover, the introduction of COF can greatly reduce the electrode reaction resistance (R_2), primarily because COF inhibits the agglomeration of catalysts and further exposes more active sites for electrocatalytic reaction (Figure 17b,c). These results clearly evidence that organic electrocatalysts are much more suitable for assembling MEA compared with other electrocatalysts due to their great compatibility.

Another reason for adopting organic electrocatalysts in MEA is that organic electrocatalysts with functional groups and great compatibility can finely combine with graphitized carbon materials to achieve better electrocatalytic performance. As shown in Figure 17d, the composite of thiophene-enriched fully conjugated 3D COF and CNT (BUCT-COF-11/CNT) exhibits much

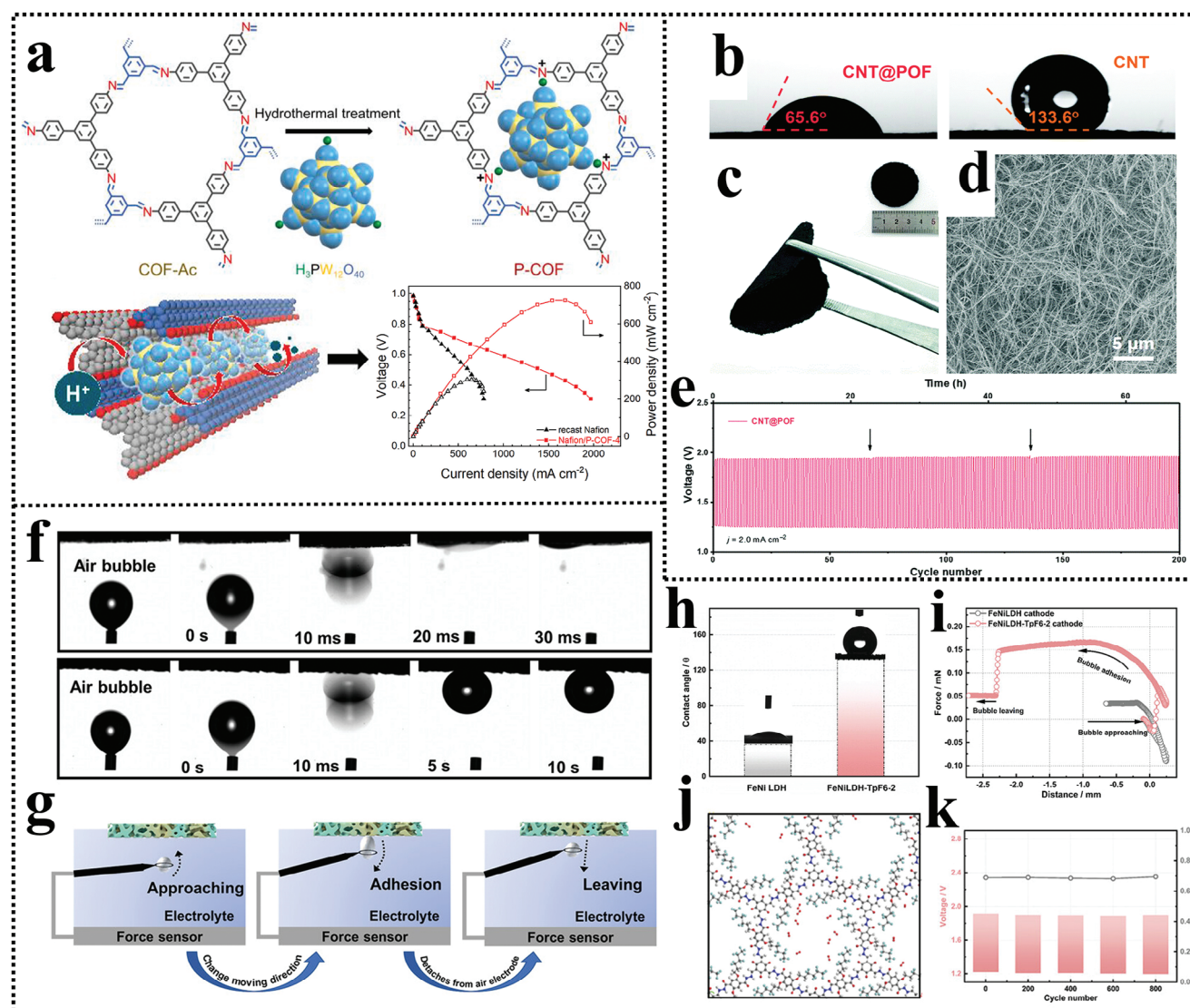


Figure 16. a) Synthesis and discharge performance of P-COF in PEMFC. Reproduced with permission.^[167] Copyright 2023, Elsevier. b) Contact angle measurement of CNT and CNT integrated with POF. c) Optic photo and d) SEM image of the CNT@POF interwoven film. e) Long-term charging/discharging test of Zn-air battery with CNT@POF cathode. Reproduced with permission.^[169] Copyright 2018, RSC. f) Optic photos of FeNi LDH and FeNi LDH-TpF6-2 during OER. g) Models for gas adhesion property measurement. h) Contact angle and i) oxygen adhesion measurements of FeNi LDH and FeNi LDH-TpF6-2. j) Simulated oxygen transportation of TpF6. k) Long-term cycling test of Zn-air battery with FeNi LDH-TpF6-2 cathode. Reproduced with permission.^[71e] Copyright 2023, Wiley-VCH.

better ORR catalytic performance than CNT and BUCT-COF-11.^[171] This is because the CNT can greatly boost the conductivity and further transport more electrons to the active site for ORR, which fully utilizes the highly efficient active sites on BUCT-COF-11. This successful combination between BUCT-COF-11 and CNT is mostly due to the unique properties of organic electrocatalysts. With massive functional groups, the BUCT-COF-11 can combine with CNT through both chemical bonds and van der Waals interactions, resulting in the superior catalytic performance of their composite product. Therefore, this property of organic electrocatalysts can be perfectly utilized in the area of fuel cell/water electrolyzer electrode designing because graphitic carbon conductive enhancer is an essential part of

MEA. The assembled AEMFC with BUCT-COF-11/CNT in MEA exhibits much higher maximum power density than AEMFC with BUCT-COF-11 in MEA (Figure 17e,f), which is also because the superior combination between BUCT-COF-11 and CNT.

Designing MEA systems with ultralow inner resistances is also appealing for the development of a water electrolyzer under large currents. Organic electrocatalysts with massive functional groups can also easily be in situ decorated on the current collector. Yue et al. in situ decorated a trimetallic MOF on nickel foam to obtain a binder-free electrode through a coronation/electrochemical transformation synthesis (Figure 17g).^[154] The binder-free electrode only needs an

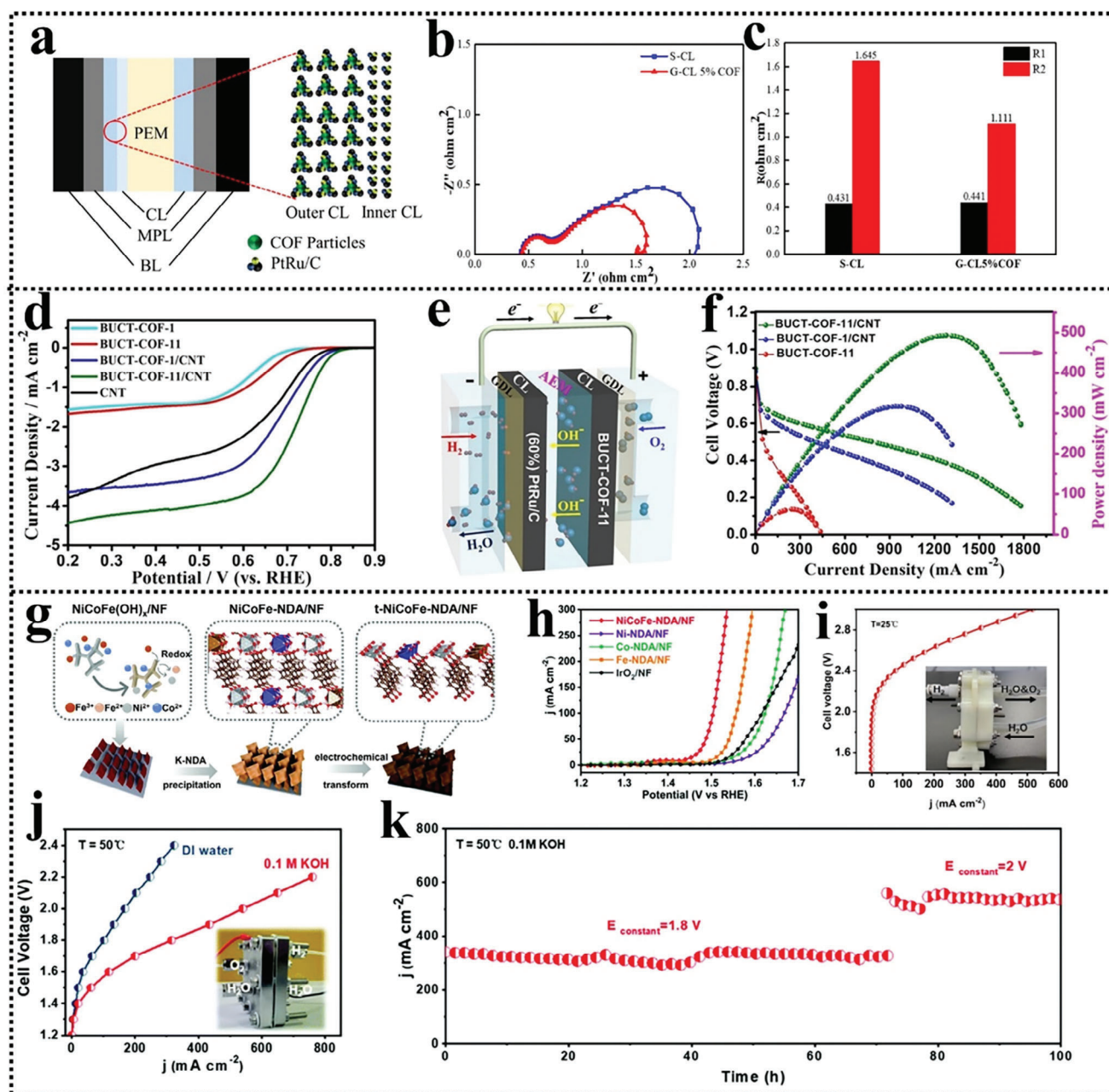


Figure 17. a) Graphic illustration of the MEA with G-CL structure. b) Measured EIS curves and c) calculated resistance values of MEAs. Reproduced with permission.^[170] Copyright 2022, Elsevier. d) LSV curves of BUCT-COF-11/CNT and its counterparts. e) Illustration of the AEMFC structure. f) Discharge performance of AEMFCs with different cathodic electrocatalysts. Reproduced with permission.^[171] Copyright 2023, Wiley-VCH. g) Synthesis of the binder-free electrode with trimetallic MOF. h) LSV curves of binder-free electrodes with MOFs. Polarization curves of i) AEMWE and j) PEMWE using MOF decorated binder-free electrodes. k) Long-term stability measurement of MOF binder-free electrode in AEMWE cell. Reproduced with permission.^[154] Copyright 2021, RSC.

overpotential of $\approx 300 \text{ mV}$ to reach a large current density of 300 mA cm^{-2} , which is also attributed to the low charge resistance (Figure 17h). Furthermore, when assembled in MEA systems, the performance of the trimetallic MOF binder-free electrode can be further revealed. Due to the dissolution of Ni current collector, the performance of PEMWE with trimetallic MOF binder-free electrode is moderate (Figure 17i). Nonetheless,

when this kind of MOF is assembled in AEMWE, due to the high compatibility of MOF, the integration between MOF and Ni current collector is compact with ultralow charge resistance. Moreover, the assembly of MEA further reduces the inner resistance of the water electrolyzer, which is beneficial for achieving large current density under a low cell voltage. The onset potential of AEMWE with trimetallic MOF binder-free electrode in

both deionized water and 0.1 M KOH is only 1.4 V (Figure 17j). Furthermore, at a constant external cell voltage of 1.8 and 2.0 V, the AEMWE with trimetallic MOF binder-free electrode exhibits nearly no current attenuation under large currents after 100 h, manifesting the superior stability of the MEA system with self-supported electrode (Figure 17k).

4.4. Optimization of the Affinity with Electrolyte

The aggregation of active species is one of the important factors causing the degradation of an electrocatalyst during long-term use. This substantially hinders the practical application of most small molecule and oligomer-based organic electrocatalysts, which have a low molecular weight and a high tendency to aggregate. To overcome this weakness, strategies should focus on optimizing the affinity of organic electrocatalysts with the electrolyte to prevent aggregation and increase dispersity. For instance, Sun et al. used an rGO substrate to immobilize and disperse eight layers of Ni-/Co-porphyrin complexes ($\text{Ni}^{2+}/\text{THPP}/\text{Co}^{2+}/\text{THPP}$)₈ with rich oxygen-containing functional groups through hydrogen bond and π - π stacking, and the rGO/($\text{Ni}^{2+}/\text{THPP}/\text{Co}^{2+}/\text{THPP}$)₈ composite exhibited superior stability in water, which can remain stable and uniform dispersion for 5 months (Figure 18a).^[172] This improved water affinity greatly contributed to the better stability of rGO/($\text{Ni}^{2+}/\text{THPP}/\text{Co}^{2+}/\text{THPP}$)₈ compared to the Ir/C benchmark in the alkaline aqueous electrolyte (Figure 18b). Furthermore, the addition of a solution medium in the electrolyte can also modulate the affinity of organic electrocatalysts to enhance stability. Ruan et al. reported that the OER stability of N-substituted glycine oligomer $\text{Cu}_2(\text{BEE})_2$ electrocatalyst was enhanced by adding a borate buffer solution medium. This medium coordinated with $\text{Cu}_2(\text{BEE})_2$ to stabilize the metal center of $\text{Cu}_2(\text{BEE})_2$ via H-bonding (Figure 18c,d).^[29b] The UV-vis spectra of $\text{Cu}_2(\text{BEE})_2$ before and after controlled potential electrolysis displayed that the structure of $\text{Cu}_2(\text{BEE})_2$ remained nearly intact after OER (Figure 18e). Moreover, the attenuation of charge accumulation and evolved oxygen was less than 10% after four repeating controlled potential electrolysis (CPE) cycles (Figure 18f,g).

4.5. Corrosion-Resistant Species Employment

Another significant challenge for the long-term use of electrocatalysts is the corrosion of active species. Fortunately, organic electrocatalysts usually possess confirmed active sites, making it easier to discern the corrosion of active sites. Despite this, organic electrocatalysts, especially those with metal active sites are still susceptible to corrosion.^[173] Introducing corrosion-resistant species into the system is a promising strategy to inhibit the corrosion of organic electrocatalysts and further extend their service life. For instance, one of the main challenges of producing hydrogen through electrolysis in seawater is that the hypochlorite byproduct on the anode can corrode the electrocatalysts leading to rapid degradation. To prevent the formation of harmful hypochlorite, N_2H_4 was added into the seawater electrolyte to prevent the corrosion of the MIL-(IrNiFe) MOF electrocatalyst (Figure 19a).^[174] Because the theoretical potential for hydrazine

oxidation reaction (HzOR) is much lower than those of OER and chlorine evolution reaction (CLER),^[175] the added N_2H_4 can not only negatively shift anodic oxidation potential for reducing the splitting voltage of water, but also serve as a type of corrosion-resistant species to prevent the activation of CLER for generating corrosion sources. Therefore, the overpotential to reach the current densities of 200, 400, 600, 800, and 1000 mA cm^{-2} was significantly reduced after adding N_2H_4 (Figure 19b), and the long-term stability of the seawater electrolyzer with the addition of N_2H_4 is significantly improved at large current densities (Figure 19c,d). Apart from that, the corrosion-resistant species (or its precursor) can also be directly decorated on organic electrocatalysts for stability enhancement. Fan et al. prepared an MOF-based electrocatalyst consisting of MOF and CoB on carbon cloth (denoted as CoB@MOF@CC) for overall water splitting.^[176] The CoB in the electrocatalyst serves as a type of protective phase and undergoes partial oxidation during OER. During this process, an ultrathin layer of CoOOH was formed as a corrosion-resistant species to prevent the corrosion of the MOF active defect site during long-term use under harsh conditions. The FTIR spectra show that peak positions of both post-HER and post-OER samples were nearly unvaried, demonstrating superior structural maintenance and electrochemical stability of CoB@MOF@CC (Figure 19e). As a consequence, the in situ transformed protective anticorrosion layer can be considered as the predominant factor resulting in the excellent durability of CoB@MOF@CC toward 360 h overall water splitting in various kinds of harsh electrolytes including alkaline solution with NaCl/seawater/rainwater/urea (Figure 19f-i).

In all, the application of organic electrocatalysts with promising catalytic activity and stability to various practical applications requires careful consideration. Not only their electron transfer and mass transfer processes on the electrode ought to be considered to avoid exhibiting mismatched suboptimal performance, but their affinity with the electrolyte and the system's anticorrosion property of the system should also be taken into account to ensure long-term stability. The unique characteristics of organic electrocatalysts should be exploited in practical applications to fully reveal their inherent activity. First, owing to the high compatibility of organic electrocatalysts, they can be compactly decorated on other conductive supports to form integrated electrodes with low charge resistance. Second, the high tunability of organic electrocatalysts plays a key role in determining the surface wettability of the electrode, which can greatly affect the mass transfer and effective collision between reactants and active sites. Third, through assembling MEA, both the charge and mass transfer on the electrocatalyst can be greatly enhanced and the catalytic efficiency (usually identified by the reaction current) can be improved exponentially. Besides, to achieve satisfactory stability of organic electrocatalysts in practical applications, it is highly recommended to optimize both the structure of organic electrocatalysts and the additional conductive species in the system. Initially, the electrolyte affinity of organic electrocatalysts can be optimized by designing ideal functional groups that can stabilize the reaction intermediate or coordinate with the solution medium, significantly inhibiting the aggregation of active species. Taking second place, the employment of special anticorrosion species in the system can effectively protect the active sites on the organic electrocatalyst from corrosion during

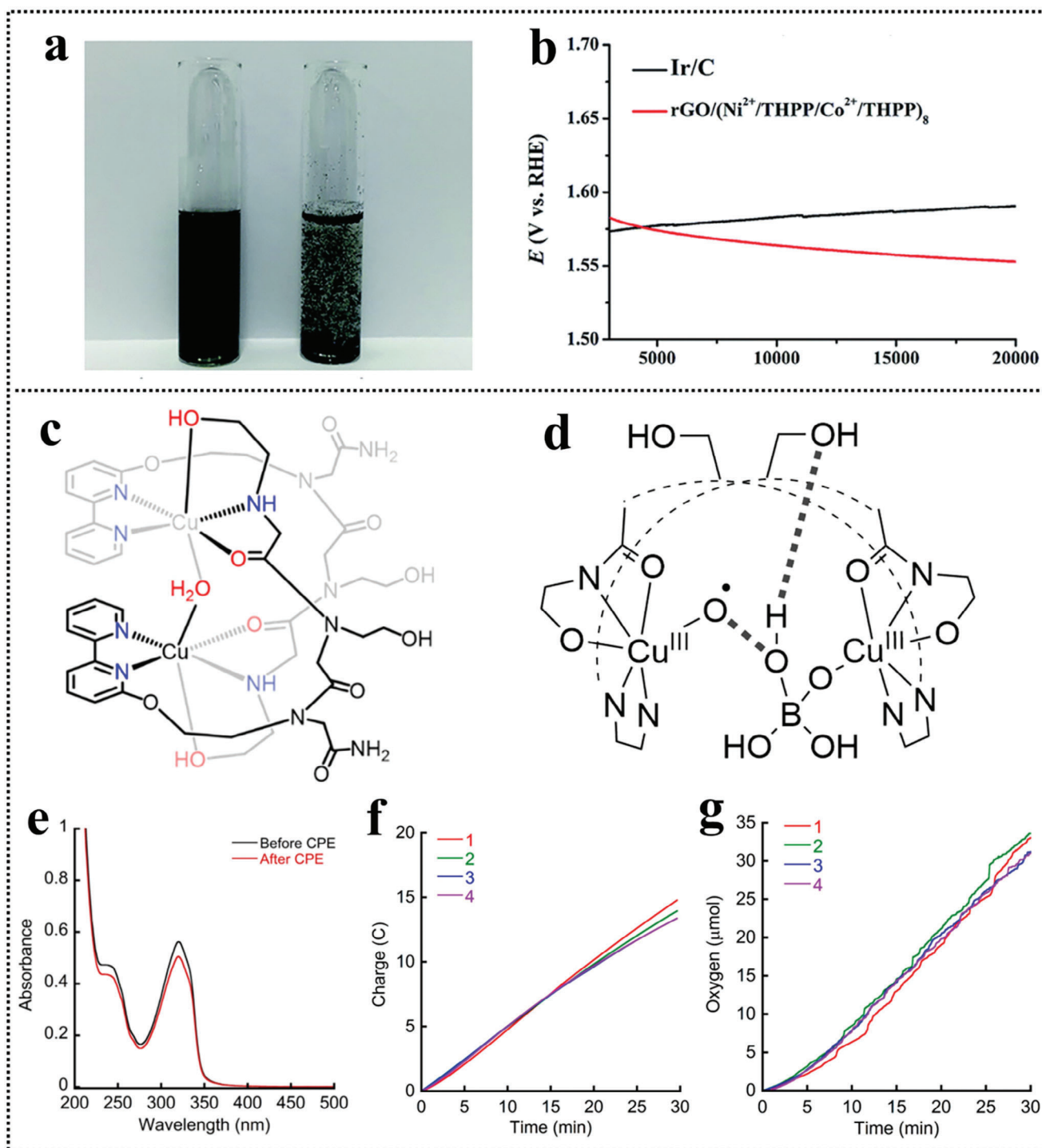


Figure 18. a) Dispersed suspensions of $\text{rGO}/(\text{Ni}^{2+}/\text{THPP}/\text{Co}^{2+}/\text{THPP})_8$ (left) and rGO (right) after aging for 5 months. b) Chronopotentiometry curves of $\text{rGO}/(\text{Ni}^{2+}/\text{THPP}/\text{Co}^{2+}/\text{THPP})_8$ and Ir/C benchmark. Reproduced with permission.^[172] Copyright 2016, RSC. Configuration of c) $\text{Cu}_2(\text{BEE})_2$ and d) $\text{Cu}_2(\text{BEE})_2$ adsorbed with borate buffer solution medium. e) UV-vis spectra of $\text{Cu}_2(\text{BEE})_2$ before and after CPE test. f) Charge accumulation and g) evolved oxygen during repeat CPE cycles. Reproduced with permission.^[29b] Copyright 2021, American Chemical Society.

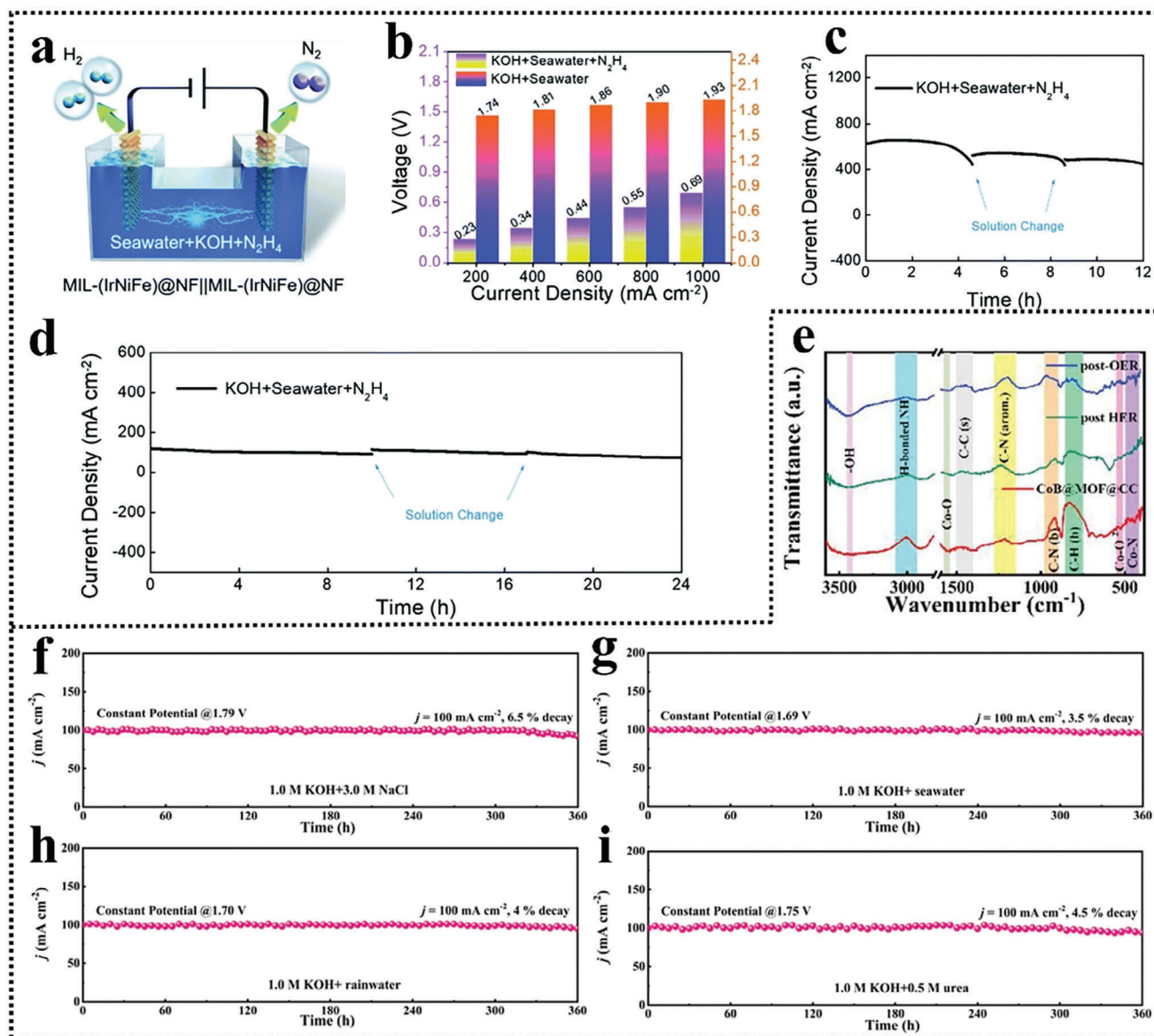


Figure 19. a) Schematic illustration of the MIL-(IrNiFe) MOF seawater electrolyzer. b) Water splitting voltage of the MIL-(IrNiFe) MOF seawater electrolyzer with/without N₂H₄ in the electrolyte. c,d) Chronopotentiometry curves of the MIL-(IrNiFe) MOF under different current densities. Reproduced with permission.^[174] Copyright 2021, RSC. e) FTIR spectra of raw, post-OER, and post-HER CoB@MOF@CC. Chronopotentiometry curve of CoB@MOF@CC for overall water splitting at 100 mA cm⁻² in alkaline electrolyte with f) 3 M NaCl, g) seawater, h) rainwater, and i) 0.5 M urea. Reproduced with permission.^[176] Copyright 2022, Wiley-VCH.

electrocatalytic reactions, thereby extending their lifetime. Taking everything into account, a systematic overview is also depicted based on the aforementioned optimization strategies from the perspectives of both the matching degree between the exhibited performance and laboratory-measured activity and stability during long-term use. This overview addresses the primary challenges and provides a considerable future enhancement of organic electrocatalysts for practical applications (Figure 20). All these strategies are instrumental in achieving large-scale application and commercialization of organic electrocatalysts in various energy storage/harvesting devices.

5. Conclusion and Prospect

5.1. Conclusion of Design and Application of Cost-Efficient Organic Electrocatalyst

In the realm of cost-effective electrocatalysts devoid of noble metals, organic compounds emerge as promising and exceptionally viable candidates, thanks to their inherent advantages. For instance, their recyclability and degradability render them a more sustainable and environmentally friendly choice when employed as electrocatalysts. Furthermore, their pronounced periodicity and well-defined structure simplify the identification of

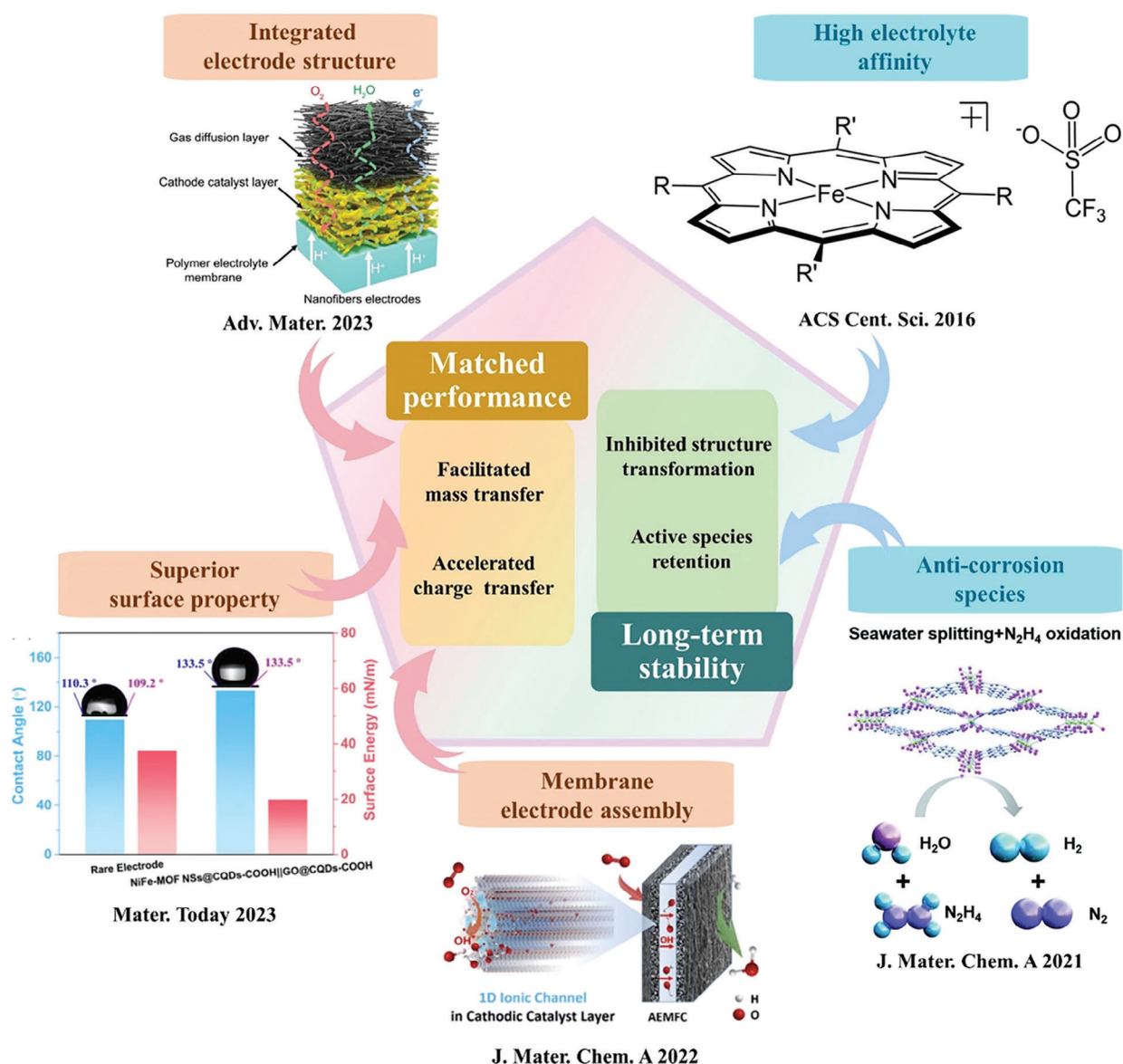


Figure 20. Prospects on the future enhancement of organic electrocatalysts for practical applications. Reproduced with permission.^[19a,158,174,177] Copyright 2023, Wiley-VCH. Copyright 2023, Elsevier. Copyright 2022, RSC. Copyright 2021, RSC. Copyright 2016, ACS.

the factor that determines activity when catalyzing various types of electrocatalytic reactions. Additionally, their innate compatibility ensures thorough contact with other components when assembling electrodes for practical applications. These advantages collectively indicate that the development of affordable organic electrocatalysts holds significant promise for cost reduction in a wide range of green energy devices. The four primary categories of organic electrocatalysts—small organic molecules, oligomers, polymers, and organic frameworks exhibit unique physicochemical properties. Consequently, the structural and physicochemical characteristics influencing the observed electrocatalytic performance also vary among these categories. To elucidate the catalytic mechanism of these organic electrocatalysts and establish a distinctive structure–activity relationship, we have introduced four key electrochemical attributes: number

of active sites, mass transfer, charge transfer, and intrinsic activity. This approach aims to provide a comprehensive understanding of the connection between electrocatalytic activity and the structural/physicochemical properties of these catalysts. Utilizing the identified electrochemical characteristics, the structural and physicochemical properties of various organic electrocatalysts can be employed as indicators or descriptors of their electrocatalytic activities. This categorization can offer valuable insights to inform the strategic development of cost-effective organic electrocatalysts.

More importantly, based on the development timeline for optimizing and preparing well-performed organic electrocatalysts, a systematic roadmap for combining all the advantages of optimizations from various aspects (number of active sites, mass transfer, charge transfer, and intrinsic activity) on one

organic electrocatalyst, can be proposed. Through selecting building blocks, nearly all physicochemical properties that can be recognized as activity indicators/descriptors (pore/channel structure, surface group, charge distribution, electron state, conjugation degree, etc.), can be effectively controlled and modulated. The main structure of organic electrocatalysts usually consists of C, H, N, and O. Moreover, most organic electrocatalysts do not contain metallic elements (such as metal-free small organic molecules, polymers, and COFs), indicating they are unrestricted by mineral resource reserves. The geometry and size of building blocks directly determine the pore/channel structure and conjugation degree and configurations of linked functional groups are more related to the efficiency of active sites for electrocatalytic reactions. Given that the elemental, structural, and geometric variables of organic catalysts adhere to clear and defined rules, machine learning will be a valuable tool for expediting the process of identifying the optimal organic catalyst in terms of activity, stability, cost-effectiveness, and scalability, provided that we have access to an initial high-quality dataset. After optimizing organic electrocatalysts in terms of both morphology and molecular structure through repeated screening of building blocks and measuring the electrocatalytic performance of the final product, these catalysts not only possess a well-designed interconnected pore/channel structure to expose numerous active sites and facilitate mass diffusion but also an optimized molecular structure with a conductive skeleton and high-quality active sites.

Furthermore, by evaluating the technology readiness levels of organic electrocatalysts, future-stage goals for these catalysts are also outlined. In the near future, a comprehensive system, including theoretical simulation, batch screening, scaling up production, and application under operational conditions, could be established to design efficient and applicable organic electrocatalysts, thus achieving comprehensive commercialization.

At last, to enhance the viability of well-designed organic electrocatalysts in actual devices, five strategies including tuning the surface property of the electrode, constructing integrated electrode structure, fabricating membrane electrode assembly, electrolyte affinity regulating, and corrosion-resistant species applying have been discussed. These strategies can either enhance the mass/charge transfer ability on the electrode or the durability of the whole electrocatalytic system, which are favorable for fully revealing the original electrocatalytic activity and achieving long-term stability of these organic electrocatalysts in practical applications. Overall, we have thoroughly summarized the classification, activity-determining structural/physicochemical properties, and electrode-designing strategies of organic electrocatalysts. By gaining a deeper understanding of these properties in organic electrocatalysts, a robust structure–activity relationship can be established, effectively bridging the gap between measured electrocatalytic activity and our understanding of it.

5.2. Current Challenges and Future Prospects

Despite our progress, persistent challenges remain. While we have successfully categorized structural and physicochemical properties as indicators or descriptors of the activity of organic electrocatalysts based on their impact on specific electrochemical characteristics, it is important to note that certain properties

may influence multiple electrochemical characteristics simultaneously. For instance, structural/physicochemical properties that affect the mass transfer of organic electrocatalysts can also indirectly affect the number of active sites, and properties determining the intrinsic activity can somehow more or less affect the charge transfer. Although we have categorized these structural and physicochemical properties in this paper based on the electrochemical characteristics they predominantly affect, it is essential to acknowledge that when designing organic electrocatalysts, the potential impact of these properties on other electrochemical characteristics should also be taken into consideration. From a theoretical perspective, simulations of organic electrocatalysts should be broadened to encompass multiple electrochemical characteristics simultaneously. In simulating mass transfer, it is imperative to not only calculate the diffusion concentration and rate of the reactants but also incorporate considerations of their affinity and mobility. Similarly, for simulating the intrinsic activity of active sites in organic electrocatalysts, the electron mobility in the overall material during electrocatalysis should also be incorporated. Furthermore, it is crucial to take into account the effects of solvation to achieve precise theoretical simulations of organic electrocatalysts under practical conditions. Additionally, there is a need for more advanced theoretical analysis methods to offer fresh insights into the rational design of organic electrocatalysts. Machine learning serves as an exemplary approach that can rapidly screen and predict electroactive organic electrocatalysts. However, the effective implementation of machine learning relies on a substantial amount of accurate and high-quality raw input datasets. Traditional electrocatalysts often suffer from unclear structures, indistinct active sites, and inaccurate theoretical models, leading to subpar input data quality. Organic electrocatalysts typically exhibit clear molecular structures and precise theoretical models. This provides a favorable condition for accurately constructing structure–activity relationships when coupled with first-principles calculations. The robust correlation between activity and structure offers a high-quality raw input dataset for machine learning, facilitating the accurate and efficient prediction of new cost-efficient organic electrocatalysts and the successful construction of materials genome of organic electrocatalysts. These findings have profound significance for further exploring the electrocatalytic mechanism and optimizing the performance of newly designed organic electrocatalysts and similar electrocatalysts in the future. Moreover, as the raw input dataset accumulates, the optimization rate of the machine learning model is expected to significantly improve, accelerating the overall machine learning process. From an experimental standpoint, it is advisable to measure a broader range of structural and physicochemical properties that can influence the performance of electrocatalysts, including factors like spin state, entropy, and gas adsorption efficiency. This multifaceted approach aims to provide a more comprehensive assessment of the designed organic electrocatalysts. Moreover, these characteristics play a pivotal role in delineating the electrocatalytic activity of organic electrocatalysts, in conjunction with theoretical analysis. This combined insight provides valuable guidance for the rational design of nonprecious, highly efficient organic electrocatalysts. Additionally, another major concern of organic electrocatalysts is to pertinently overcome their inherent shortcomings including agglomeration tendency and unstratified conductivity.

Consequently, integrating them with an electrocatalytic active or highly conductive substrate can significantly prevent agglomeration and enhance electron transfer efficiency, thereby improving the electrocatalytic performance. Ultimately, these cost-effective organic electrocatalysts will be all-roundly developed and applicable to green energy devices.

In terms of practical applications, a critical limitation in the practical use of organic electrocatalysts is the frequent disparity between electrocatalytic activity observed in laboratory tests and that experienced in practical operational settings. Subsequent studies should focus on a thorough evaluation of organic electrocatalyst performance in real-world systems to bridge this gap. Furthermore, while numerous meticulously engineered organic electrocatalysts exhibit electrocatalytic activity comparable to or even surpassing noble-metal benchmarks, their durability during long-term operation is inferior. Hence, it is imperative that future research prioritizes the investigation of structural degradation and transformation phenomena during extended practical applications. This will lead to a deeper understanding of the durability of designed organic electrocatalysts in real-world scenarios. Only by taking all these factors into consideration can we substantially advance the development of practical organic electrocatalysts and foster the large-scale widespread adoption of various green energy devices.

Acknowledgements

This work was financially supported by the National Natural Science Foundation of China (No. 51874197) and Natural Science Foundation of Shanghai (Nos. 21ZR1429400 and 22ZR1429700).

Conflict of Interest

The authors declare no conflict of interest.

Keywords

electrode fabrication, organic electrocatalysts, reaction mechanisms, structure–activity relationships

Received: February 9, 2024

Published online:

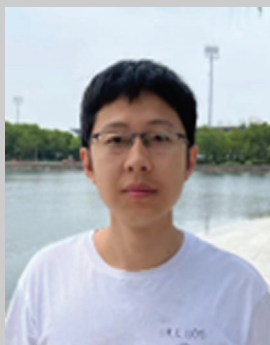
- [1] a) R. Cheng, K. Li, Z. Li, M. Jiang, F. Wang, Z. Yang, T. Zhao, P. Meng, C. Fu, *J. Power Sources* **2023**, 556, 232476; b) N. Du, C. Roy, R. Peach, M. Turnbull, S. Thiele, C. Bock, *Chem. Rev.* **2022**, 122, 11830; c) S. J. Peighambardoust, S. Rowshanzamir, M. Amjadi, *Int. J. Hydrogen Energy* **2010**, 35, 9349.
- [2] a) Y. Gao, D. Zheng, Q. Li, W. Xiao, T. Ma, Y. Fu, Z. Wu, L. Wang, *Adv. Funct. Mater.* **2022**, 32, 2203206; b) Y. Yang, C. R. Peltier, R. Zeng, R. Schimmenti, Q. Li, X. Huang, Z. Yan, G. Potsi, R. Selhorst, X. Lu, W. Xu, M. Tader, A. V. Soudackov, H. Zhang, M. Krumov, E. Murray, P. Xu, J. Hitt, L. Xu, H.-Y. Ko, B. G. Ernst, C. Bundschu, A. Luo, D. Markovich, M. Hu, C. He, H. Wang, J. Fang, R. A. DiStasio Jr., L. F. Kourkoutis, et al., *Chem. Rev.* **2022**, 122, 6117; c) X. Peng, T. J. Omasta, E. Magliocca, L. Wang, J. R. Varcoe, W. E. Mustain, *Angew. Chem., Int. Ed.* **2019**, 58, 1046; d) R. Cheng, K. Li, H. Li, F. Sun, X. He, T. Zhao, J. Zhang, C. Fu, *Nano Res.* **2023**, <https://doi.org/10.1007/s12274-023-6240-7>; e) M. R. Kandel, U. N. Pan, P. P. Dhakal, R. B. Ghising, T. T. Nguyen, J. Zhao, N. H. Kim, J. H. Lee, *Appl. Catal., B* **2023**, 331, 122680; f) L. Chong, G. Gao, J. Wen, H. Li, H. Xu, Z. Green, J. D. Sugar, A. J. Kropf, W. Xu, X.-M. Lin, H. Xu, L.-W. Wang, D.-J. Liu, *Science* **2023**, 380, 609.
- [3] a) R. Balaji, T. T. Nguyen, K. Harish, N. H. Kim, J. H. Lee, *J. Mater. Chem. A* **2022**, 10, 3782; b) X. Wei, S. Song, W. Cai, X. Luo, L. Jiao, Q. Fang, X. Wang, N. Wu, Z. Luo, H. Wang, Z. Zhu, J. Li, L. Zheng, W. Gu, W. Song, S. Guo, C. Zhu, *Chem* **2023**, 9, 181.
- [4] a) Y. Liu, Q. Sun, W. Li, K. R. Adair, J. Li, X. Sun, *Green Energy Environ.* **2017**, 2, 246; b) Y. Zhou, R. Abazari, J. Chen, M. Tahir, A. Kumar, R. R. Ikreedeegh, E. Rani, H. Singh, A. M. Kirillov, *Coord. Chem. Rev.* **2022**, 451, 214264; c) R. Cheng, K. Li, H. Li, T. Zhao, Y. Wang, Q. Xue, J. Zhang, C. Fu, *J. Energy Chem.* **2024**, 88, 103; d) Y. Song, Y. Peng, S. Yao, P. Zhang, Y. Wang, J. Gu, T. Lu, Z. Zhang, *Chin. Chem. Lett.* **2022**, 33, 1047.
- [5] H. Li, Y. Gong, H. Zhou, J. Li, K. Yang, B. Mao, J. Zhang, Y. Shi, J. Deng, M. Mao, Z. Huang, S. Jiao, Y. Kuang, Y. Zhao, S. Luo, *Nat. Commun.* **2023**, 14, 6407.
- [6] Y. Yao, J. Wu, Q. Feng, K. Zeng, J. Wan, J. Zhang, B. Mao, K. Hu, L. Chen, H. Zhang, Y. Gong, K. Yang, H. Zhou, Z. Huang, H. Li, *Small* **2023**, 19, 2302015.
- [7] X. Yang, X. Zheng, H. Li, B. Luo, Y. He, Y. Yao, H. Zhou, Z. Yan, Y. Kuang, Z. Huang, *Adv. Funct. Mater.* **2022**, 32, 2200397.
- [8] a) Q. Che, Q. Li, Y. Tan, X. Chen, X. Xu, Y. Chen, *Appl. Catal., B* **2019**, 246, 337; b) X. Zou, Y. Liu, G.-D. Li, Y. Wu, D.-P. Liu, W. Li, H.-W. Li, D. Wang, Y. Zhang, X. Zou, *Adv. Mater.* **2017**, 29, 1700404.
- [9] a) L. Liu, G. Zeng, J. Chen, L. Bi, L. Dai, Z. Wen, *Nano Energy* **2018**, 49, 393; b) S. S. Sekhon, J. Lee, J.-S. Park, *J. Energy Chem.* **2022**, 65, 149.
- [10] X. Xing, R. Liu, K. Cao, U. Kaiser, C. Streb, *Chem.-Eur. J.* **2019**, 25, 11098.
- [11] X. Cui, L. Gao, R. Ma, Z. Wei, C.-H. Lu, Z. Li, Y. Yang, *J. Mater. Chem. A* **2021**, 9, 20985.
- [12] a) Y. Chen, H. Dai, K. Fan, G. Zhang, M. Tang, Y. Gao, C. Zhang, L. Guan, M. Mao, H. Liu, T. Zhai, C. Wang, *Angew. Chem., Int. Ed.* **2023**, 62, 202302539; b) P. Peng, L. Shi, F. Huo, C. Mi, X. Wu, S. Zhang, Z. Xiang, *Sci. Adv.* **2019**, 5, eaaw2322.
- [13] L. Zhong, L. He, N. Wang, Y. Chen, X. Xie, B. Sun, J. Qian, S. Komarneni, W. Hu, *Appl. Catal., B* **2023**, 325, 122343.
- [14] a) Z. You, B. Wang, Z. Zhao, Q. Zhang, W. Song, C. Zhang, X. Long, Y. Xia, *Adv. Mater.* **2023**, 35, 2209129; b) F. Sun, G. Wang, Y. Ding, C. Wang, B. Yuan, Y. Lin, *Adv. Energy Mater.* **2018**, 8, 1800584.
- [15] J.-S. Qin, D.-Y. Du, W. Guan, X.-J. Bo, Y.-F. Li, L.-P. Guo, Z.-M. Su, Y.-Y. Wang, Y.-Q. Lan, H.-C. Zhou, *J. Am. Chem. Soc.* **2015**, 137, 7169.
- [16] N. Huang, P. Wang, D. Jiang, *Nat. Rev. Mater.* **2016**, 1, 16068.
- [17] a) B. C. Patra, S. Bhattacharya, *Chem. Mater.* **2021**, 33, 8512; b) P. Pachfule, S. Kandmabath, A. Mallick, R. Banerjee, *Chem. Commun.* **2015**, 51, 11717.
- [18] a) X. Sun, Y. Li, H. Su, X. Zhang, Y. Xu, W. Zhou, M. Liu, W. Cheng, Q. Liu, *Appl. Catal., B* **2022**, 317, 121706; b) S. Singh, M. K. Ghorai, K. K. Kar, *J. Mater. Chem. A* **2023**, 11, 8003; c) M. Liu, S. Liu, C.-X. Cui, Q. Miao, Y. He, X. Li, Q. Xu, G. Zeng, *Angew. Chem., Int. Ed.* **2022**, 61, 202213522.
- [19] a) B. Yang, Q. Han, L. Han, Y. Leng, T. O'Carroll, X. Yang, G. Wu, Z. Xiang, *Adv. Mater.* **2023**, 35, 2208661; b) J. Tang, Z. Liang, H. Qin, X. Liu, B. Zhai, Z. Su, Q. Liu, H. Lei, K. Liu, C. Zhao, R. Cao, Y. Fang, *Angew. Chem., Int. Ed.* **2023**, 62, 202214449; c) C. Ding, M. Breunig, J. Timm, R. Marschall, J. Senker, S. Agarwal, *Adv. Funct. Mater.* **2021**, 31, 2106507; d) R. Yang, S. Liu, Q. Sun, Q. Liao, K. Xi, B. Su, *J. Am. Chem. Soc.* **2022**, 144, 11778.
- [20] S. H. DuVall, R. L. McCreery, *J. Am. Chem. Soc.* **2000**, 122, 6759.

- [21] X. Hu, B. M. Cossairt, B. S. Brunschwig, N. S. Lewis, J. C. Peters, *Chem. Commun.* **2005**, 37, 4723.
- [22] a) Z. P. Li, B. H. Liu, *J. Appl. Electrochem.* **2010**, 40, 475; b) Y. Zhao, X. Yang, J. Tian, F. Wang, L. Zhan, *J. Power Sources* **2010**, 195, 4634.
- [23] a) Y. Ren, G. H. Chia, Z. Gao, *Nano Today* **2013**, 8, 577; b) K. Sakaushi, M. Antonietti, *Acc. Chem. Res.* **2015**, 48, 1591.
- [24] a) S. Bhunia, A. Peña-Duarte, H. Li, H. Li, M. F. Sanad, P. Saha, M. A. Addicoat, K. Sasaki, T. A. Strom, M. J. Yacamán, C. R. Cabrera, R. Seshadri, S. Bhattacharya, J.-L. Brédas, L. Echegoyen, *ACS Nano* **2023**, 17, 3492; b) J. Timoshenko, B. R. Cuenya, *Chem. Rev.* **2021**, 121, 882.
- [25] a) Y. Guan, J. Lai, G. Xu, *ChemElectroChem* **2021**, 8, 2764; b) M. K. Lee, M. Shokouhimehr, S. Y. Kim, H. W. Jang, *Adv. Energy Mater.* **2022**, 12, 2003990.
- [26] R. Cheng, Y. Min, H. Li, C. Fu, *Nano Energy* **2023**, 115, 108718.
- [27] R. Tian, F. Wang, C. Zou, Z. Pei, X. Guo, H. Yang, *J. Alloys Compd.* **2023**, 933, 167670.
- [28] X. Li, Q. Liu, B. Yang, Z. Liao, W. Yan, Z. Xiang, *Adv. Mater.* **2022**, 34, 2204570.
- [29] a) S. Ilic, U. Pandey Kadel, Y. Basdogan, J. A. Keith, K. D. Glusac, *J. Am. Chem. Soc.* **2018**, 140, 4569; b) G. Ruan, P. Ghosh, N. Fridman, G. Maayan, *J. Am. Chem. Soc.* **2021**, 143, 10614; c) M. Axelsson, C. F. N. Marchiori, P. Huang, C. M. Araujo, H. Tian, *J. Am. Chem. Soc.* **2021**, 143, 21229; d) K. Schwinghammer, S. Hug, M. B. Mesch, J. Senker, B. V. Lotsch, *Energy Environ. Sci.* **2015**, 8, 3345; e) Z. Fang, P. Wu, K. Yu, Y. Li, Y. Zhu, P. J. Ferreira, Y. Liu, G. Yu, *ACS Nano* **2019**, 13, 14368; f) X. Yan, B. Wang, J. Ren, X. Long, D. Yang, *Angew. Chem., Int. Ed.* **2022**, 61, 202209583.
- [30] G. Lu, H. Yang, Y. Zhu, T. Huggins, Z. J. Ren, Z. Liu, W. Zhang, *J. Mater. Chem. A* **2015**, 3, 4954.
- [31] Y. Y. Sun, A. Kakinin, X. Wan, N. Moriarty, C. P. J. Hunt, Y. Li, N. Andrikopoulos, A. Nandakumar, T. P. Davis, C. L. Parish, Y. Song, P. C. Ke, F. Ding, *Nano Today* **2021**, 38, 101125.
- [32] a) Y. Zhang, L. Cheng, L. Zhang, D. Yang, C. Du, L. Wan, J. Chen, M. Xie, *J. Energy Storage* **2021**, 34, 102018; b) A. F. M. El-Mahdy, A. M. Elewa, S.-W. Huang, H.-H. Chou, S.-W. Kuo, *Adv. Opt. Mater.* **2020**, 8, 2000641; c) J. Guo, D. Ma, F. Sun, G. Zhuang, Q. Wang, A. M. Al-Enizi, A. Nafady, S. Ma, *Chem* **2022**, 65, 1704; d) Z. Chen, J. Wang, M. Hao, Y. Xie, X. Liu, H. Yang, G. I. N. Waterhouse, X. Wang, S. Ma, *Nat. Commun.* **2023**, 14, 1106.
- [33] a) D. J. Boston, C. Xu, D. W. Armstrong, F. M. MacDonnell, *J. Am. Chem. Soc.* **2013**, 135, 16252; b) H. Li, F. Xie, M.-T. Zhang, *ACS Catal.* **2021**, 11, 68; c) C.-H. Lim, S. Ilic, A. Alherz, B. T. Worrell, S. S. Bacon, J. T. Hynes, K. D. Glusac, C. B. Musgrave, *J. Am. Chem. Soc.* **2019**, 141, 272.
- [34] X. Yan, D. Li, L. Zhang, X. Long, D. Yang, *Appl. Catal., B* **2022**, 304, 120908.
- [35] M. A. Hoque, J. B. Gerken, S. S. Stahl, *Science* **2024**, 383, 173.
- [36] J. Wang, J. Yu, J. Wang, K. Wang, L. Yu, C. Zhu, K. Gao, Z. Gong, Z. Li, R. Devasenathipathy, D. Cai, H. Xie, G. Lu, *Small* **2023**, 19, 2207135.
- [37] a) H. Lin, H. Wang, C. Xue, M. Ye, *Enzyme Microb. Technol.* **2002**, 31, 588; b) A. Rahimalimamaghani, D. A. Pacheco Tanaka, M. A. Llosa Tanco, F. Neira D'Angelo, F. Gallucci, *Chem. Eng. J.* **2022**, 435, 134891.
- [38] a) W. Feng, S. Wu, H. Chen, L. Meng, F. Huang, H. Liang, J. Zhang, Z. Wei, X. Wan, C. Li, Z. Yao, Y. Chen, *Adv. Energy Mater.* **2022**, 12, 2104060; b) Q. Mahmood, X. Li, L. Qin, L. Wang, W.-H. Sun, *Dalton Trans.* **2022**, 51, 14375.
- [39] B. Zhang, H. Liu, P. Zhai, R. Zhang, W. Wang, P. Khangale, D. Hildebrandt, X. Liu, S. Qiao, *Adv. Funct. Mater.* **2023**, 33, 2211440.
- [40] J. Wang, D. Li, Z. Chen, Z. Wu, B. Chen, X. Liu, *J. Mater. Chem. A* **2020**, 8, 22754.
- [41] a) J. Guo, C.-Y. Lin, Z. Xia, Z. Xiang, *Angew. Chem., Int. Ed.* **2018**, 57, 12567; b) D.-H. Yang, Y. Tao, X. Ding, B.-H. Han, *Chem. Soc. Rev.* **2022**, 51, 761.
- [42] a) Y. Li, P. Peng, Z. Liao, F. Huo, Y. Liu, X. Shao, Z. Xiang, *ACS Sustainable Chem. Eng.* **2020**, 8, 3728; b) M. Gopalakrishnan, A. A. Mohamad, M. T. Nguyen, T. Yonezawa, J. Qin, P. Thamyongkit, A. Somwangthanoj, S. Kheawhom, *Mater. Today Chem.* **2022**, 23, 100632.
- [43] Y. Li, P. Peng, F. Huo, X. Shao, Z. Xiang, *Front. Mater.* **2019**, 6, 244.
- [44] B. C. Patra, S. Khilari, R. N. Manna, S. Mondal, D. Pradhan, A. Pradhan, A. Bhaumik, *ACS Catal.* **2017**, 7, 6120.
- [45] H. Furukawa, K. E. Cordova, M. O'Keeffe, O. M. Yaghi, *Science* **2013**, 341, 1230444.
- [46] A. P. Côté, A. I. Benin, N. W. Ockwig, M. O'Keeffe, A. J. Matzger, O. M. Yaghi, *Science* **2005**, 310, 1166.
- [47] J. L. Segura, M. J. Mancheño, F. Zamora, *Chem. Soc. Rev.* **2016**, 45, 5635.
- [48] W. Zhang, L. Chen, S. Dai, C. Zhao, C. Ma, L. Wei, M. Zhu, S. Y. Chong, H. Yang, L. Liu, Y. Bai, M. Yu, Y. Xu, X.-W. Zhu, Q. Zhu, S. An, R. S. Sprick, M. A. Little, X. Wu, S. Jiang, Y. Wu, Y.-B. Zhang, H. Tian, W.-H. Zhu, A. I. Cooper, *Nature* **2022**, 604, 72.
- [49] S. Dutta, S. K. Pati, *Catal. Lett.* **2022**, 152, 3548.
- [50] F. Cheng, X. Peng, L. Hu, B. Yang, Z. Li, C.-L. Dong, J.-L. Chen, L.-C. Hsu, L. Lei, Q. Zheng, M. Qiu, L. Dai, Y. Hou, *Nat. Commun.* **2022**, 13, 6486.
- [51] C.-P. Wang, Y.-X. Lin, L. Cui, J. Zhu, X.-H. Bu, *Small* **2023**, 19, 2207342.
- [52] L. Tang, Q. Xu, Y. Zhang, W. Chen, M. Wu, *Electrochem. Energy Rev.* **2022**, 5, 32.
- [53] Z. Xue, Y. Li, Y. Zhang, W. Geng, B. Jia, J. Tang, S. Bao, H.-P. Wang, Y. Fan, Z.-w. Wei, Z. Zhang, Z. Ke, G. Li, C.-Y. Su, *Adv. Energy Mater.* **2018**, 8, 1801564.
- [54] W. Zhou, D.-D. Huang, Y.-P. Wu, J. Zhao, T. Wu, J. Zhang, D.-S. Li, C. Sun, P. Feng, X. Bu, *Angew. Chem., Int. Ed.* **2019**, 58, 4227.
- [55] C.-P. Wang, Y. Feng, H. Sun, Y. Wang, J. Yin, Z. Yao, X.-H. Bu, J. Zhu, *ACS Catal.* **2021**, 11, 7132.
- [56] C.-P. Wang, H.-Y. Liu, G. Bian, X. Gao, S. Zhao, Y. Kang, J. Zhu, X.-H. Bu, *Small* **2019**, 15, 1906086.
- [57] a) C. F. Li, J. W. Zhao, L. J. Xie, J. Q. Wu, Q. Ren, Y. Wang, G. R. Li, *Angew. Chem., Int. Ed.* **2021**, 60, 18129; b) Y. Umena, K. Kawakami, J.-R. Shen, N. Kamiya, *Nature* **2011**, 473, 55.
- [58] M. Liu, X. Zheng, L. Tang, M. Zhang, X. Chen, Z. Cai, *J. Alloys Compd.* **2023**, 961, 170976.
- [59] Y. Zhang, S. Chen, Y. Zhang, R. Li, B. Zhao, T. Peng, *Adv. Mater.* **2023**, 35, 2210727.
- [60] H. Huang, Y. Zhao, Y. Bai, F. Li, Y. Zhang, Y. Chen, *Adv. Sci.* **2020**, 7, 2000012.
- [61] a) A. J. Clough, J. W. Yoo, M. H. Mecklenburg, S. C. Marinescu, *J. Am. Chem. Soc.* **2015**, 137, 118; b) C. A. Downes, A. J. Clough, K. Chen, J. W. Yoo, S. C. Marinescu, *ACS Appl. Mater. Interfaces* **2018**, 10, 1719.
- [62] X. Sun, K.-H. Wu, R. Sakamoto, T. Kusamoto, H. Maeda, X. Ni, W. Jiang, F. Liu, S. Sasaki, H. Masunaga, H. Nishihara, *Chem. Sci.* **2017**, 8, 8078.
- [63] V. Hasija, S. Patial, P. Raizada, A. Aslam Parwaz Khan, A. M. Asiri, Q. Van Le, V.-H. Nguyen, P. Singh, *Coord. Chem. Rev.* **2022**, 452, 214298.
- [64] Z. Li, R. Gao, M. Feng, Y.-P. Deng, D. Xiao, Y. Zheng, Z. Zhao, D. Luo, Y. Liu, Z. Zhang, D. Wang, Q. Li, H. Li, X. Wang, Z. Chen, *Adv. Energy Mater.* **2021**, 11, 2003291.
- [65] Z. Fang, Y. Li, J. Li, C. Shu, L. Zhong, S. Lu, C. Mo, M. Yang, D. Yu, *Angew. Chem., Int. Ed.* **2021**, 60, 17615.
- [66] S. Huang, S. Lu, Y. Hu, Y. Cao, Y. Li, F. Duan, H. Zhu, Y. Jin, M. Du, W. Zhang, *Small Struct.* **2023**, 4, 2200387.

- [67] D. Li, C. Li, L. Zhang, H. Li, L. Zhu, D. Yang, Q. Fang, S. Qiu, X. Yao, *J. Am. Chem. Soc.* **2020**, *142*, 8104.
- [68] J. Li, P. Liu, J. Yan, H. Huang, W. Song, *Adv. Sci.* **2023**, *10*, 2206165.
- [69] a) S. S. A. Shah, M. S. Javed, T. Najam, M. A. Nazir, A. ur Rehman, A. Rauf, M. Sohail, F. Verpoort, S.-J. Bao, *Mater. Today* **2023**, *67*, 229; b) J. Li, P. Liu, J. Mao, J. Yan, W. Song, *Nanoscale* **2022**, *14*, 6126.
- [70] S. Yu, Z. Levell, Z. Jiang, X. Zhao, Y. Liu, *J. Am. Chem. Soc.* **2023**, *145*, 25352.
- [71] a) M. Lefèvre, E. Proietti, F. Jaouen, J.-P. Dodelet, *Science* **2009**, *324*, 71; b) Y. Wang, Y. Zhang, Z. Liu, C. Xie, S. Feng, D. Liu, M. Shao, S. Wang, *Angew. Chem., Int. Ed.* **2017**, *56*, 5867; c) R. Cheng, M. Jiang, K. Li, M. Guo, J. Zhang, J. Ren, P. Meng, R. Li, C. Fu, *Chem. Eng. J.* **2021**, *425*, 130603; d) K. Li, R. Cheng, Q. Xue, T. Zhao, F. Wang, C. Fu, *ACS Appl. Mater. Interfaces* **2023**, *15*, 9150; e) Q. Cao, L. Wan, Z. Xu, W. Kuang, H. Liu, X. Zhang, W. Zhang, Y. Lu, Y. Yao, B. Wang, K. Liu, *Adv. Mater.* **2023**, *35*, 2210550.
- [72] C.-Y. Lin, D. Zhang, Z. Zhao, Z. Xia, *Adv. Mater.* **2018**, *30*, 1703646.
- [73] a) J. Hu, Q. Xu, X. Wang, X. Huang, C. Zhou, Y. Ye, L. Zhang, H. Pang, *Carbon Energy* **2023**, *5*, 315; b) S. Xie, F. Li, S. Xu, J. Li, W. Zeng, *Chin. J. Catal.* **2019**, *40*, 1205.
- [74] a) W. Zhang, J. Lu, X. Gao, P. Li, W. Zhang, Y. Ma, H. Wang, B. Tang, *Angew. Chem., Int. Ed.* **2018**, *57*, 4891; b) Q. Liu, L. Xie, X. Shi, G. Du, A. M. Asiri, Y. Luo, X. Sun, *Inorg. Chem. Front.* **2018**, *5*, 1570; c) S. Mondal, B. Mohanty, M. Nurhuda, S. Dalapati, R. Jana, M. Addicoat, A. Datta, B. K. Jena, A. Bhaumik, *ACS Catal.* **2020**, *10*, 5623.
- [75] J. Chang, C. Li, X. Wang, D. Li, J. Zhang, X. Yu, H. Li, X. Yao, V. Valtchev, S. Qiu, Q. Fang, *Nano* **2023**, *15*, 159.
- [76] R. Wang, Z. Zhang, J. Suo, L. Liao, L. Li, Z. Yu, H. Zhang, V. Valtchev, S. Qiu, Q. Fang, *Chem. Eng. J.* **2023**, *478*, 147403.
- [77] C. Liu, F. Liu, H. Li, J. Chen, J. Fei, Z. Yu, Z. Yuan, C. Wang, H. Zheng, Z. Liu, M. Xu, G. Henkelman, L. Wei, Y. Chen, *ACS Nano* **2021**, *15*, 3309.
- [78] A. Q. Mugheri, M. S. Samtio, A. A. Sangah, J. H. Awan, S. A. Memon, *Int. J. Hydrogen Energy* **2021**, *46*, 35261.
- [79] T. D. Bennett, A. K. Cheetham, *Acc. Chem. Res.* **2014**, *47*, 1555.
- [80] J. Li, W. Huang, M. Wang, S. Xi, J. Meng, K. Zhao, J. Jin, W. Xu, Z. Wang, X. Liu, Q. Chen, L. Xu, X. Liao, Y. Jiang, K. A. Owusu, B. Jiang, C. Chen, D. Fan, L. Zhou, L. Mai, *ACS Energy Lett.* **2019**, *4*, 285.
- [81] Z. Sun, Y. Wang, L. Zhang, H. Wu, Y. Jin, Y. Li, Y. Shi, T. Zhu, H. Mao, J. Liu, C. Xiao, S. Ding, *Adv. Funct. Mater.* **2020**, *30*, 1910482.
- [82] D. Sheberla, L. Sun, M. A. Blood-Forsythe, S. Er, C. R. Wade, C. K. Brozek, A. Aspuru-Guzik, M. Dincă, *J. Am. Chem. Soc.* **2014**, *136*, 8859.
- [83] R. G. Mariano, O. J. Wahab, J. A. Rabinowitz, J. Oppenheim, T. Chen, P. R. Unwin, M. Dincă, *ACS Cent. Sci.* **2022**, *8*, 975.
- [84] F. Yin, Y. Liu, C. Wang, H. Liu, *Phys. Chem. Chem. Phys.* **2018**, *20*, 16159.
- [85] J. Wang, Y. Yao, C. Zhang, Q. Sun, D. Cheng, X. Huang, J. Feng, J. Wan, J. Zou, C. Liu, C. Yu, *Adv. Sci.* **2021**, *8*, 2100120.
- [86] X. Li, K. Zhang, Z. Li, Y. Yan, Y. Yuan, L. Ma, K. Xie, K. P. Loh, *Angew. Chem., Int. Ed.* **2023**, *62*, 202217869.
- [87] a) K. Dutta, in *Conjugated Polymers for Next-Generation Applications*, Vol. 1 (Eds: V. Kumar, K. Sharma, R. Sehgal, S. Kalita), Woodhead Publishing, Oxford, UK **2022**, p. 447; b) H. Jia, Y. Yao, J. Zhao, Y. Gao, Z. Luo, P. Du, *J. Mater. Chem. A* **2018**, *6*, 1188.
- [88] T. Wang, Z. Zhang, X. Wang, W. Wang, T. Ma, X. Liu, *Appl. Catal., B* **2022**, *315*, 121590.
- [89] W. Li, Z. Zhao, W. Hu, Q. Cheng, L. Yang, Z. Hu, Y. A. Liu, K. Wen, H. Yang, *Chem. Mater.* **2020**, *32*, 8553.
- [90] A. M. Dominic, Z. Wang, A. Kuc, P. Petkov, K. H. Ly, T. L. H. Pham, M. Kutzschbach, Y. Cao, J. Bachmann, X. Feng, R. Dong, I. M. Weidinger, *J. Phys. Chem. C* **2023**, *127*, 7299.
- [91] I. Liberman, R. Shimoni, R. Ifraimov, I. Rozenberg, C. Singh, I. Hod, *J. Am. Chem. Soc.* **2020**, *142*, 1933.
- [92] S. M. Scott, K. C. Gordon, A. K. Burrell, *Inorg. Chem.* **1996**, *35*, 2452.
- [93] a) K. Ge, S. Sun, Y. Zhao, K. Yang, S. Wang, Z. Zhang, J. Cao, Y. Yang, Y. Zhang, M. Pan, L. Zhu, *Angew. Chem., Int. Ed.* **2021**, *60*, 12097; b) J. Duan, S. Chen, C. Zhao, *Nat. Commun.* **2017**, *8*, 15341.
- [94] W. Wang, L. Zhang, T. Wang, Z. Zhang, X. Wang, C. Cheng, X. Liu, *J. Energy Chem.* **2023**, *77*, 543.
- [95] a) Z. Gao, L. L. Gong, X. Q. He, X. M. Su, L. H. Xiao, F. Luo, *Inorg. Chem.* **2020**, *59*, 4995; b) R. Ma, X. Cui, Y. Wang, Z. Xiao, R. Luo, L. Gao, Z. Wei, Y. Yang, *J. Mater. Chem. A* **2022**, *10*, 5918.
- [96] S. Xue, X. Lv, N. Liu, Q. Zhang, H. Lei, R. Cao, F. Qiu, *Inorg. Chem.* **2023**, *62*, 1679.
- [97] J. Zhou, Z. Han, X. Wang, H. Gai, Z. Chen, T. Guo, X. Hou, L. Xu, X. Hu, M. Huang, S. V. Levchenko, H. Jiang, *Adv. Funct. Mater.* **2021**, *31*, 2102066.
- [98] a) W. Zhang, Y. Wang, H. Zheng, R. Li, Y. Tang, B. Li, C. Zhu, L. You, M.-R. Gao, Z. Liu, S.-H. Yu, K. Zhou, *ACS Nano* **2020**, *14*, 1971. b) S. Zhao, C. Tan, C.-T. He, P. An, F. Xie, S. Jiang, Y. Zhu, K.-H. Wu, B. Zhang, H. Li, J. Zhang, Y. Chen, S. Liu, J. Dong, Z. Tang, *Nat. Energy* **2020**, *5*, 881.
- [99] J. Zhou, Y. Dou, X.-Q. Wu, A. Zhou, L. Shu, J.-R. Li, *Small* **2020**, *16*, 1906564.
- [100] S. Zhao, Y. Wang, J. Dong, C.-T. He, H. Yin, P. An, K. Zhao, X. Zhang, C. Gao, L. Zhang, J. Lv, J. Wang, J. Zhang, A. M. Khattak, N. A. Khan, Z. Wei, J. Zhang, S. Liu, H. Zhao, Z. Tang, *Nat. Energy* **2016**, *1*, 16184.
- [101] X. Yin, L. Lin, U. Martinez, P. Zelenay, *ACS Appl. Energy Mater.* **2019**, *2*, 7272.
- [102] S. An, X. Li, S. Shang, T. Xu, S. Yang, C.-X. Cui, C. Peng, H. Liu, Q. Xu, Z. Jiang, J. Hu, *Angew. Chem., Int. Ed.* **2023**, *62*, 202218742.
- [103] Z. Yang, Y. Gao, L. Zuo, C. Long, C. Yang, X. Zhang, *ACS Catal.* **2023**, *13*, 4790.
- [104] L. Liu, L. Kang, A. Chutia, J. Feng, M. Michalska, P. Ferrer, D. C. Grinter, G. Held, Y. Tan, F. Zhao, F. Guo, D. G. Hopkinson, C. S. Allen, Y. Hou, J. Gu, I. Papakonstantinou, P. R. Shearing, D. J. L. Brett, I. P. Parkin, G. He, *Angew. Chem., Int. Ed.* **2023**, *62*, 202303525.
- [105] Z. Zhang, W. Wang, X. Wang, L. Zhang, C. Cheng, X. Liu, *Chem. Eng. J.* **2022**, *435*, 133872.
- [106] J.-Y. Yue, Y.-T. Wang, X. Wu, P. Yang, Y. Ma, X.-H. Liu, B. Tang, *Chem. Commun.* **2021**, *57*, 12619.
- [107] Z. Wu, L. Feng, Z. Lu, X. Yu, Y. Zhao, J. Luo, S. Wang, X. Tian, Q. Chen, *Nano Mater. Sci.* **2023**, <https://doi.org/10.1016/j.nanoms.2023.10.002>.
- [108] R. Gao, J. Wang, Z.-F. Huang, R. Zhang, W. Wang, L. Pan, J. Zhang, W. Zhu, X. Zhang, C. Shi, J. Lim, J.-J. Zou, *Nat. Energy* **2021**, *6*, 614.
- [109] R. Cheng, K. Li, H. Li, T. Zhao, Y. Wang, Q. Xue, J. Zhang, C. Fu, *J. Energy Chem.* **2024**, *88*, 103.
- [110] J. Hu, Q. Xu, X. Wang, X. Huang, C. Zhou, Y. Ye, L. Zhang, H. Pang, *Carbon Energy* **2023**, *5*, 315.
- [111] H. Wu, S. Huang, F. Ding, Y. Ma, Q. Zhai, Y. Ren, Y. Yang, L. Chen, S. Tang, X. Meng, *J. Phys. Chem. C* **2022**, *126*, 19715.
- [112] Z. Xue, K. Liu, Q. Liu, Y. Li, M. Li, C.-Y. Su, N. Ogiwara, H. Kobayashi, H. Kitagawa, M. Liu, G. Li, *Nat. Commun.* **2019**, *10*, 5048.
- [113] H. B. Aiyappa, J. Thote, D. B. Shinde, R. Banerjee, S. Kurungot, *Chem. Mater.* **2016**, *28*, 4375.
- [114] X. Li, M. Fan, D. Wei, M. Li, Y. Wang, *Electrochim. Acta* **2020**, *354*, 136682.
- [115] Q. Zhang, Y. Hu, H. Wu, X. Zhao, M. Wang, S. Wang, R. Feng, Q. Chen, F. Song, M. Chen, P. Liu, *ACS Nano* **2023**, *17*, 1485.
- [116] H.-L. Meng, S.-Y. Lin, J.-J. Feng, L. Zhang, A.-J. Wang, *J. Colloid Interface Sci.* **2022**, *610*, 573.
- [117] C. E. Park, R. A. Senthil, G. H. Jeong, M. Y. Choi, *Small* **2023**, *19*, 2207820.
- [118] Y. Dou, A. Wang, L. Zhao, X. Yang, Q. Wang, M. Shire Sudi, W. Zhu, D. Shang, *J. Colloid Interface Sci.* **2023**, *650*, 943.

- [119] Y. Zhao, Y. Liang, D. Wu, H. Tian, T. Xia, W. Wang, W. Xie, X.-M. Hu, X. Tian, Q. Chen, *Small* **2022**, *18*, 2107750.
- [120] S. Ruidas, B. Mohanty, P. Bhanja, E. S. Erakulan, R. Thapa, P. Das, A. Chowdhury, S. K. Mandal, B. K. Jena, A. Bhaumik, *ChemSusChem* **2021**, *14*, 5057.
- [121] Y. Wang, Y. Jiao, H. Yan, G. Yang, C. Tian, A. Wu, Y. Liu, H. Fu, *Angew. Chem., Int. Ed.* **2022**, *61*, 202116233.
- [122] H. Yuan, D. Jiang, Z. Li, X. Liu, Z. Tang, X. Zhang, L. Zhao, M. Huang, H. Liu, K. Song, W. Zhou, *Adv. Mater.* **2024**, *36*, 2305375.
- [123] S. Wang, B. Xu, W. Huo, H. Feng, X. Zhou, F. Fang, Z. Xie, J. K. Shang, J. Jiang, *Appl. Catal., B* **2022**, *313*, 121472.
- [124] a) W. Zhou, L. Yang, F.-Y. Zhou, Q.-W. Deng, X. Wang, D. Zhai, G.-Q. Ren, K.-L. Han, W.-Q. Deng, L. Sun, *Chem.-Eur. J.* **2020**, *26*, 7720; b) Y. Song, J.-J. Zhang, Z. Zhu, X. Chen, L. Huang, J. Su, Z. Xu, T. H. Ly, C.-S. Lee, B. I. Jakobson, B. Z. Tang, R. Ye, *Appl. Catal., B* **2021**, *284*, 119750.
- [125] M. Jahan, Z. Liu, K. P. Loh, *Adv. Funct. Mater.* **2013**, *23*, 5363.
- [126] L. Liu, D.-W. Zha, Y. Wang, J.-B. He, *Int. J. Hydrogen Energy* **2014**, *39*, 14712.
- [127] R. Dong, M. Pfeffermann, H. Liang, Z. Zheng, X. Zhu, J. Zhang, X. Feng, *Angew. Chem., Int. Ed.* **2015**, *54*, 12058.
- [128] T. Fukushima, W. Drisdell, J. Yano, Y. Surendranath, *J. Am. Chem. Soc.* **2015**, *137*, 10926.
- [129] C. Che, M. Vagin, K. Wijeratne, D. Zhao, M. Warczak, M. P. Jonsson, X. Crispin, *Adv. Sustainable Syst.* **2018**, *2*, 1800021.
- [130] W. Zhou, Z. Xue, Q. Liu, Y. Li, J. Hu, G. Li, *ChemSusChem* **2020**, *13*, 5647.
- [131] L. Fan, H. Deng, Y. Zhang, Q. Du, D. Y. C. Leung, Y. Wang, K. Jiao, *Energy Environ. Sci.* **2023**, *16*, 1466.
- [132] H. Wang, Y. Pei, K. Wang, Y. Zuo, M. Wei, J. Xiong, P. Zhang, Z. Chen, N. Shang, D. Zhong, P. Pei, *Small* **2023**, *19*, 2304863.
- [133] H. Xu, Y. Zhao, G. He, H. Chen, *Int. J. Hydrogen Energy* **2022**, *47*, 14257.
- [134] A. Pedersen, A. Bagger, J. Barrio, F. Maillard, I. E. L. Stephens, M.-M. Titirici, *J. Mater. Chem. A* **2023**, *11*, 23211.
- [135] a) U. Khan, A. Nairan, J. Gao, Q. Zhang, *Small Struct.* **2023**, *4*, 2200109; b) M. El Hanafi, A. BaQais, M. Saadi, H. Ait Ahsaine, *Energy Fuels* **2023**, *37*, 10869.
- [136] G. Lu, Y. Zhu, K. Xu, Y. Jin, Z. J. Ren, Z. Liu, W. Zhang, *Nanoscale* **2015**, *7*, 18271.
- [137] J. Ji, C. Zhang, S. Qin, P. Jin, *Sustainable Energy Fuels* **2021**, *5*, 5615.
- [138] H. Mai, T. C. Le, D. Chen, D. A. Winkler, R. A. Caruso, *Chem. Rev.* **2022**, *122*, 13478.
- [139] C. Yang, Z.-D. Yang, H. Dong, N. Sun, Y. Lu, F.-M. Zhang, G. Zhang, *ACS Energy Lett.* **2019**, *4*, 2251.
- [140] M. Martínez-Fernández, E. Martínez-Periñán, A. de la Peña, J. Cabrera-Trujillo, J. A. R. Navarro, F. Aguilar-Galindo, D. Rodríguez-San-Miguel, M. M. Ramos, R. Vismara, F. Zamora, E. Lorenzo, J. L. Segura, *Angew. Chem., Int. Ed.* **2023**, *62*, 202313940.
- [141] a) Q. Dang, Y. Sun, X. Wang, W. Zhu, Y. Chen, F. Liao, H. Huang, M. Shao, *Appl. Catal., B* **2019**, *257*, 117905; b) Z. Che, X. Lu, B. Cai, X. Xu, J. Bao, Y. Liu, *Nano Res.* **2022**, *15*, 1269.
- [142] C.-H. Hsu, H.-Y. Liao, P.-L. Kuo, *J. Phys. Chem. C* **2010**, *114*, 7933.
- [143] A. A. Alekseenko, V. E. Guterma, S. V. Belenov, V. S. Menshikov, N. Y. Tabachkova, O. I. Safonov, E. A. Moguchikh, *Int. J. Hydrogen Energy* **2018**, *43*, 3676.
- [144] A. N. Borodin, A. I. Sologubov, L. A. Chernenko, P. I. Zolkin, H. M. Aberyahimov, G. A. Grigoriev, in *MICC 90: Moscow Int. Composites Conf. 1990* (Eds: I. N. Fridlyander, V. I. Kostikov), Springer, Dordrecht, Netherlands **1991**, p. 464.
- [145] C. Ma, P. Fang, Z.-R. Liu, S.-S. Xu, K. Xu, X. Cheng, A. Lei, H.-C. Xu, C. Zeng, T.-S. Mei, *Sci. Bull.* **2021**, *66*, 2412.
- [146] a) Z. Xue, Y. Wang, M. Yang, T. Wang, H. Zhu, Y. Rui, S. Wu, W. An, *Int. J. Hydrogen Energy* **2022**, *47*, 34025; b) Z. Wang, L. Dong, W. Huang, H. Jia, Q. Zhao, Y. Wang, B. Fei, F. Pan, *Nano* **2021**, *13*, 73.
- [147] M. Liu, L. Kong, X. Wang, J. He, X.-H. Bu, *Small* **2019**, *15*, 1903410.
- [148] E. Mirzakulova, R. Khatmullin, J. Walpita, T. Corrigan, N. M. Vargas-Barbosa, S. Vyas, S. Oottikkal, S. F. Manzer, C. M. Hadad, K. D. Glusac, *Nat. Chem.* **2012**, *4*, 794.
- [149] A. V. Dolganov, B. S. Tanaseichuk, D. N. Moiseeva, V. Y. Yurova, J. R. Sakanyan, N. S. Shmelkova, V. V. Lobanov, *Electrochem. Commun.* **2016**, *68*, 59.
- [150] M. A. Hoque, M. Gil-Sepulcre, A. de Aguirre, J. A. A. W. Elemans, D. Moonshiram, R. Matheu, Y. Shi, J. Benet-Buchholz, X. Sala, M. Malfois, E. Solano, J. Lim, A. Garzón-Manjón, C. Scheu, M. Lanza, F. Maseras, C. Gimbert-Suriñach, A. Llobet, *Nat. Chem.* **2020**, *12*, 1060.
- [151] S. Karak, K. Koner, A. Karmakar, S. Mohata, Y. Nishiyama, N. T. Duong, N. Thomas, T. G. Ajithkumar, M. S. Hossain, S. Bandyopadhyay, S. Kundu, R. Banerjee, *Adv. Mater.* **2023**, 2209919.
- [152] V. Rajagopal, M. Ragunath, N. A. Khan, M. Kathiresan, V. Suryanarayanan, L. A. Jones, S. Kundu, *Mater. Today Chem.* **2023**, *27*, 101327.
- [153] Y.-F. Yao, Z.-Y. Huang, W.-Y. Xie, S.-J. Huang, Z.-Y. Liu, G. Yang, J.-S. Ye, H.-Y. Liu, X.-Y. Xiao, *Catal. Sci. Technol.* **2023**, *13*, 6321.
- [154] K. Yue, J. Liu, Y. Zhu, C. Xia, P. Wang, J. Zhang, Y. Kong, X. Wang, Y. Yan, B. Y. Xia, *Energy Environ. Sci.* **2021**, *14*, 6546.
- [155] W. Ahn, M. G. Park, D. U. Lee, M. H. Seo, G. Jiang, Z. P. Cano, F. M. Hassan, Z. Chen, *Adv. Funct. Mater.* **2018**, *28*, 1802129.
- [156] Y. Luo, X. Yang, L. He, Y. Zheng, J. Pang, L. Wang, R. Jiang, J. Hou, X. Guo, L. Chen, *ACS Appl. Mater. Interfaces* **2022**, *14*, 46374.
- [157] S.-W. Ke, W. Li, Y. Gu, J. Su, Y. Liu, S. Yuan, J.-L. Zuo, J. Ma, P. He, *Sci. Adv.* **2023**, *9*, 2398.
- [158] R. Ren, L. Yang, Z. Lin, X. Li, S. Zhang, T. Zheng, D. Wu, J. Wang, Z. Wei, W. Ding, N. Huang, M. Gu, Q. He, *J. Mater. Chem. A* **2022**, *10*, 22781.
- [159] Q. Wang, F. Wei, D. Manoj, Z. Zhang, J. Xiao, X. Zhao, F. Xiao, H. Wang, S. Wang, *Chem. Commun.* **2019**, *55*, 11307.
- [160] H. Xu, B. Fei, G. Cai, Y. Ha, J. Liu, H. Jia, J. Zhang, M. Liu, R. Wu, *Adv. Energy Mater.* **2020**, *10*, 1902714.
- [161] a) Q. Sun, B. Aguila, G. Verma, X. Liu, Z. Dai, F. Deng, X. Meng, F.-S. Xiao, S. Ma, *Chem* **2016**, *1*, 628; b) G. Huang, Q. Yang, Q. Xu, S.-H. Yu, H.-L. Jiang, *Angew. Chem., Int. Ed.* **2016**, *55*, 7379.
- [162] D. Xu, H. Zhang, L. Zhou, X. Gao, X. Lu, *ChemPhysMater* **2022**, *1*, 86.
- [163] X. Wu, Y.-I. Hong, B. Xu, Y. Nishiyama, W. Jiang, J. Zhu, G. Zhang, S. Kitagawa, S. Horike, *J. Am. Chem. Soc.* **2020**, *142*, 14357.
- [164] S. Yuan, X. Li, J. Zhu, G. Zhang, P. Van Puyvelde, B. Van der Bruggen, *Chem. Soc. Rev.* **2019**, *48*, 2665.
- [165] S. R. Holmes-Farley, C. D. Bain, G. M. Whitesides, *Langmuir* **1988**, *4*, 921.
- [166] K. Artyushkova, M. J. Workman, I. Matanovic, M. J. Dzara, C. Ngo, S. Pylypenko, A. Serov, P. Atanassov, *ACS Appl. Energy Mater.* **2018**, *1*, 68.
- [167] S. Zhai, Z. Lu, Y. Ai, X. Jia, Y. Yang, X. Liu, M. Tian, X. Bian, J. Lin, S. He, *J. Power Sources* **2023**, *554*, 232332.
- [168] a) C. Zhao, J. Long, B. Zhou, R. Zheng, M. He, R. Li, Y. Pan, A. Hu, C. Shu, *J. Mater. Chem. A* **2022**, *10*, 17267; b) C. Vogt, B. M. Weckhuysen, *Nat. Rev. Chem.* **2022**, *6*, 89.
- [169] B.-Q. Li, S.-Y. Zhang, B. Wang, Z.-J. Xia, C. Tang, Q. Zhang, *Energy Environ. Sci.* **2018**, *11*, 1723.
- [170] Z. Chang, L. Guan, J. Zhang, W. Zhang, Q. Ma, A. Shah, L. Xing, H. Su, Q. Xu, *Int. J. Hydrogen Energy* **2022**, *47*, 37013.

- [171] R. Bao, Z. Xiang, Z. Qiao, Y. Yang, Y. Zhang, D. Cao, S. Wang, *Angew. Chem., Int. Ed.* **2023**, 62, 202216751.
- [172] J. Sun, H. Yin, P. Liu, Y. Wang, X. Yao, Z. Tang, H. Zhao, *Chem. Sci.* **2016**, 7, 5640.
- [173] F.-M. Li, L. Huang, S. Zaman, W. Guo, H. Liu, X. Guo, B. Y. Xia, *Adv. Mater.* **2022**, 34, 2200840.
- [174] X. Zhai, Q. Yu, G. Liu, J. Bi, Y. Zhang, J. Chi, J. Lai, B. Yang, L. Wang, *J. Mater. Chem. A* **2021**, 9, 27424.
- [175] X. Xu, H.-C. Chen, L. Li, M. Humayun, X. Zhang, H. Sun, D. P. Debecker, W. Zhang, L. Dai, C. Wang, *ACS Nano* **2023**, 17, 10906.
- [176] J. Fan, C. Fu, R. Liang, H. Lv, C. Fang, Y. Guo, W. Hao, *Small* **2022**, 18, 2203588.
- [177] a) D. Song, H. Guo, K. Huang, H. Zhang, J. Chen, L. Wang, C. Lian, Y. Wang, *Mater. Today* **2022**, 54, 42; b) M. L. Pegis, B. A. McKeown, N. Kumar, K. Lang, D. J. Wasylenko, X. P. Zhang, S. Rauegi, J. M. Mayer, *ACS Cent. Sci.* **2016**, 2, 850.



Ruiqi Cheng is currently a Ph.D. student in the School of Materials Science and Engineering, Shanghai Jiao Tong University under the supervision of Prof. Chaopeng Fu. He received his B.S. from Huazhong University of Science and Technology in 2018 and M.S. from Shanghai Jiao Tong University in 2021. His research interests focus on multifunctional hydrogen and oxygen electrocatalysts for clean energy conversion and storage devices.



Huanxin Li is currently a research fellow in UCL Electrochemical Innovation Lab, as well as a senior academic visiting scholar in Department of Chemistry at University of Oxford. In 2022, he worked on Electrochemistry at the Department of Chemistry, University of Oxford. Prior to this, he was a research associate at University of Cambridge from 2020 to 2022. Through his academic career, he made substantial breakthroughs in the development of novel electrochemical energy devices, thermal cells, and sensors to promote the Net-Zero goal.



Chaopeng Fu received his Ph.D. from Hunan University in 2011 and undertook postdoctoral work at Nanyang Technological University, Singapore (2012–2012) and University of Oxford, UK (2013–2016). He is a research professor at School of Materials Science and Engineering, Shanghai Jiao Tong University. His main research interests focus on advanced metal materials and processing for energy storage.